

**DYNAMIC ANALYSIS OF CONSTRAINED OBJECT MOTION FOR  
MECHANICAL TRANSFER OF LIVE PRODUCTS**

A Thesis  
Presented to  
The Academic Faculty

by

Daxue Wang

In Partial Fulfillment  
of the Requirements for the Degree  
Master of Science in the  
School of Mechanical Engineering

Georgia Institute of Technology  
May 2009

**DYNAMIC ANALYSIS OF CONSTRAINED OBJECT MOTION FOR  
MECHANICAL TRANSFER OF LIVE PRODUCTS**

Approved by:

Dr. Kok-Meng Lee, Advisor  
School of Mechanical Engineering  
*Georgia Institute of Technology*

Dr. Shreyes N.Melkote  
School of Mechanical Engineering  
*Georgia Institute of Technology*

Dr. A.Bruce Webster  
School of Poultry Science  
*University of Georgia*

Date Approved: 04/03/09

## ACKNOWLEDGEMENTS

My sincere gratitude goes first to my thesis advisor, Dr. Kok-Meng Lee. His valuable, insightful advice and guidance on my graduate studies provide me the possibility to complete this thesis, which has provided me with precious experiences that will definitely help me in the future as well. I would like to thank Dr. Shreyes Melkote for his interest and valuable feedback on this thesis as well as agreeing to be on my thesis committee. I would also like to thank Dr. Bruce Webster for his contribution towards this project, and for his interest and advice in my thesis.

A great appreciation must be given to Chihhsing Liu for working together with me on the final project of ME6124 Finite Element Method in Spring 2008. I must also thank Shaohui Foong, for many of his valuable help, discussions and advices on my work throughout my study. I would also like to deliver my special thanks to Kun Bai, Jiajie Guo, Jungyoul Lim and Yang Xie for their support and memorable friendship over a span of two-year graduate study.

I would like to take this opportunity to thank my parents, Guiwen Wang and Xiufen Guo, for providing both mental and economical support to help me finish this thesis. Without their support and deep love, this thesis cannot be completed.

The thesis research was in part supported by the Georgia Agricultural Technology Research Program, the U.S. Poultry and Eggs Association, and the Georgia FoodPAC.

# TABLE OF CONTENTS

	Page
ACKNOWLEDGEMENTS	iii
LIST OF TABLES	vi
LIST OF FIGURES	vii
NOMENCLATURE	x
SUMMARY	xv
 <u>CHAPTER</u>	
1 INTRODUCTION AND BACKGROUND	1
1.1 Introduction	1
1.2 Review of Prior and Related Work	2
1.3 Research Objectives	11
1.4 Thesis Outline	12
 2 SYSTEM OVERVIEW	 14
2.1 Introduction	14
2.2 System Overview	14
2.3 Bird Model and Assumptions	19
2.4 Generalized Coordinates, Constraints and Redundancy	24
2.4.1 Forward Kinematics	24
2.4.2 Constraints	27
2.4.3 Redundancy	27
2.5 Summary	28

3	DYNAMIC MODELING	29
3.1	Introduction	29
3.2	Lagrange Equation of Motion	29
3.3	System Forces	35
3.4	Numerical Algorithm	39
3.5	Verification of the Computational Algorithm	42
3.6	Summary	46
4	NUMERICAL DESIGN ANALYSIS	50
4.1	Introduction	50
4.2	Simulation Parameters	50
4.3	Simulation of Three Consecutive Functions	53
4.4	Discussions of Integrated Three-function Simulation	62
4.5	Effects of Bird Sizes	64
4.5.1	Position, Velocity and Orientation of the Body Center	65
4.5.2	Bird Size Effects on the Shackle Force	69
4.6	Preliminary Studies	72
4.6.1	Effects of Body Rotation on Head Motion	72
4.6.2	Effects of the Shackle Sidewalls and Gravity in SF-2a	75
4.7	Summary	77
5	CONCLUSIONS AND FUTURE WORK	79
	APPENDIX A: DAMPING COEFFICIENTS OF THE RUBBER FINGER	81
	REFERENCES	84

## LIST OF TABLES

	Page
Table 2-1: Symbols used for the derivation	26
Table 3-1: Inertia matrix properties	33
Table 3-2: Jacobian sub-matrices	34
Table 3-3: Non-constrained forces	36
Table 3-4: Constrained forces	38
Table 4-1: Bird properties	51
Table 4-2: Parameters and initial conditions	51
Table A-1: Equipment properties	82

## LIST OF FIGURES

	Page
Figure 1-1: Automated transfer mechanism and leg kinematics	4
Figure 1-2: Compliant constant force and its pseudo-rigid-body model	6
Figure 1-3: Parallel manipulator	7
Figure 1-4: Three link mechanism and its applications in the space station	7
Figure 1-5: Stick model of human leg	8
Figure 1-6: A lumped-parameter model of human leg	9
Figure 1-7: Kip performance of a human gymnast and optimized trajectory	9
Figure 1-8: Three-link under-actuated mechanical system	10
Figure 1-9: Push task and model with external force to the manipulator	11
Figure 2-1: CAD modeling of live transfer system	15
Figure 2-2: Schematics illustrating function 1	16
Figure 2-3: External finger force and moment	17
Figure 2-4: Schematics illustrating function 2 (plan view)	18
Figure 2-5: Broiler body model	20
Figure 2-6: Bird leg model (side view)	21
Figure 2-7: Bird leg model (plan view)	22
Figure 2-8: Contact kinematic constraints	22
Figure 2-9: Bird mass components	23
Figure 3-1: Free body diagram of impulse force analysis	35
Figure 3-2: Simulation flowchart	40
Figure 3-3: Convergence check	45
Figure 3-4: Inversion process (SF-2b on the XY plane, $\omega_z = 8.727\text{rad/s}$ )	47

Figure 3-5: Rotation process (SF-2a on the XZ plane, $\omega_y = 4.514\text{rad/s}$ )	48
Figure 3-6: Percentage error of $Y_c$ (SF-2b)	49
Figure 3-7: Percentage error of $Z_c$ (SF-2a)	49
Figure 4-1: Contact force time plot ( $F_{max}=25.35\text{N}$ )	52
Figure 4-2: Snap shots of three consecutive functions	54
Figure 4-3: Trajectory (center and orientation in F-1)	55
Figure 4-4: Center position and velocity (F-1)	55
Figure 4-5: Shackle force on joint 1 (F-1)	56
Figure 4-6: Constrained force and moment (body center in F-1)	56
Figure 4-7: Constrained torque on joints (F-1)	57
Figure 4-8: Trajectory (center and orientation in SF-2a)	58
Figure 4-9: Center position and velocity (SF-2a)	58
Figure 4-10: Shackle force on joint 1 (SF-2a)	59
Figure 4-11: Constrained force and moment (body center in SF-2a)	59
Figure 4-12: Constrained torque on joints (SF-2a)	60
Figure 4-13: Trajectory (center and orientation in SF-2b)	60
Figure 4-14: Center position and velocity (SF-2b)	60
Figure 4-15: Shackle force on Joint 1 (SF-2b)	61
Figure 4-16: Constrained force on body center and toe joint (SF-2b)	61
Figure 4-17: Constrained torque on the joints (SF-2b)	62
Figure 4-18: Trajectory (center and orientation)	66
Figure 4-19: Center velocities	67
Figure 4-20: Shackle force	70
Figure 4-21: Head and its pseudo-rigid-model (plan view)	73
Figure 4-22: System input and output	74

Figure 4-23: Pseudo-rigid-model motion	74
Figure 4-24: Pseudo-rigid-link trajectory	75
Figure 4-25: Snapshots in SF-2a (with sidewalls and gravity)	76
Figure 4-26: Trajectory comparison	76
Figure 4-27: Bird motion in 3D	76
Figure A-1: Experimental setup (6-inch finger)	81
Figure A-2: Response of the 6-inch finger	82

## NOMENCLATURE

### Capitalized letters

$\mathbf{C}(q, \dot{q})$	Centrifugal-Coriolis matrix
$D$	Distance between shackle point and pivot point
$D_p$	Projected $D$ on the XZ plane
$D_r$	Rayleigh dissipation function
$E$	Young's modulus
$\mathbf{F}(q, \dot{q})$	System non-constrained force
$\mathbf{F}_c$	Constrained force vector
$\mathbf{F}$	External finger force
$I_i$	Moment of inertia of $i^{\text{th}}$ link
$I_l$	Total moment of inertia of the bird limbs
$J_1$	The toe joint
$J_2$	The hock joint
$J_3$	The knee joint
$J_4$	The hip joint
$J_5$	Center of the bird body
$\mathbf{J}_i$	Position vector of $i^{\text{th}}$ joint
$\mathbf{J}_{15}$	Length between the toe joint and the body center
$L_1$	Length of bird foot
$L_2$	Length of bird leg
$L_3$	Length of bird thigh
$L_4$	Length between the hip joint and ellipse center
$L_b$	Projected $L_4$ on the XZ plane

$L_p$	Shackle length on the XZ plane
$L_s$	Shackle length
$L_t$	Projected total length of the foot, leg and thigh on the XZ plane
$\mathbf{M}(\mathbf{q})$	Inertia matrix
$\mathbf{M}$	Net moment from external force
$\mathbf{M}_c$	Constrained moment acting on the body center
$\mathbf{P}$	System parameter vector
$\mathbf{P}_1$	Position vector of the foot mass
$\mathbf{P}_2$	Position vector of the leg mass
$\mathbf{P}_3$	Position vector of the thigh mass
$\mathbf{P}_4$	Position vector of the body mass
$\mathbf{P}_5$	Position vector of the shackle mass
$\mathbf{Q}$	External force vector
$\mathbf{V}_1$	Velocity vector of the foot mass
$\mathbf{V}_2$	Velocity Vector of the leg mass
$\mathbf{V}_3$	Velocity Vector of the thigh mass
$\mathbf{V}_4$	Velocity Vector of the body mass
$\mathbf{V}_5$	Velocity Vector of the shackle mass
$T$	Total kinetic energy
$T_{z1}$	Non-constrained moment on the toe joint
$T_{z2}$	Non-constrained moment on the hock joint
$T_{z3}$	Non-constrained moment on the knee joint
$T_{z4}$	Non-constrained moment on the hip joint
$V$	Total potential energy
(X,Y,Z)	Global coordinate system

## Lower Case Letters

$a$	First lengthwise semi axis of ellipsoid
$\mathbf{a}(\mathbf{q})$	Jacobian Matrix
$b$	Second lengthwise semi axis of ellipsoid
$b_1$	Torsional damping coefficient of the toe joint
$b_2$	Torsional damping coefficient of the hock joint
$b_3$	Torsional damping coefficient of the knee joint
$b_4$	Torsional damping coefficient of the hip joint
$c$	Third lengthwise semi axis of ellipsoid
$f$	Constraint equation
$g$	Gravitational acceleration
$h$	Time step in the numerical algorithm
$m$	Number of constraint equations
$m_1$	Mass of the foot
$m_2$	Mass of the leg
$m_3$	Mass of the thigh
$m_4$	Mass of the bird body
$m_5$	Mass of shackle
$m_l$	Total mass of three limbs (foot, leg, thigh)
$n$	Number of generalized coordinates
$k_1$	Torsional spring constant of toe joint
$k_2$	Torsional spring constant of hock joint
$k_3$	Torsional spring constant of knee joint
$k_4$	Torsional spring constant of hip joint
$\mathbf{q}$	Generalized coordinate vector

$\dot{\mathbf{q}}$	Generalized velocity vector
$\ddot{\mathbf{q}}$	Generalized acceleration vector
$t_{max}$	Total time in simulation
$v_c$	Conveyor speed

### Greek Letters

$\alpha$	Angle between $\mathbf{J}_{15}$ and semi axis of bird body b
$\beta_1$	Angle of the toe joint on the XZ plane
$\beta_4$	Angle of the hip joint on the XZ plane
$\beta_e$	Orientation angle of bird body on the XZ plane
$\gamma$	Swing angle of the bird head on the XZ plane
$\theta_p$	Orientation angle of rotating shackle on the XY plane
$\theta_y$	Orientation angle of rotating shackle on the XZ plane
$\lambda$	Lagrange multiplier vector
$\tau_{z1}$	Constrained moment on the toe joint
$\tau_{z2}$	Constrained moment on the hock joint
$\tau_{z3}$	Constrained moment on the knee joint
$\tau_{z4}$	Constrained moment on the hip joint
$\phi_4$	Horizontal angle of the foot
$\phi_5$	Horizontal angle of the leg
$\phi_6$	Horizontal angle of the thigh
$\phi_7$	Horizontal angle of $L_4$
$\varphi_1$	Angle of the foot with respect to the shackle

$\varphi_2$	Angle between the foot and the leg
$\varphi_3$	Angle between the leg and the thigh
$\varphi_4$	Angle between the leg and $L_4$
$\varphi_5$	Angle between a and $L_4$
$\varphi_e$	Orientation angle of bird body
$\omega_d$	Angular velocity of the rotating drum
$\omega_y$	Angular velocity of the rotating shackle on the XZ plane
$\omega_z$	Angular velocity of the rotating shackle on the XY plane

### Subscripts

0	Equilibrium angle of the $i^{\text{th}}$ joint
1	The toe joint
2	The hock joint
3	The knee joint
4	The hip joint
5	The body center
N	Normal direction
T	Tangential direction
X	X component
Y	Y component

## SUMMARY

This thesis is motivated by practical problems encountered in handling live products in the poultry processing industry, where live birds are manually transferred by human labors. As the task of handling live products is often unpleasant and hazardous, it is an ideal candidate for automation. To reduce the number of configurations and live birds to be tested, this thesis focuses on developing analytical models based on the Lagrange method to predict the effect of mechanical inversion on the shackled bird. Unlike prior research which focused on the effect of different inversion paths on the joint force/torque of a free-falling shackled bird, this thesis research examines the effect of kinematic constraints (designed to support the bird body) on the shackled bird. Unlike free-falling, the imposed kinematic constraints enable the shackled bird to rotate about its center of mass, and thus minimize wing flapping. In this thesis, birds are geometrically approximated as ellipsoids while the lower extremity is modeled as a pair of multi-joint serial manipulators. With the constraint equations formulated into a set of differential algebraic equations, the equations of motion as well as Lagrange multipliers characterizing kinematical constraints are numerically solved for the bird motion, specifically the position, velocity, and orientation and hence the forces and torques of the joints. The dynamic models are verified by comparing simulation results against those obtained using a finite element method. The outcomes of this thesis will provide some intuitive insights essential to design optimization of a live-bird transfer system.

# CHAPTER I

## INTRODUCTION AND BACKGROUND

### 1.1 Introduction

Automation plays an important role in the global economy and daily processes; while not only increases productivity and reduce costs, but also offers manufacturing flexibility and improves quality of products. In poultry processing, such application includes handling, meat processing and packaging.

One of the major tasks in poultry meat processing is the handling of live broilers, which requires human workers to grasp and invert the bird body followed by inserting both legs of the bird into a shackle at a typical production rate of 120-180 birds per minute. Work environment is often dark and unpleasant for human beings. Potential injuries to handlers include scratching from flapping birds. These are potential causes responsible for high turnover rates and difficulties to recruit new workers. Therefore, transferring of live broilers is an ideal candidate for automation.

In this thesis, birds are geometrically approximated as ellipsoids while its legs are modeled as a pair of multi-joint serial manipulators. By imposing kinematic constraints that enable the shackled bird to rotate about its center of mass, the effects of kinematic constraints (designed to support the bird body) on the shackled bird are investigated. With the constraint equations formulated into a set of differential algebraic equations, the equations of motion as well as Lagrange multipliers characterizing kinematical constraints are numerically solved for the bird motion, specifically the position, velocity, and orientation and hence the forces and torques of the joints.

The remainder of this chapter is organized as follows: a review of prior and related works on dynamic modeling is presented below. Next, the research objectives for this thesis are explained. An outline of the remainder of this thesis is given at the end of this chapter.

## 1.2 Review of Prior and Related Work

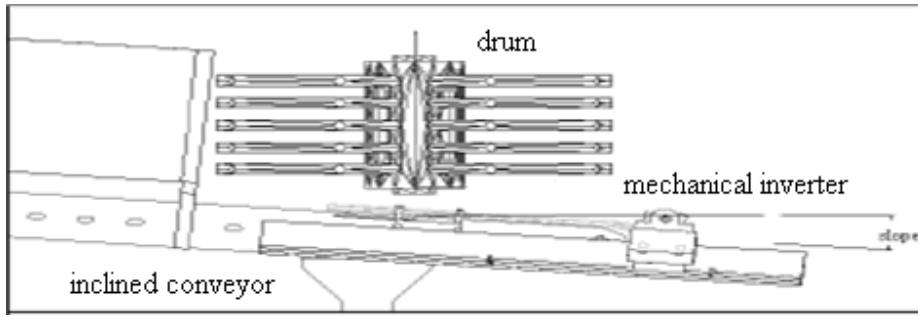
This thesis is a continuation of an ongoing project entitled “Intelligent Automated High Speed Transfer of Live Birds” proposed by Lee *et al.* [1997]. The goal is to develop a mechanical system to transfer live birds from conveyors to shackle lines while maintaining production requirements which include cycle time and cost. The basic process includes separating, shackling and inverting live birds.

### Early research on bird handling

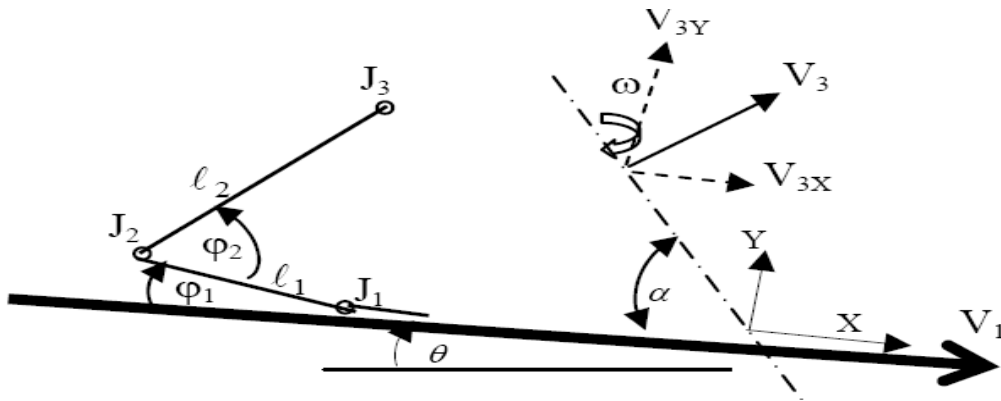
Many ideas have been developed on harvesting, handling and shackling live birds in the processing plant, as surveyed by Lee [1996]. Parker [1980] suggested shackling the bird before transporting it from the farm. Then the shackle became a part of coop structure on which the bird was constrained. At the processing plant, the shackles with birds are loaded on the conveyor for subsequent processes. The advantage of Parker’s method is reducing human operations required for bird shackling thus saving labor costs. However, from studies conducted by Scott [1993] and Kettlewell [1995], they concluded that birds suffered more bruising when held stationary than they did when transported unrestrained. As an important aspect in this automated high-speed live-bird transfer system, a few methods have been proposed to properly orient the bird and present their legs to the shackle. Keiter [1992] claimed that when birds travel on an incline, they naturally orient themselves to face up the slope. Heemskerk [1992] suggested that

spraying water or gas under the abdomens of the broilers could make them stand up, thus making both legs easier for shackling. The experimental study of two methods introduced above was done on an empirical basis, and the results were determined subjectively.

Differing from the work by other people, where designs were based upon a subjective assessment, Lee [1999] developed an analytical model to provide a means to understand the bird's natural reactions to mechanical transfer processes for tests with live birds [Lee *et al.*, 1999]. This understanding subsequently led to the development of a compliant grasping mechanism consisting of a pair of counter-rotating drums with rubber fingers. In [Lee, 2001], the concept and design criteria of an automated live bird transfer system are presented. As shown in Figure 1-1, the live-bird transfer system consists of a rotating body grasper, an inclined conveyor and a shackle inverter. The operating principle of the transfer system is as follows. The bird is guided to the grasper where its body is constrained by rubber fingers on two counter-rotating drums. The downward-inclined conveyor allows the bird to extend its legs freely between the conveyor and grasper into a pair of feet grippers built in the shackle. Hence the bird legs can be kinematically manipulated by controlling the body-feet velocity difference using the drum and conveyor speeds. Once the bird's legs are shackled, the momentum along with gravity will cause the body to rotate with the shackle at the end of the conveyor [Lee, 2000]. This proof of concept feasibility led to significant interests in automating the transfer of live products [Webster and Lee, 2002] and [Webster and Lee, 2003].



(a) Side view of live bird transfer system



(b) Leg kinematics on a moving conveyor

Figure 1-1 Automated transfer mechanism and leg kinematics [8]

To reduce the number of design configurations for the fabrication and birds used, some fundamental researches were performed at Georgia Tech in [Lee *et al.*, 2001], [Lee and Yin, 2001] and [Yin and Lee, 2002]. To provide a good understanding on the effect of rotating finger on the live broilers, Joni [2001] conducted an experimental study and performed a 2D finite-element analysis (FEA) to predict the forces acting on a rigid body by the rubber fingers. His experimental results suggested that the finger force could be analyzed quasi-statically since it was independent of the drum angular velocity. In addition, because the finger is highly compliant, large deformations occur on the finger instead of the bird body hence reducing the possibility of damaging the bird. To further

investigate the rotating finger effects, Yin [2002] conducted both quasi-static and dynamic analyses, he also derived a closed-form solution to determine contact points and forces by modeling the finger as a flexible beam, and validated it through experiments. To identify the design parameters that affect the gripping process, Summer [2002] developed a design algorithm (combining the kinematic model of the bird leg and the pallet motion) for designing a drop cam trajectory profile. To study the body rotational dynamics under free fall when the bird is being inverted, [Lee and Shumway, 2003] developed dynamic models by Lagrange method considering constraints imposed by an external mechanical system on which the body was transported. This model (validated experimentally with mechanical birds) has provided a means to identify parameters (such as inversion path) which could influence joint forces and body dynamics.

All the aforementioned researches provide a good basis for this thesis research topic. As in Lee *et al*, [2001] , [Lee and Yin, 2001], and [Lee and Shumway, 2003], the models developed in this thesis incorporate the kinematic constraints from the bird limbs and the shackle, and the rotational dynamics of bird (such as trajectory and velocity of the body center) will be obtained by numerically solving Lagrange equations of motion. However, unlike prior work [Shumway,2002] focusing on the effect of different inversion paths of a free-falling shackled bird on the joint force/torque, the effects of kinematic constraints (designed to support the bird's body and enable it to rotate about its center of mass) will be examined. Some research publications related to this thesis are reviewed in the following subsections.

Research on methods of dynamic modeling

Boyle [2001] derived a closed-form dynamic model as shown in Figure 1-2 for a constant-force mechanism based on Lagrange equation of motion to simplify kinematic and dynamic analyses, which converts the compliant mechanism to its counterpart rigid-body model.

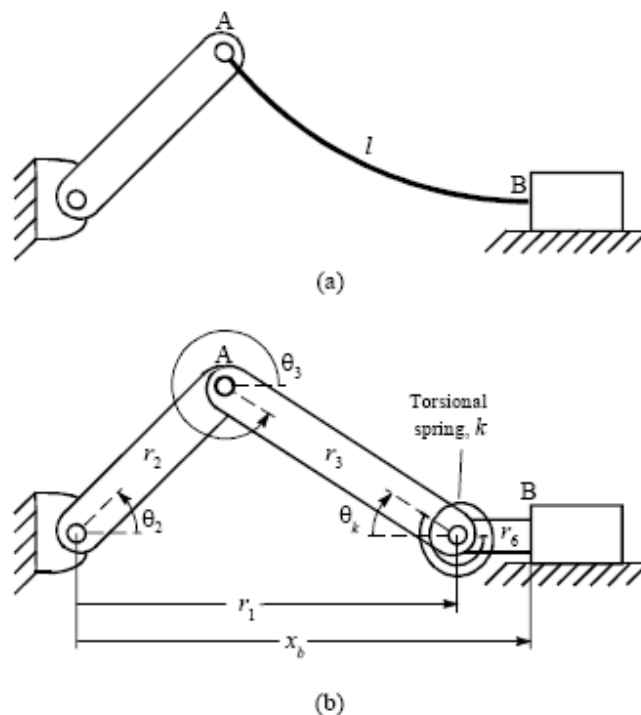


Figure 1-2 Compliant constant force and its pseudo-rigid-body model [2]

Dynamic modeling of flexible planar manipulators has been widely researched in robotics. Kang and Mills [2001] formulated the Lagrange equations of motion to model a parallel manipulator, where they used Lagrange multipliers to account for the geometrical constraints in multiple closed loop chains in Figure 1-3.

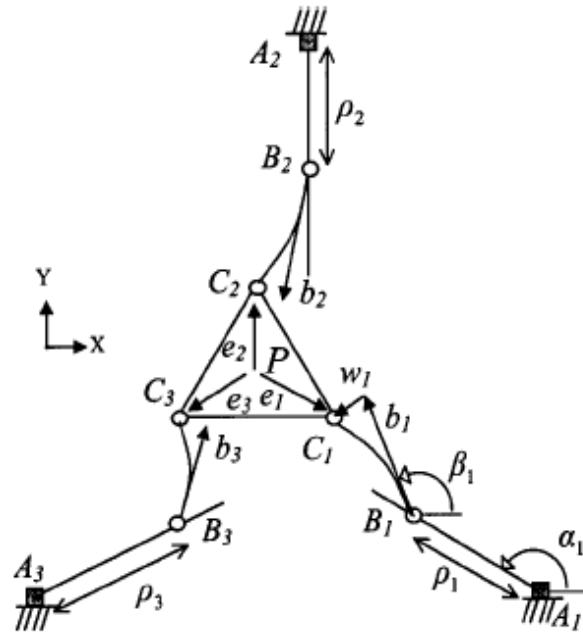


Figure 1-3 Parallel manipulator [6]

Similar work was developed on constrained robot systems. By Kovacs *et al.* [2003], a constrained robotic system, as shown in Figure 1-4, was modeled with kinematical constraints explicitly considered in analysis, by using nonlinear holonomic constraint equations.

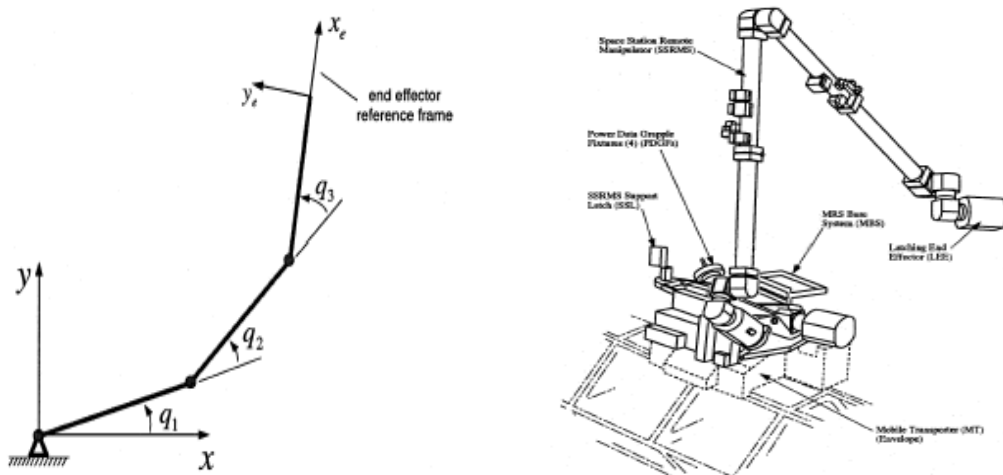


Figure 1-4 Three link mechanism and its applications in the space station [7]

Research on body and leg modeling

Lumped-parameter approaches have been commonly used in modeling biological mechanics, most notably, on modeling human legs. A bond graph technique was proposed by Patla *et al.*[2000] to describe human locomotion and model human dynamics. They model connections between the foot, leg and thigh as combinations of spring and dashpot elements, as shown in Figure 1-5. Similarly, Wojcik [2003] proposed another bond graph approach in the form of lumped parameter of human legs, as shown in Figure 1-6, to represent muscular functions and rigid body motion, it provides an effective means to examine the global spring and damping effects of biological muscles and other soft tissues.

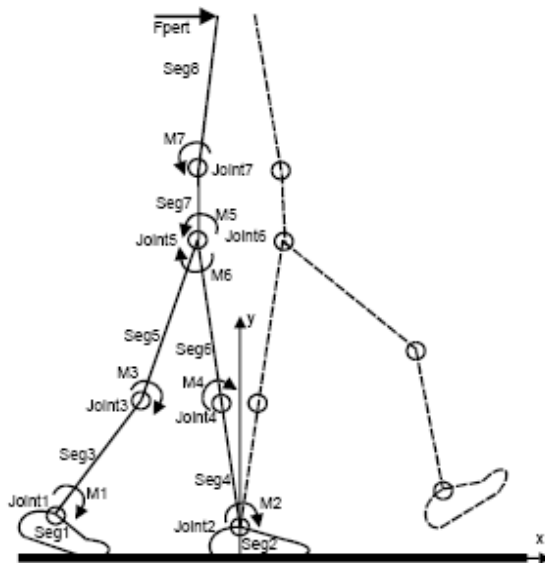


Figure 1-5 Stick model of human leg [23]

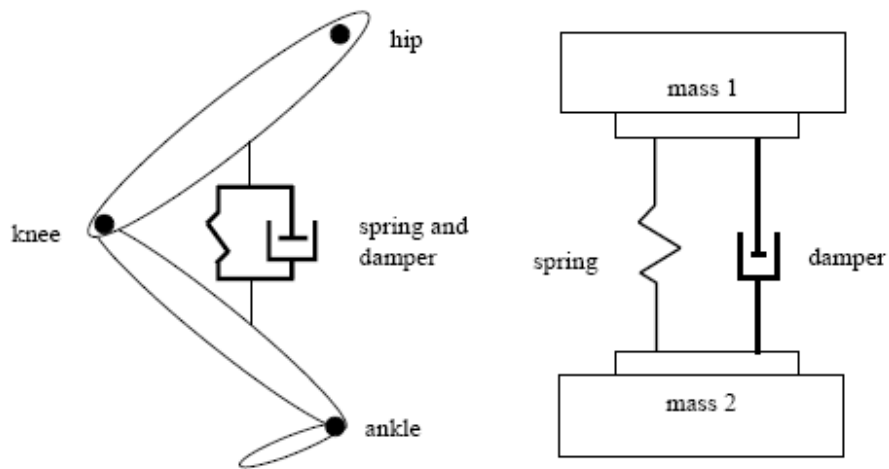


Figure 1-6 A lumped-parameter model of human leg [29]

Some relevant researches were conducted in the area of sports. Miyazaki *et al.* [1998] presented a system for coaching novice gymnasts in performing the kip. By modeling human body as a pendulum with three links, they simulated a trajectory to describe the center of mass and to determine an optimal trajectory, as seen in Figure 1-7.

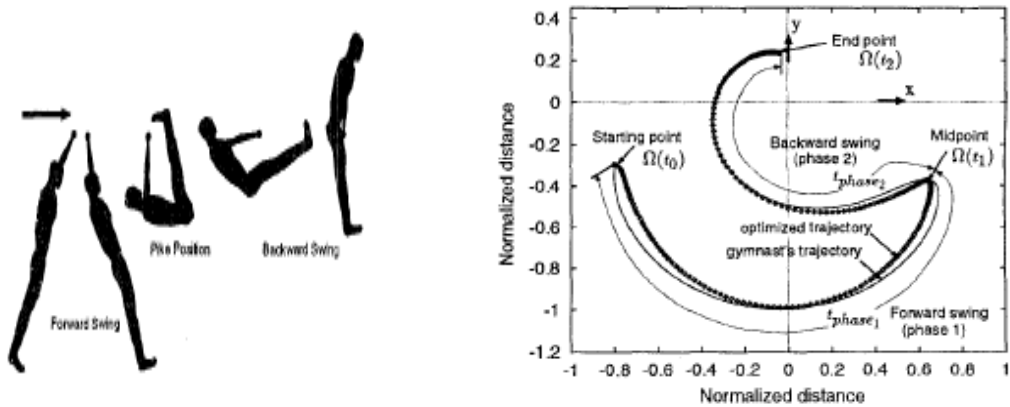


Figure 1-7 Kip performance of a human gymnast and optimized trajectory [20]

Similarly, Yamakita *et al.* [2001] modeled a gymnast on a horizontal bar as a three-link under-actuated acrobat robot, as shown in Figure 1-8. By implementing the acrobat robot

model by the heuristic control method and considering the limits of each joint angles, performance of several skillful motions from a gymnast, such as, swinging from pendulum state, forward upward circling and giant swing, can be realized.

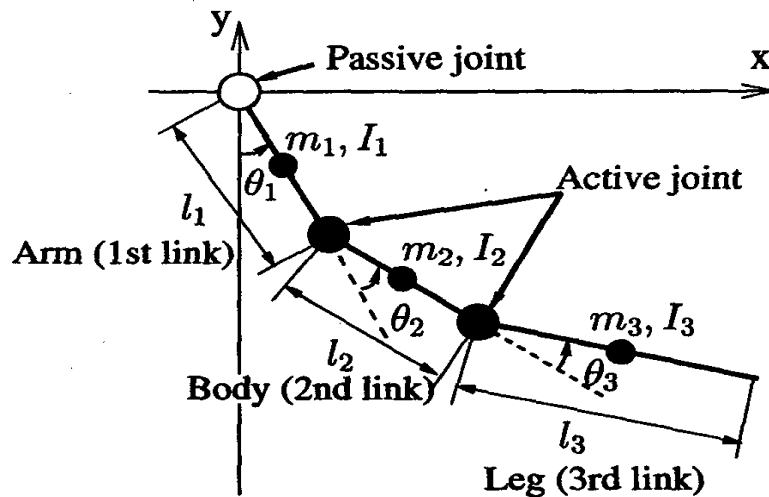


Figure 1-8 Three-link under-actuated mechanical system [19]

Research on pushing operations

Research on pushing operations has important applications on humanoid robots. Arai *et al.* [2005] worked on a pushing task by a humanoid robot and using a balancing control when an external force is acting on the end effectors, as shown in Figure 1-9. They proposed a new method of implementing an impedance controller to manipulate the walk velocity of humanoid robot, therefore, by controlling pushing force, the walking pattern can be adjusted to different operation environments, such as changed target object or disturbed travel.

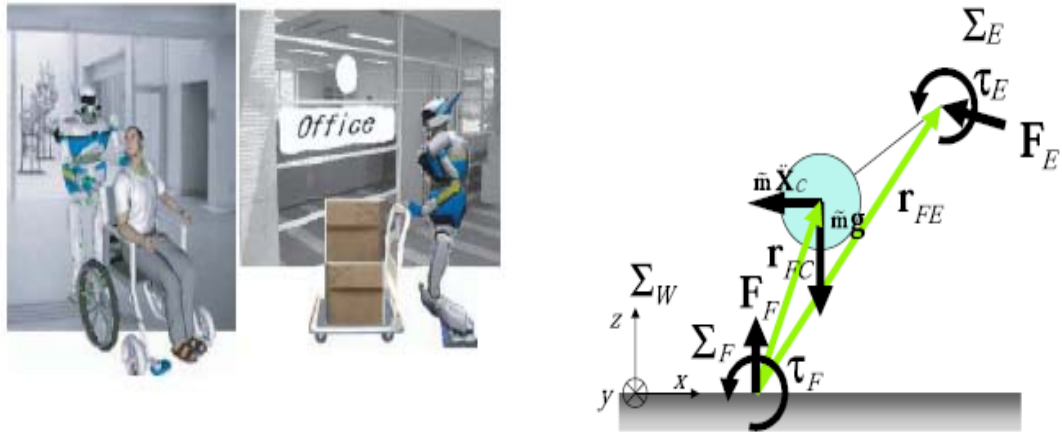


Figure 1-9 Push task and model with external force to the manipulator [26]

### 1.3 Research Objectives

One of the key concerns in developing an automated live broiler transfer system is to maintain the welfare of the birds, and avoid carcass bruising on their bodies as well as their legs during inversion and other rotation process. For this reason, the primary objective of this thesis is to develop a dynamic model and a numerical algorithm to simulate body motions while considering effects of gravity and grasping finger force. Additionally, influences from kinematic constraints and different bird sizes on body motions are investigated.

Realistic dynamic models improve understanding of the bird body motions and provide a reference for design of a cost-effective transfer system, thus minimizing the possibility of injuring the birds by reducing unwanted reactions during the entire process.

Since experiments of the automated transfer system require fabrication of mechanical components and sensing devices, as well as considerable amount of time to set up the system involving live birds, it is very costly. Science-based numerical simulation can be effective before setting up an experiment; thus, this thesis offers

computer simulation results using dynamic modeling of the bird motion with verification against finite element results to provide a foundation for designing and implementing real experiments for this automated live bird transfer system.

#### 1.4 Thesis Outline

This thesis is outlined as follows. Chapter 1 introduces the motivation of this thesis, followed by a description on the background of the project and a review of past and related research work. Then the research objectives are discussed. Contents of the remainder of this thesis are organized below.

Chapter 2 provides an overview of automated live bird transfer system, which consists of three subsystems; a finger-drum system, a rotating shackle, and a bird. A typical operation process of the system involving three consecutive functions is introduced. As a basis for the subsequent chapters, the assumptions including the bird model are made; the generalized coordinates are defined; and the kinematic constraints and redundancy are discussed.

Chapter 3 begins with the derivation of the Lagrange equations of motion along with the formulation of the inertia matrix, Jacobian matrix (derived from kinematic constraints), the acceleration terms of generalized coordinates, and the Lagrange multipliers. The Lagrange equations of motion are explicitly solved from a compact form of equations. System forces including both non-constrained and constrained forces are also derived. A numerical algorithm for simulating the body dynamics is presented. A verification of the computational algorithm is obtained by comparing results against FEA.

Chapter 4 performs a numerical analysis on the system design. Simulation parameters including the bird properties and initial conditions are defined. Then a

simulation of three consecutive functions is made to illustrate the rotation dynamics and constrained forces on the bird based on the geometrical and mass properties of a medium size bird. A comparison is then made to illustrate the effects of the bird size on the dynamics and the constrained forces, especially the normal force and the tangential force imposed by the shackle.

Chapter 5 draws the conclusion of this thesis work. Recommendations and topics for future research are presented at the end of this chapter.

## CHAPTER 2

### SYSTEM OVERVIEW

#### 2.1 Introduction

This chapter begins with an introduction of the automated live-transfer system being developed at Georgia Tech. Three sub functions (supporting, rotating and inverting the bird body) are described. System assumptions (including the bird model) are made. Generalized coordinates, constraint equations and redundancy for the formulations in the subsequent chapter are also discussed in this chapter.

#### 2.2 System Overview

Figure 2-1 shows a CAD model of an automated live-bird transfer system [Lee *et al.* 2009], which consists of the following mechanical processes:

1. body-cradling for leg-shackling [Lee, 2000], and
2. body-inversion [Lee and Shumway, 2003].

A typical working cycle begins with transporting the broilers on the conveyor (moving at a constant surface speed  $v_c$ ) towards a pair of “mechanical hands” where (during the first process) the broiler is grasped by its body while both of its legs are guided into a pair of leg-grippers. The “hands” are essentially two counter-rotating drums with flexible rubber fingers (driven by a servo motor rotating at a constant speed  $\omega_d$ ). While the broiler body is held by the “hands”, both legs of the broiler are manipulated with respect to its body by adjusting the speeds of the drum and conveyor. The legs are secured before the broiler slides along the shackling platform under its momentum.

As mentioned in Chapter 1, this thesis primarily focuses on the second process where the shackled broiler is inverted by means of two consecutive functions:

- Function 1 is to support the shackled bird exiting from the rotating fingers onto a pallet.
- Function 2 is to rotate and invert the pallet (on which the bird is shackled) out of the shackling area.

Unlike the earlier mechanism described in [Lee and Shumway, 2003] where the shackled broilers were rotating around an inversion path, the mechanism discussed here supports the broiler body with the control effort derived from the exit momentum and gravity. A description of these two functions is introduced below:

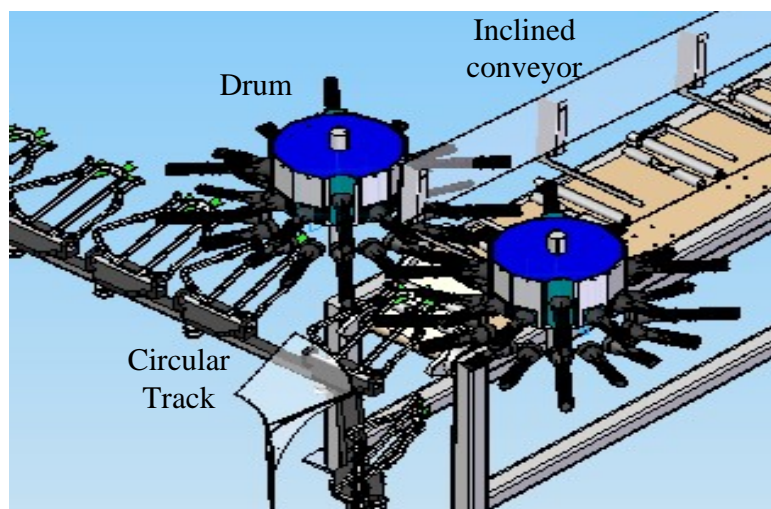


Figure 2-1 CAD modeling of live transfer system [11]

Function 1(F-1): Support the exiting shackled bird

Figure 2-2 shows the schematics of the live bird transfer system, where XYZ defines the global Cartesian coordinate system with its origin O at the pivot point of the shackle. In Figure 2-2, the XZ is a horizontal plane and the Y-axis is parallel to the rotating axis of the drums and perpendicular to the XZ plane.

As shown in Figure 2-2, the shackle is rotatable about the Z axis with the angular velocity  $\omega_z = d\theta_p/dt$ . For this function, the shackle is inclined at a constant angle  $\theta_p$  and therefore  $\omega_z = 0$ . Because the rotating fingers exert contact forces on the broiler as the drums continue to rotate, the bird exits with a momentum while both of its legs are shackled on the pallet at a distance of  $D$  from the origin. This momentum (which depends on the drum rotation  $\omega_d$ ) along with the gravitational force and the conveyor velocity  $v_c$  causes the bird to rotate about the shackled point.

In addition to the gravity, the system input variables are the force  $F$  and moment  $M$  acting on the bird (center of mass) due to the fingers, as shown in Figure 2-3. Given these system inputs, the interest here is to determine the bird exit trajectory, and contact locations and forces encountered in this process.

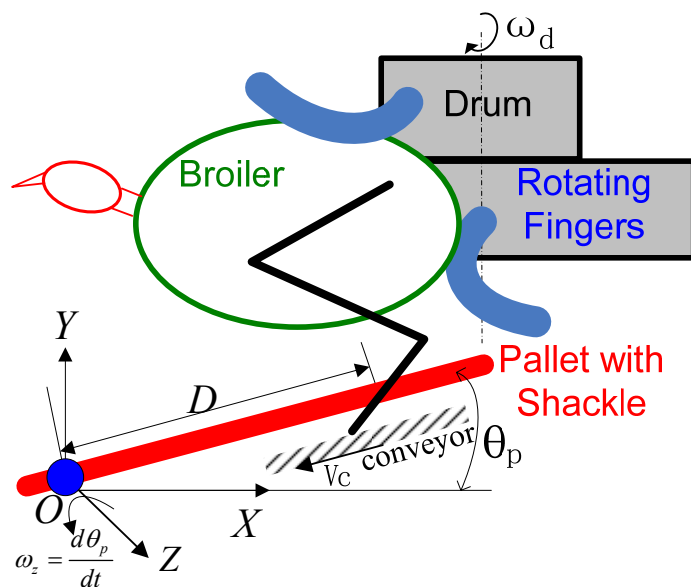


Figure 2-2 Schematics illustrating function 1

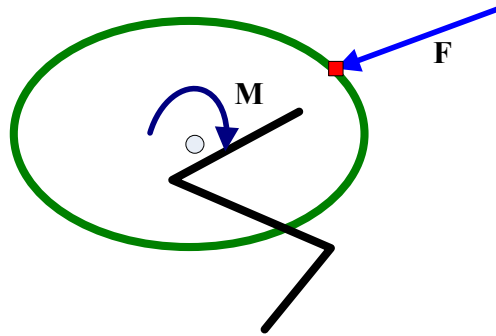


Figure 2-3 External finger force and moment

Function 2: Rotate shackled bird out of the grasping region

Figure 2-4 shows the plan view illustrating the bird rotation out of the grasping region when being shackled. This function is sub-divided into two portions:

*Sub-function 2a (SF-2a)* takes place on the inclined plane at the angle  $\theta_p$  with respect to the X-Z (or the horizontal) plane:

As illustrated earlier in Figure 2-1, once the shackled bird is free from the fingers, the pallet (driven by an external motor) with the shackled bird rotates about the point  $O$  at a constant angular velocity  $\omega_y = d\theta_y / dt$  along the track while both legs remain shackled at the point (distance  $D \cos \theta_p$  from the origin), as shown in Figure 2-4. The rotational dynamics can be determined from  $\omega_y$  during the process. Given that the distance between the pivot and the origin, bird body position, velocity, orientation and joint forces/torques can be determined.

*Sub-function 2b (SF-2b)* happens on the X-Y (or the vertical) plane.

Next, the pallet will rotate at a constant angular speed  $\omega_z$  in an anticlockwise direction from the initial position  $\theta_p$ , as seen from Figure 2-2. As compared to function 1, the only difference is that the effect from the rotating finger and drum will no longer be considered here. Therefore, only the forces due to gravity and that under the influence of system input  $\omega_z = d\theta_p / dt$  will cause the bird to rotate about the shackled point.

The broiler body will continue rotating until it is in contact with the pallet surface.

In this process, the dynamic model is to determine the rotational dynamics of bird body as well as constrained force and torques for the given shackle point distance  $D$  and

angular velocity  $\omega_z$ . Once the pallet is rotated to its vertical position, the inverted broiler continues to travel along the track as shown in Figure 2-1 to a stunning bath. The predicted swinging trajectory of the bird head during rotation offers a rational basis for the design of a head constraining mechanism for subsequent handling of the bird head.

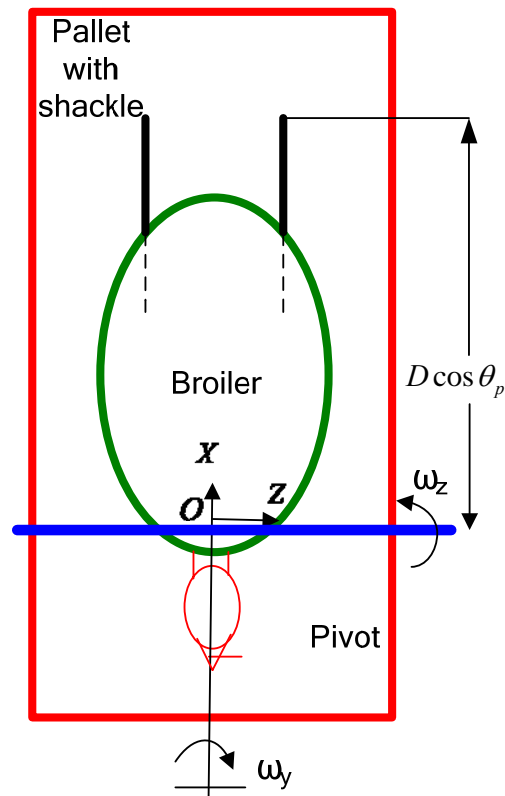


Figure 2-4 Schematics illustrating function 2 (plan view)

Objective of the dynamic analysis

In summary, the objective of this thesis is to study the constrained motion of bird during the inversion as well as in the along-track-rotation. The approach to this problem is to derive and solve the equations of motions (with associated constraint equations) using the Lagrange method. As compared to the setup analyzed in the previous thesis by Shumway [2002] where the broiler is allowed to free fall, in this

thesis the forces from the flexible rubber fingers and the body force from shackle surface are utilized leading to a more gentle body inversion.

### 2.3 Bird Model and Assumptions

To reduce the equations of motion to a more tractable form, several assumptions are made. These assumptions are broadly divided into the following types.

#### Bird model

The broiler body is approximated as an ellipsoid as shown in the Figure 2-5(a) based on the skeleton model of a broiler [Shumway, 2002]. In 2D side view, it can be considered as an ellipse, with  $a$  and  $b$  denoting major and minor axes respectively. Figure 2-5(b) shows a plan view of broiler body, which is also a 2-D ellipse, with  $a$  and  $c$  denoting its major and minor axes.

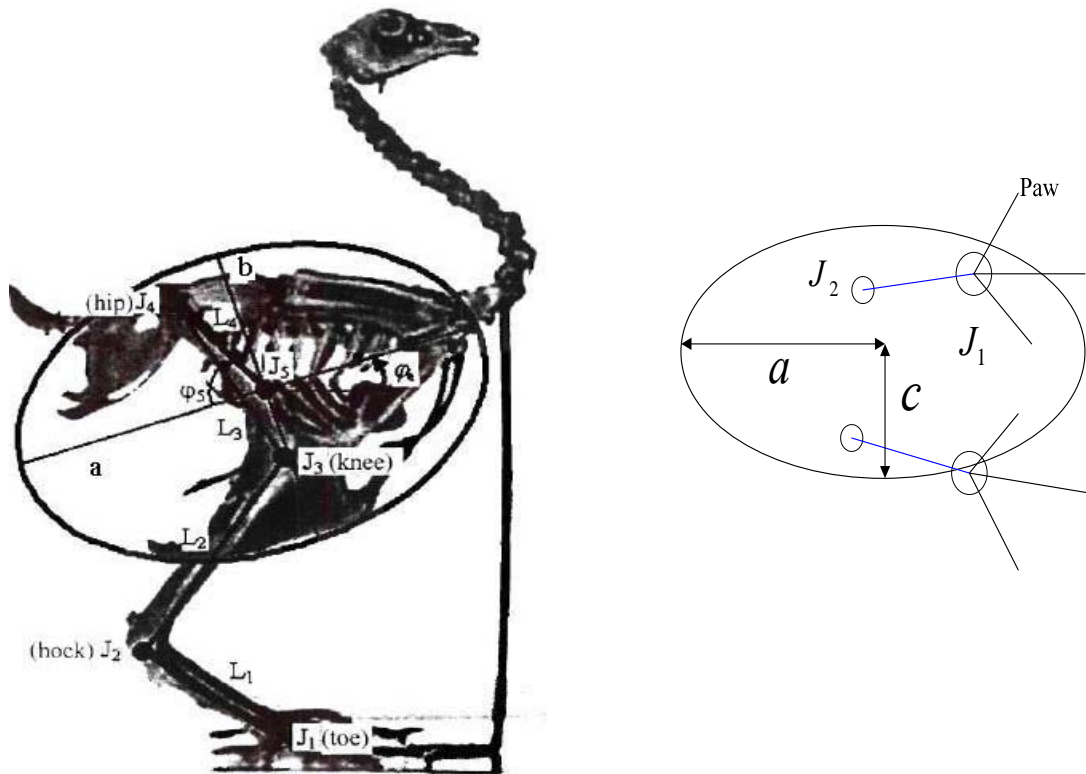
The broiler is modeled as a multi-joint structural mechanism in Figure 2-6 where

- $J_1, J_2, J_3, J_4,$  and  $J_5$  represent the toe, hock, knee, hip, the center of ellipse respectively;
- $L_1, L_2,$  and  $L_3$  denote the lengths of the foot, leg and thigh respectively; and
- $L_4$  is the length between the hip joint  $J_4$  and the ellipse center  $J_5$ .

In Figure 2-6, the following angles are defined to facilitate the discussions:

- $\varphi_1$  is the angle between the foot and the shackle plane;
- $\varphi_2, \varphi_3$  and  $\varphi_4$  are the angles between two adjacent limbs;
- $\varphi_5$  is the fixed angle between  $L_4$  and the major axis of the ellipse (side view); and
- $\varphi_e$  characterizes the bird orientation.

In addition, we define the angles  $\phi_4, \phi_5$  and  $\phi_6$  to describe the orientation of the link with respect to X-axis.



(a) Broiler skeleton model [25]

(b) Plan view of body

Figure 2-5 Broiler body model

Bird relative to shackle

In the motion analysis, the following assumptions are made:

*Assumption 1:* The bird has been shackled such that Joint  $J_1$  is fixed with respect to the shackle throughout the operation.

*Assumption 2:* Because of soft biologic tissues, the bird body is flattened after it contacts with shackle surface. The shackled bird slides but not rolls, and its orientation remains parallel to the shackle surface,

*Assumption 3:* During rotation, the pallet (with the shackled bird) swings on the projected X-Z plane. In other words, there is no displacement on the center of mass along the Y-axis.

*Assumption 4:* The segments of the lower extremity are modeled as masses located approximately at their geometrical center.

*Assumption 5:* The effect of the finger forces is modeled as a force and a moment acting at the bird center.

*Assumption 6:* Since Joints  $J_2$  and  $J_3$  are modeled as pin joints, they are extensible in the lengthwise direction in the plan view (Sub-function-2a).

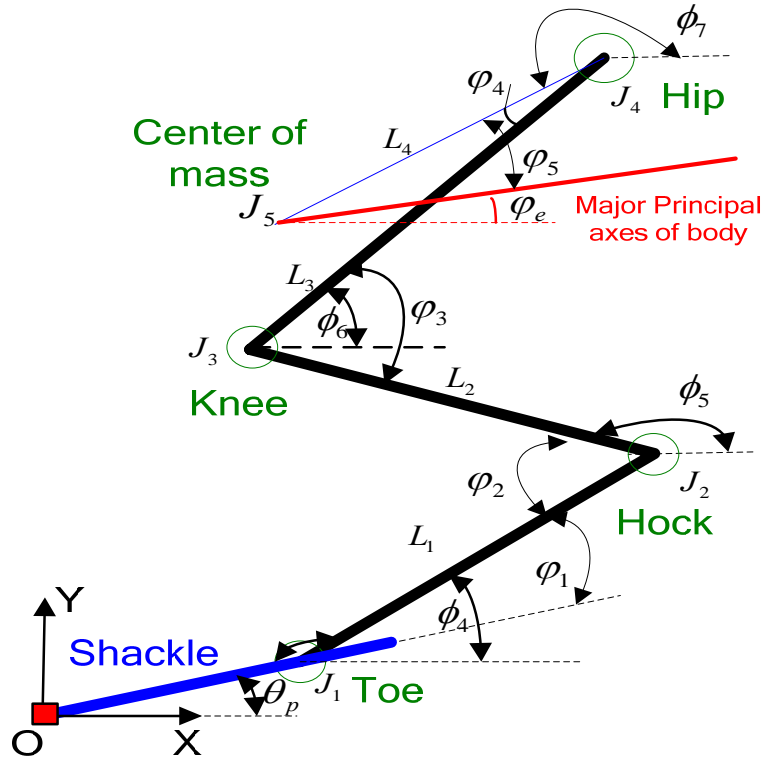


Figure 2-6 Bird leg model (side view)

Figure 2-7 is a projected view on the XZ plane, which illustrates the assumptions and the following angles relating the shackled bird with respect to the shackle:

- $L_b$  is the projected length between the hip joint and the ellipse center; and
- $L_t$  denotes the projected total length of the foot, leg and thigh.
- $\beta_j$  is the angle between the foot and the X-axis;
- $\beta_4$  are angles between  $L_t$  and  $L_b$ ; and
- $\beta_e$  denotes the bird orientation.

The contact kinematic constraints (corresponding to Assumptions 1 and 2) are shown in Figure 2-8, where the angles are defined as follows:

- $\alpha$  is the angle between the line  $J_1J_5$  and the minor axis of ellipse  $b$ ; and
- $\varphi_e$  denotes the bird orientation.

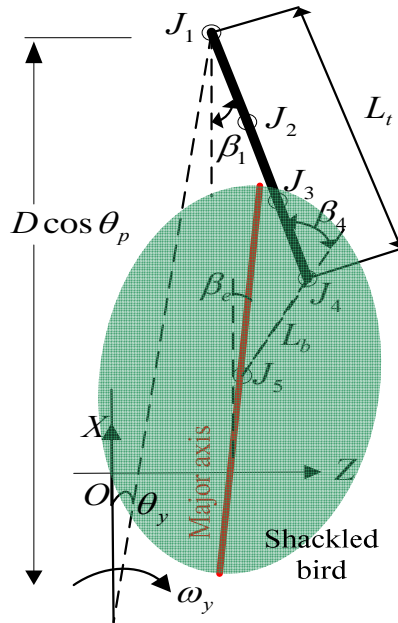


Figure 2-7 Bird leg model (plan view)

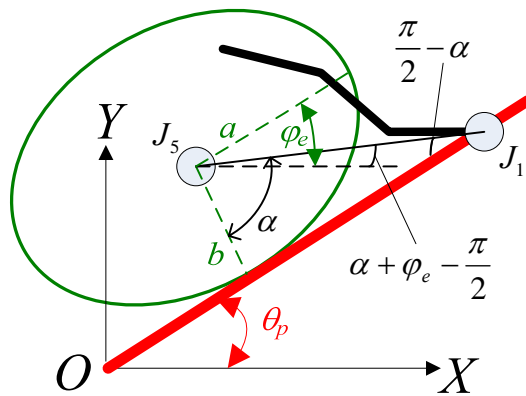


Figure 2-8 Contact kinematic constraints

As the Lagrange formulation requires the derivation of potential and kinetic energies, the position and velocity vectors are defined according on the lumped-parameter assumption in Figure 2-9:

- $m_1, m_2, m_3,$  and  $m_4$  denote the masses of the foot, leg, thigh, body of the bird respectively; and  $m_5$  is the mass of the shackle. For simplicity, we let the total mass and moment of inertia of the bird leg respectively be

$$m_l = m_1 + m_2 + m_3 \text{ and } I_l = I_1 + I_2 + I_3$$

- $P_1, P_2$  and  $P_3$  denote the center of gravity of the respective masses for the foot, leg, thigh respectively;  $P_4$  is the bird center  $J_5$ ; and  $P_5$  is the mass center of the shackle (measured from the origin).
- $I_i$  ( $i=1, \dots, 5$ ) are the moments of inertia about the centroid of the  $i^{\text{th}}$  component.

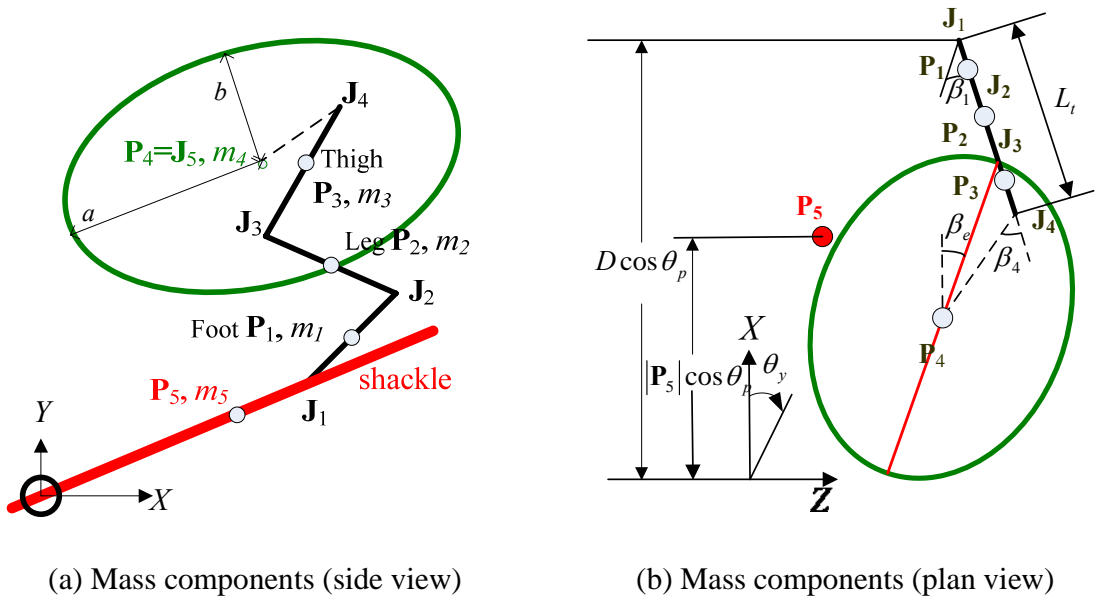


Figure 2-9 Bird mass components

## 2.4 Generalized Coordinates, Constraints and Redundancy

The generalized coordinates of the bird model are defined in Equation (2-1):

$$\mathbf{q} = \left[ \mathbf{J}_1^T \quad \mathbf{J}_5^T \quad \varphi_1 \quad \varphi_2 \quad \varphi_3 \quad \varphi_e \quad \varphi_4 \right]^T \quad (2-1)$$

Although the bird rotates in 3D space, the overall problem is subdivided so that each of the functions can be analyzed in 2D; function 1 and sub-function 2b on the XY plane, and sub-function 2a on the XZ plane. Thus, the equations of motion along with the kinematic constraints of the joints with respect to the shackle can be expressed in 2D. For clarity, the common symbols used and their correspondences in the respective functions are summarized in Table 2-1.

### 2.4.1 Forward Kinematics

Given the defined input  $\theta$ , the toe joint  $\mathbf{J}_1$  has the following form:

$$\mathbf{J}_1 = \begin{bmatrix} D_{c1} \\ D_{s1} \end{bmatrix} = \begin{bmatrix} D_p \cos \theta \\ D_p \sin \theta \end{bmatrix} \quad (2-2)$$

The corresponding joints (hock joint  $\mathbf{J}_2$ , knee joint  $\mathbf{J}_3$ , hip joint  $\mathbf{J}_4$  and bird center  $\mathbf{J}_5$ ) can be expressed using (2-3), where  $i = 1, 2, 3$ , and 4:

$$\mathbf{J}_{i+1} = \mathbf{J}_i + (-1)^{i-1} \mathbf{L}_i \quad (2-3)$$

$$\mathbf{L}_i = \begin{bmatrix} L_{ci} \\ L_{si} \end{bmatrix} = \begin{bmatrix} L_{ip} \cos \phi_{i+3} \\ L_{ip} \sin \phi_{i+3} \end{bmatrix} \quad (2-4)$$

### Position vectors

The position vectors  $\mathbf{P}_1$ ,  $\mathbf{P}_2$  and  $\mathbf{P}_3$  for the foot, leg and thigh are shown below:

$$\mathbf{P}_1 = \begin{bmatrix} P_{1x} \\ P_{1y} \end{bmatrix} = \mathbf{J}_1 + \frac{1}{2} \begin{bmatrix} L_{c1} \\ L_{s1} \end{bmatrix} \quad (2-5)$$

$$\mathbf{P}_n = \mathbf{P}_{n-1} + \frac{1}{2} \sum_{i=n-1}^n (-1)^{i-1} \mathbf{L}_i \quad \text{where } n=2, 3 \quad (2-6)$$

For ease of indexing, we define the position vectors,  $\mathbf{P}_4$  and  $\mathbf{P}_5$ , for the bird center and the shackle in (2-7) and (2-8) respectively:

$$\mathbf{P}_4 = \mathbf{J}_5 \quad (2-7)$$

$$\mathbf{P}_5 = \begin{bmatrix} L_{c\theta} \\ L_{s\theta} \end{bmatrix} = \begin{bmatrix} L_p \cos \theta \\ L_p \sin \theta \end{bmatrix} \quad (2-8)$$

### Velocity vectors

Taking the time derivatives of the position vectors, the velocity vectors for the link components can be given from Equation (2-9) to (2-12):

For  $\mathbf{P}_1$ ,

$$\mathbf{V}_1 = \dot{\mathbf{P}}_1 = \dot{\mathbf{J}}_1 + \frac{\dot{\phi}_4}{2} \begin{bmatrix} -L_{c1} \\ L_{s1} \end{bmatrix} \text{ where } \dot{\mathbf{J}}_1 = \dot{\theta} \begin{bmatrix} -D_{s1} \\ D_{c1} \end{bmatrix} \quad (2-9)$$

For  $\mathbf{P}_2$  and  $\mathbf{P}_3$ ,

$$\mathbf{V}_n = \mathbf{V}_{n-1} + \frac{1}{2} \sum_{i=n-1}^n (-1)^{i-1} \mathbf{V}_{L_i}, \text{ where } \mathbf{V}_{L_i} = \dot{\mathbf{L}}_i = \dot{\phi}_{i+3} \begin{bmatrix} -L_{si} \\ L_{ci} \end{bmatrix} \quad (2-10)$$

For the center of mass  $\mathbf{P}_4 = \mathbf{J}_5$ ,

$$\mathbf{V}_4 = \dot{\mathbf{J}}_1 + \sum_{i=1}^4 (-1)^{i-1} \mathbf{V}_{L_i} \quad (2-11)$$

For the shackle  $\mathbf{P}_5$ ,

$$\mathbf{V}_5 = \dot{\mathbf{P}}_5 = \dot{\theta} \begin{bmatrix} -L_{s\theta} \\ L_{c\theta} \end{bmatrix} \quad (2-12)$$

Table 2-1 Symbols used for the derivation

	Symbol used	F-1 (XY)	SF-2a (XZ)	SF-2b (XY)
<b>Bird</b>	$\varphi_i$ ( $i=1,2,3,4$ )	$\varphi_i$	$\beta_i$	$\varphi_i$
	$\varphi_e$	$\theta_p + \sum_{i=1}^4 (-1)^{i-1} \varphi_i - \varphi_5$	$\theta_y + \beta_1 - \beta_4$	$\theta_p + \sum_{i=1}^4 (-1)^{i-1} \varphi_i - \varphi_5$
	$L_{ip}$ ( $i=1,2,3$ )	$L_i$	$L_i \cos \theta_p$	$L_i$
	$L_{4p}$	$L_4$	$L_b$	$L_4$
	$\phi_n$ ( $n=4, 5, 6$ )	$\theta_p + \sum_{m=1}^{n-3} (-1)^{m-1} \varphi_m$	$\theta_y + \beta_1$	$\theta_p + \sum_{m=1}^{n-3} (-1)^{m-1} \varphi_m$
	$\phi_7$	$\varphi_5 + \varphi_e$	$\beta_e$	$\varphi_5 + \varphi_e$
	$\dot{\phi}_n$ ( $n=4,5,6$ )	$\dot{\theta}_p + \sum_{m=1}^{n-3} (-1)^{m-1} \dot{\varphi}_m$	$\dot{\theta}_y + \dot{\beta}_1$	$\dot{\theta}_p + \sum_{m=1}^{n-3} (-1)^{m-1} \dot{\varphi}_m$
	$\dot{\phi}_7$	$\dot{\theta}_p + \sum_{i=1}^4 (-1)^{i-1} \dot{\varphi}_i$	$\dot{\theta}_y + \dot{\beta}_1 - \dot{\beta}_4$	$\dot{\theta}_p + \sum_{i=1}^4 (-1)^{i-1} \dot{\varphi}_i$
<b>Shackle</b>	$D_p$	$D$	$D \cos \theta_p$	$D$
	$L_p$	$ \mathbf{P}_5 $	$ \mathbf{P}_5  \cos \theta_p$	$ \mathbf{P}_5 $
<b>System input, <math>\theta</math></b>		$0$	$\theta_y$	$\theta_p$
<b>Generalized coordinates</b>	Number	9	7	9
	$\mathbf{q}^T = [q_1 \quad q_2 \quad \dots]$	$J_{1x}, J_{1y}, J_{5x}, J_{5y}$ $\varphi_i$ ( $i=1,2,3$ ), $\varphi_e, \varphi_4$	$J_{1x}, J_{1z}, J_{5x}, J_{5z}$ $\beta_1, \beta_e, \beta_4$	$J_{1x}, J_{1y}, J_{5x}, J_{5y}$ $\varphi_i$ ( $i=1,2,3$ ), $\varphi_e, \varphi_4$
<b>Generalized force <math>\mathbf{Q}^T</math></b>		$Q_3 = F_x; Q_4 = F_y; Q_8 = F_y = M$	[0]	[0]
<b>Constraints</b>	Number	5	5	7
	Equations	(2-13a,b), (2-16a,b)	(2-13a,b), (2-16a,b)	(2-13a,b), (2-14), (2-15), (2-16a,b)
<b>Degrees of freedom</b>		3	2	3
<b>Redundancy</b>		1	0	1

#### 2.4.2 Constraints

With the aid of Figures 2-6 and 2-7, the following kinematic constraints can be obtained from the assumptions made in Section 2.3. From Assumptions 1, we have

$$|\mathbf{J}_1| = D_p \text{ and } \arg(\mathbf{J}_1) = \theta \quad (2-13a,b)$$

Assumption 2 implies that the major axis of the bird and the shackle surface are parallel:

$$|\mathbf{J}_1 - \mathbf{J}_5| \cos \left[ \frac{\pi}{2} - \theta_p + \arg(\mathbf{J}_1 - \mathbf{J}_5) \right] = b \quad (2-14)$$

$$\varphi_e = \theta_p \quad (2-15)$$

The point position and orientation of the serial mechanism are defined by the joint kinematics:

$$\mathbf{P}_4 = \mathbf{J}_5 \text{ and } \varphi_e = \begin{cases} \theta_p + \sum_{i=1}^4 (-1)^{i-1} \varphi_i - \varphi_5 & \text{F-1 and SF-2b} \\ \theta_y + \beta_1 - \beta_4 & \text{SF-2a} \end{cases} \quad (2-16a,b)$$

The above constraints have the form suggested in (3-17):

$$f_\ell(\mathbf{q}, t) = 0 \text{ where } \ell = \begin{cases} 5 & \text{F-1} \\ 5 & \text{SF-2a} \\ 7 & \text{SF-2b} \end{cases} \quad (2-17)$$

where the constraints for each case are summarized in Table 2-1.

#### 2.4.3 Redundancy

As described in the aforementioned subsections, the set of generalized coordinates and constraints are summarized for each of the 2D problems; F1 and SF-2b are on the XY plane and SF-2a on the XZ plane. For a typical 2D problem, there are generally three degrees of freedom (DOF), two translational and one rotational freedom.

For F-1, there are 9 generalized coordinates and 5 constraints. The degree of mobility is four, which is larger than the DOF of three. That means, one degree of redundancy exists in this system. A common approach is to reduce the number of variables. Alternatively, it can be solved by transforming this problem into a constrained linear optimization problem. In this thesis, the solution to this redundancy problem is to determine the unique leg position that is physical realizable.

For SF-2a, there are 7 generalized coordinates and 5 constraints. Obviously, this bird model is over constrained; hence, no redundancy will exist in the model and there are only two DOF.

For SF-2b, there are 9 generalized coordinates. When the bird body is no contact with the shackle, as F-1 there are 5 constraints and one degree of redundancy. Once the bird body is in contact with the shackle, two additional constraints are imposed according to *Assumption 2* and hence the system is over constrained reducing the DOF to 2 (with no redundancy as in SF-2a).

## 2.5 Summary

This chapter presented an overview of the Live Bird Transfer System. Specifically three sub-functions have been described for bird shackling; the first supports the bird body; the second rotates the pallet out of shackling area; and the third inverts the pallet. Six assumptions are made for the subsequent formulations to simplify the relationship among the bird, the shackle, and the effects of the finger force so that the analyses in 3D space can be reduced to multiple 2D problems and solved using a lumped parameter approach. The generalized coordinates, joint kinematics and constraint equations for formulating the bird motion have been described. Nine generalized coordinates are selected in order to analyze the force/moment acting between the toe joint and the shackle, the leg kinematics and the body position/orientation. The effects of assumptions and constraints imposed on the number of degrees of freedom and redundancy are summarized in Table 2-1.

# CHAPTER 3

## DYNAMIC MODELING

### 3.1 Introduction

This chapter formulates the dynamics of three functions F-1, SF-2a and SF-2b using the Lagrange method and is organized as follows. The chapter starts with a general formulation of constrained Lagrange equations of motion in terms of system energies of kinetics, potential and dissipation subject to the external forces and constraints. Next, the associated inertia and Jacobian matrices, along with system forces including non-constrained and constrained forces, are derived. This is followed by illustrating the numerical algorithm that solves the equations of motion with two examples. Results are compared against those obtained using finite element analysis (FEA) for verification.

### 3.2 Lagrange Equations of Motion

Given the generalized external force  $\mathbf{Q}$  in Table 2-1, the Lagrange's formula for the equation of motion augmented by the Jacobian matrix  $[a(\mathbf{q})]$  and Lagrange multiplier vector  $\boldsymbol{\lambda}$  to account for the contributions from the constrained equations is given by

Equation (3-1):

$$\frac{d}{dt} \left( \frac{\partial T}{\partial \dot{\mathbf{q}}} \right) - \frac{\partial (T - V)}{\partial \mathbf{q}} + \frac{\partial D_r}{\partial \dot{\mathbf{q}}} = \mathbf{Q} + [a(\mathbf{q})]^T \boldsymbol{\lambda} \quad (3-1)$$

In Equation (3-1),  $T(\mathbf{q}, \dot{\mathbf{q}})$  and  $V(\mathbf{q})$  are the kinetic and potential energies respectively; and  $D_r$  is the Raleigh dissipation function modeling the damper characteristics. These energy terms are given by (3-2a) – (3-2c):

$$T = \frac{1}{2} \sum_{i=1}^5 m_i |\mathbf{V}_i|^2 + \frac{1}{2} \left( \sum_{i=1}^3 (I_i \dot{\phi}_i^2) + I_4 \dot{\phi}_e^2 + I_5 \dot{\theta}^2 \right) \quad (3-2a)$$

$$V = \sum_{i=1}^5 m_i g P_{iY} + \frac{1}{2} \sum_{i=1}^4 k_i (\phi_i - \phi_{i,0})^2 \quad (3-2b)$$

$$D_r = \sum_{i=1}^4 \frac{1}{2} b_i \dot{\phi}_i^2 \quad (3-2c)$$

In Equations (3-2b,c), the equivalent torsion spring and damping constants at the  $i^{\text{th}}$  joint of the bird ( $k_i$  and  $b_i$  respectively) are experimentally determined in [Shumway, 2002]; and  $\phi_{i,0}$  are the equilibrium angle of the  $i^{\text{th}}$  joint.

The first term in Equation (3-1) can be expressed as

$$\frac{d}{dt} \left( \frac{\partial T}{\partial \dot{\mathbf{q}}} \right) = \mathbf{M}(\mathbf{q}) \ddot{\mathbf{q}} + \dot{\mathbf{M}}(\mathbf{q}) \dot{\mathbf{q}} \quad (3-3)$$

where  $\mathbf{M}(\mathbf{q})$  is the inertia matrix, and since the terms  $\dot{\mathbf{M}}(\mathbf{q}) \dot{\mathbf{q}}$  in (3-3) and  $\partial T / \partial \mathbf{q}$  in Equation (3-1) are both quadratic in the generalized velocities  $\dot{\mathbf{q}}$  with coefficients that depends on generalized coordinates  $\mathbf{q}$ , Equation (3-3) can be rewritten as

$$\mathbf{M}(\mathbf{q}) \ddot{\mathbf{q}} + [-a(\mathbf{q})]^T \boldsymbol{\lambda} = \mathbf{Q} - \mathbf{F}(\mathbf{q}, \dot{\mathbf{q}}) \quad (3-4)$$

where

$$\mathbf{F}(\mathbf{q}, \dot{\mathbf{q}}) = \mathbf{C}(\mathbf{q}) \dot{\mathbf{q}} + \frac{\partial V}{\partial \mathbf{q}} + \frac{\partial D}{\partial \dot{\mathbf{q}}} \quad (3-4a)$$

$$\mathbf{C}(\mathbf{q}) \dot{\mathbf{q}} = \dot{\mathbf{M}}(\mathbf{q}) \dot{\mathbf{q}} - \frac{\partial T}{\partial \mathbf{q}} \quad (3-4b)$$

and

$$[a(\mathbf{q})]^T \boldsymbol{\lambda} = \mathbf{F}_c \quad (3-4c)$$

Equations (3-4a, b, c) define the non-constrained force  $\mathbf{F}(\mathbf{q}, \dot{\mathbf{q}})$ , the Centrifugal-Coriolis, and the constraint forces respectively.

In Equation (3-4), there are  $n$  equations with  $(n+m)$  unknowns, which are  $n$  elements of the vector  $\ddot{\mathbf{q}}$  and  $m$  elements of the vector  $\boldsymbol{\lambda}$ . Additional acceleration

kinematic constraint equations can be obtained by differentiating Equation (2-17) twice with respect to time leading to  $m$  number of ODEs in Equation (3-5):

$$-[a(\mathbf{q})]\ddot{\mathbf{q}} = [\dot{a}(\mathbf{q})]\dot{\mathbf{q}} \quad (3-5)$$

The combined Equations (3-1) and (3-5) form a system of  $(n + m)$  augmented equations of motion with  $(n + m)$  unknowns:

$$\begin{bmatrix} \mathbf{M}(\mathbf{q}) & -[a(\mathbf{q})]^T \\ -[a(\mathbf{q})] & [0] \end{bmatrix} \begin{bmatrix} \ddot{\mathbf{q}} \\ \lambda \end{bmatrix} = \begin{bmatrix} \mathbf{Q} - \mathbf{F}(\mathbf{q}, \dot{\mathbf{q}}) \\ [a(\mathbf{q})]\dot{\mathbf{q}} \end{bmatrix} \quad (3-6)$$

which can be simultaneously solved for the acceleration and Lagrange multipliers:

$$\begin{bmatrix} \ddot{\mathbf{q}} \\ \lambda \end{bmatrix} = \begin{bmatrix} \mathbf{M}(\mathbf{q}) & -[a(\mathbf{q})]^T \\ -[a(\mathbf{q})] & [0] \end{bmatrix}^{-1} \begin{bmatrix} \mathbf{Q} - \mathbf{F}(\mathbf{q}, \dot{\mathbf{q}}) \\ [a(\mathbf{q})]\dot{\mathbf{q}} \end{bmatrix} \quad (3-7)$$

The solution to Equation (3-7) requires the kinematic constraints expressed in the form of a Jacobian:

$$[a(\mathbf{q})] = \begin{bmatrix} \frac{\partial f_1}{\partial q_1} & \dots & \frac{\partial f_1}{\partial q_n} \\ \vdots & & \vdots \\ \frac{\partial f_\ell}{\partial q_1} & \dots & \frac{\partial f_\ell}{\partial q_n} \end{bmatrix} \quad (3-8)$$

where  $\ell$  is the number of the constrained equations  $f_i(\mathbf{q}, t)$  in Equation (2-17).

Inertia matrix

As seen from the definition in Equation (3-3), the inertia matrix  $[\mathbf{M}]$  is square and symmetric. Since the kinetic energy  $T$  in Equation (3-2a) is independent of the last generalized coordinate  $\varphi_4$ , the elements of the last row and last column of the inertia matrix  $[\mathbf{M}]$  are zeros. Hence,  $[\mathbf{M}]$  is a positive semi-definite matrix and has the following form:

$$[\mathbf{M}] = \begin{bmatrix} \mathbf{M}_1 & \mathbf{M}_2 & \mathbf{M}_3 \\ \mathbf{M}_4 & \mathbf{M}_5 & \mathbf{M}_6 \\ \mathbf{M}_7 & \mathbf{M}_8 & \mathbf{M}_9 \end{bmatrix} \quad \text{where } [\mathbf{M}] \in \begin{cases} \mathbf{R}^{9 \times 9} & \text{F-1} \\ \mathbf{R}^{7 \times 7} & \text{SF-2a} \\ \mathbf{R}^{9 \times 9} & \text{SF-2b} \end{cases} \quad (3-9)$$

In (3-9), the sub-matrix  $\mathbf{M}_{ij}$  ( $i, j=1, 2, 3$ ) corresponding to F-1, SF-2a and SF2b are defined in Table 3-1.

In Table 3-1, the elements in  $\mathbf{M}_2$  for F-1 and F-2b (XY plane) are given below:

$$M_{15} = \frac{1}{2} \sum_{i=1}^3 [(-1)^i m_i L_{si}] - (m_2 + m_3) L_{s1} + m_3 L_{s2} \quad M_{16} = \frac{1}{2} \sum_{i=2}^3 [(-1)^{i-1} m_i L_{si}] - m_3 L_{s2} \quad M_{17} = -\frac{1}{2} m_3 L_{s3}$$

$$M_{25} = \frac{1}{2} \sum_{i=1}^3 [(-1)^{i-1} m_i L_{ci}] - (m_2 + m_3) L_{c1} + m_3 L_{c2} \quad M_{26} = \frac{1}{2} \sum_{i=2}^3 [(-1)^i m_i L_{ci}] - m_3 L_{c2} \quad M_{27} = \frac{1}{2} m_3 L_{c3}$$

As shown in Table 3-1,  $\mathbf{M}_5$  is symmetric; and is a scalar element for SF-2a. Thus, only six elements in  $\mathbf{M}_5$  for F-1 and SF-2b are needed as given below:

$$M_{55} = \frac{1}{4} \sum_{i=1}^3 [m_i L_i^2] + (m_2 + m_3) L_1^2 + m_3 L_2^2 - (m_2 + 2m_3) L_1 L_2 \cos \varphi_2 + m_3 L_3 [L_1 \cos(\varphi_2 - \varphi_3) - L_2 \cos \varphi_3] + \sum_{i=1}^3 I_i$$

$$M_{56} = -\frac{1}{4} \sum_{i=2}^3 [m_i L_i^2] - m_3 L_2^2 + \frac{1}{2} (m_2 + 2m_3) L_1 L_2 \cos \varphi_2 - m_3 L_3 \left[ \frac{1}{2} L_1 \cos(\varphi_2 - \varphi_3) - L_2 \cos \varphi_3 \right] - \sum_{i=2}^3 I_i$$

$$M_{57} = \frac{1}{4} m_3 L_3^2 + \frac{1}{2} m_3 L_3 [L_1 \cos(\varphi_2 - \varphi_3) - L_2 \cos \varphi_3] + I_3$$

$$M_{66} = \frac{1}{4} \sum_{i=2}^3 [m_i L_i^2] + m_3 L_2^2 - m_3 L_2 L_3 \cos \varphi_3 + \sum_{i=2}^3 I_i$$

$$M_{67} = \frac{1}{2} m_3 L_2 L_3 \cos \varphi_3 - \frac{1}{4} m_3 L_3^2 - I_3$$

$$M_{77} = \frac{1}{4}m_3L_3^2 + I_3$$

Table 3-1 Inertia matrix properties

F-1 and F-2b (XY plane)		
$\mathbf{M}_1 = \text{diag}[m_\ell \quad m_\ell \quad m_4 \quad m_4]$ where $m_\ell = m_1 + m_2 + m_3$	$\mathbf{M}_2 = \begin{bmatrix} M_{15} & M_{16} & M_{17} \\ M_{25} & M_{26} & M_{27} \\ [0]_{2 \times 3} \end{bmatrix}$	$\mathbf{M}_3 = [0]_{4 \times 2}$
$\mathbf{M}_4 = \mathbf{M}_2^T$	$\mathbf{M}_5 = \begin{bmatrix} M_{55} & M_{56} & M_{57} \\ M_{56} & M_{66} & M_{67} \\ M_{57} & M_{67} & M_{77} \end{bmatrix}$	$\mathbf{M}_6 = [0]_{3 \times 2}$
$\mathbf{M}_7 = [0]_{2 \times 4}$	$\mathbf{M}_8 = [0]_{2 \times 3}$	$\mathbf{M}_9 = \begin{bmatrix} I_4 & 0 \\ 0 & 0 \end{bmatrix}$
F-2a (XZ plane)		
$\mathbf{M}_1$	$\mathbf{M}_2 = \begin{bmatrix} \frac{1}{2} \sum_{i=1}^3 m_i L_{si} \\ -\frac{1}{2} \sum_{i=1}^3 m_i L_{ci} \\ [0]_{2 \times 1} \end{bmatrix}$	$\mathbf{M}_3$
$\mathbf{M}_4 = \mathbf{M}_3^T = [0]_{2 \times 4}$	$\mathbf{M}_5 = \frac{1}{4} \sum_{i=1}^3 m_i \left( \sum_{i=1}^3 L_{ip} \right)^2 + \sum_{i=1}^3 I_{ip}$	$\mathbf{M}_6 = [0]_{1 \times 2}$
$\mathbf{M}_7$	$\mathbf{M}_8 = [0]_{2 \times 1}$	$\mathbf{M}_9$

Jacobian matrix

Since the constrained equations (Chapter 2) depend only on positions, they are holonomic constraints. The Jacobian matrix can be obtained by taking the partial derivatives of Equations (2-13) to (2-16) with respect to each of the generalized coordinates. As shown in Table 2-1, F-1 and SF-2a each has 5 constraints and SF-2b has 7 constraints. The Jacobian matrices have the following forms:

$$[a(\mathbf{q})] = \begin{bmatrix} \mathbf{a}_1 & \mathbf{a}_2 \\ \mathbf{a}_3 & \mathbf{a}_4 \end{bmatrix}_{\text{SF-2a}}^{\text{F-1}} \quad \text{and} \quad [a(\mathbf{q})] = \begin{bmatrix} \mathbf{a}_1 & \mathbf{a}_2 \\ \mathbf{a}_3 & \mathbf{a}_4 \\ \mathbf{a}_5 & \mathbf{a}_6 \end{bmatrix}_{\text{SF-2b}} \quad \text{where} \quad [a(\mathbf{q})] \in \begin{cases} \mathbf{R}^{5 \times 9} & \text{F-1} \\ \mathbf{R}^{5 \times 7} & \text{SF-2a} \\ \mathbf{R}^{7 \times 9} & \text{SF-2b} \end{cases} \quad (3-10)$$

where the sub-matrices are defined under different functions, as listed in Table 3-2. The elements of  $\mathbf{a}_5$  in Table 3-2 are given below:

$$a_{61} = \frac{J_{15x}}{|\mathbf{J}_{15}|} S_{\theta_p} + \frac{J_{15y}}{|\mathbf{J}_{15}|} C_{\theta_p} \quad a_{62} = \frac{J_{15y}}{|\mathbf{J}_{15}|} S_{\theta_p} - \frac{J_{15x}}{|\mathbf{J}_{15}|} C_{\theta_p} \quad a_{63} = -\frac{J_{15x}}{|\mathbf{J}_{15}|} S_{\theta_p} - \frac{J_{15y}}{|\mathbf{J}_{15}|} C_{\theta_p} \quad a_{64} = -\frac{J_{15y}}{|\mathbf{J}_{15}|} S_{\theta_p} + \frac{J_{15x}}{|\mathbf{J}_{15}|} C_{\theta_p}$$

$$a_{71} = -\frac{bJ_{15x} + J_{15y}S}{|\mathbf{J}_{15}|^2 S} \quad a_{72} = \frac{-bJ_{15y} + J_{15x}S}{|\mathbf{J}_{15}|^2 S} \quad a_{73} = \frac{bJ_{15x} + J_{15y}S}{|\mathbf{J}_{15}|^2 S} \quad a_{74} = \frac{b(J_{15y} - J_{15x}S)}{|\mathbf{J}_{15}|^2 S}$$

where  $J_{15x} = J_{1x} - J_{5x}$ ;  $J_{15y} = J_{1y} - J_{5y}$ ;  $\mathbf{J}_{15} = \mathbf{J}_1 - \mathbf{J}_5$ ;  $S_{\theta_p} = \sin[\theta_p - \arg(\mathbf{J}_{15})]$ ;

$C_{\theta_p} = \cos[\theta_p - \arg(\mathbf{J}_{15})]$ ; and  $S = \sqrt{4|\mathbf{J}_{15}|^2 - b^2}$ .

Table 3-2 Jacobian sub-matrices

<b>F-1 and SF-2b</b> (XY plane, 9 generalized coordinates)	
$\mathbf{a}_1 = \begin{bmatrix} 2J_{1x} & 2J_{1y} \\ -J_{1y}/ \mathbf{J}_1 ^2 & -J_{1x}/ \mathbf{J}_1 ^2 \end{bmatrix}$	$\mathbf{a}_2 = [0]_{2 \times 7}$
$\mathbf{a}_3 = \begin{bmatrix} [\mathbf{I}]_{2 \times 2} & -[\mathbf{I}]_{2 \times 2} \\ [0]_{1 \times 4} & \end{bmatrix}$	$\mathbf{a}_4 = \begin{bmatrix} -L_{s1} + L_{s2} - L_{s3} & -L_{s2} + L_{s3} & -L_{s3} & L_{s4} & 0 \\ L_{c1} - L_{c2} + L_{c3} & L_{c2} - L_{c3} & L_{c3} & -L_{c4} & 0 \\ 1 & -1 & 1 & -1 & -1 \end{bmatrix}$
$\mathbf{a}_5 = \begin{bmatrix} a_{61} & a_{62} & a_{63} & a_{64} \\ a_{71} & a_{72} & a_{73} & a_{74} \end{bmatrix}$	$\mathbf{a}_6 = \begin{bmatrix} 0 & 0 \\ [0]_{2 \times 3} & -1 & 0 \end{bmatrix}$
<b>SF-2a</b> (XZ plane, 7 generalized coordinates)	
$\mathbf{a}_1$ with $J_{1y}$ replaced $J_{1z}$	$\mathbf{a}_2 = [0]_{2 \times 5}$
$\mathbf{a}_3 = \begin{bmatrix} [\mathbf{I}]_{2 \times 2} & -[\mathbf{I}]_{2 \times 2} \\ [0]_{1 \times 4} & \end{bmatrix}$	$\mathbf{a}_4 = \begin{bmatrix} L_{s1} + L_{s2} + L_{s3} & L_{s4} & 0 \\ -(L_{c1} + L_{c2} + L_{c3}) & -L_{c4} & 0 \\ -1 & 1 & 1 \end{bmatrix}$

### 3.3 System Forces

The solution to the Lagrange equation of motion requires the derivation of the non-constrained force  $\mathbf{F}(\mathbf{q}, \dot{\mathbf{q}})$  in addition to the specification of the generalized forces  $\mathbf{Q}$ . Once the generalized coordinates and the Lagrange multipliers are solved, the constrained forces can be calculated from  $\mathbf{F}_c = [a(\mathbf{q})]^T \boldsymbol{\lambda}$ . As shown in Figure 3-1,  $\tau_{zi}$  (where  $i=1,2,3,4$ ) denotes for the constrained torque on the  $i^{\text{th}}$  joint angle  $\phi_i$ ;  $F_{c1x}$  and  $F_{c1y}$  are the constrained force on  $J_1$  imposed by the shackle;  $F_{J5C}$  and  $M_c$  are the constrained force and moment on the bird body center, accounting for the net force and moment respectively.

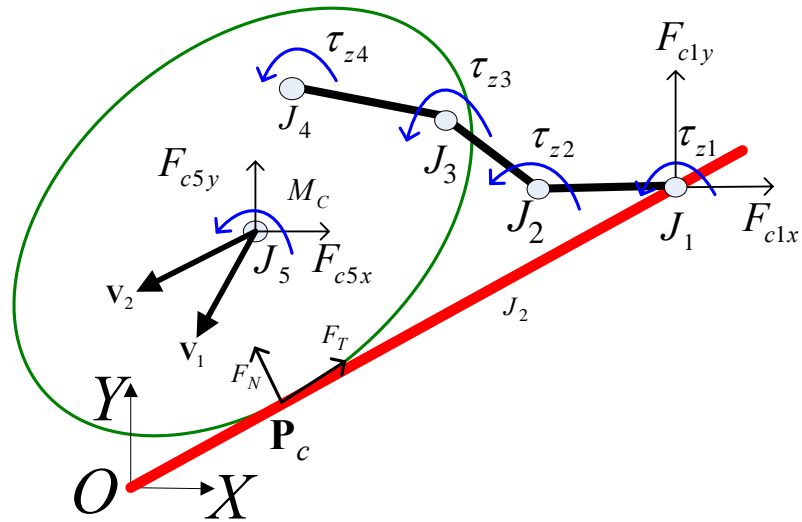


Figure 3-1 Free body diagram of impulse force analysis

#### Non-constrained forces

The non-constrained forces are categorized into different functions in Table 3-3.

For F-1 and SF-2b, the X and Y components of the force at Joint 1 are given by (3-11a, b)

where  $m_a = \frac{1}{2} m_1 + m_2 + m_3$ , and  $\dot{\phi}_{12} = \dot{\phi}_1 - \dot{\phi}_2$ .

$$F_{1x} = -m_a L_{c1} \dot{\varphi}_1 \dot{\varphi}_4 + \frac{1}{2} m_2 L_{c2} (\dot{\varphi}_{12} + \dot{\theta}_p) \dot{\varphi}_{12} + m_3 L_{c2} [\dot{\varphi}_{12} (\dot{\varphi}_1 + \dot{\theta}_p) - \dot{\varphi}_1 \dot{\varphi}_2] - m_3 L_{c3} \left[ \frac{1}{2} \dot{\varphi}_{12} (\dot{\varphi}_{12} + \dot{\theta}_p) + \dot{\varphi}_3 \left( \frac{1}{2} \dot{\varphi}_3 + \dot{\varphi}_{12} + \frac{1}{2} \dot{\theta}_p \right) \right] \quad (3-11a)$$

$$F_{1y} = -m_a L_{s1} \dot{\varphi}_1 \dot{\varphi}_4 + \frac{1}{2} m_2 L_{s2} (\dot{\varphi}_{12} + \dot{\theta}_p) \dot{\varphi}_{12} + m_3 L_{s2} [\dot{\varphi}_{12} (\dot{\varphi}_1 + \dot{\theta}_p) - \dot{\varphi}_1 \dot{\varphi}_2] - m_3 L_{s3} \left[ \frac{1}{2} \dot{\varphi}_{12} (\dot{\varphi}_{12} + \dot{\theta}_p) + \dot{\varphi}_3 \left( \frac{1}{2} \dot{\varphi}_3 + \dot{\varphi}_{12} + \frac{1}{2} \dot{\theta}_p \right) \right] + m_l g \quad (3-11b)$$

Table 3-3 Non-constrained forces

	F-1 and F-2b	F-2a
$\mathbf{F}_{J1}$	$\begin{bmatrix} F_{1x} & F_{1y} \end{bmatrix}^T$	$\left[ \frac{1}{2} \sum_{i=1}^3 m_i \dot{\beta}_1 \dot{\varphi}_{i+3} L_{ci} \quad \frac{1}{2} \sum_{i=1}^3 m_i \dot{\beta}_1 \dot{\varphi}_{i+3} L_{si} \right]^T$
$\mathbf{F}_{J5}$	$\begin{bmatrix} 0 & m_4 g \end{bmatrix}^T$	$\begin{bmatrix} \frac{\sqrt{3}}{3} m_4 g & 0 \end{bmatrix}^T$
$T_e$	0	0
$T_i$ where $i=1, 2, 3, 4$	$T_{z1}, T_{z2}, T_{z3}, T_{z4}$	$T_{y1}, T_{y2} = T_{y3} = 0, T_{y4}$

The non-constrained moment  $T_i$  on the bird joint angles  $\varphi_i (i = 1, 2, 3, 4)$  are given

by Equations (3-12) to (3-17), where  $m_b = \frac{1}{2} m_2 + m_3$ ;  $\varphi_{23} = \varphi_2 - \varphi_3$ ; and  $\dot{\varphi}_{23} = \dot{\varphi}_2 - \dot{\varphi}_3$ .

$$T_{z1} = \frac{g}{2} \sum_{i=1}^3 (-1)^{i-1} m_i L_{ci} + (m_2 + m_3) g L_{c1} - m_3 g L_{c2} + \left[ m_a (L_{c1} \dot{J}_{1x} + L_{s1} \dot{J}_{1y}) - m_b (L_{c2} \dot{J}_{1x} + L_{s2} \dot{J}_{1y}) + \frac{1}{2} m_3 (L_{c3} \dot{J}_{1x} - L_{s3} \dot{J}_{1y}) \right] \dot{\theta}_p + (m_2 + 2m_3) L_1 L_2 \sin \varphi_2 \left( \dot{\varphi}_1 - \frac{1}{2} \dot{\varphi}_2 + \dot{\theta}_p \right) \dot{\varphi}_2 + m_3 L_2 L_3 \sin \varphi_3 \left( \dot{\varphi}_{12} + \frac{1}{2} \dot{\varphi}_3 + \dot{\theta}_p \right) \dot{\varphi}_3 + m_3 L_1 L_3 \sin \varphi_{23} \left[ \frac{1}{2} (\dot{\varphi}_2^2 + \dot{\varphi}_3^2) - (\dot{\varphi}_1 + \dot{\theta}_p) \dot{\varphi}_{23}^2 \right] + k_{1z} (\varphi_1 - \varphi_{1,0}) + b_{1z} \dot{\varphi}_1 \quad (3-12)$$

$$\begin{aligned}
T_{z2} = & m_b g L_{c2} - \frac{1}{2} m_3 g L_{c3} + \left[ m_b (L_{c2} \dot{J}_{1x} + L_{s2} \dot{J}_{1y}) - \frac{1}{2} m_3 (L_{c3} \dot{J}_{1x} + L_{s3} \dot{J}_{1y}) \right] \dot{\theta}_p \\
& - m_b L_1 L_2 \sin \varphi_2 (\dot{\varphi}_1 + \dot{\theta}_p)^2 - m_3 L_2 L_3 \sin \varphi_3 \left( \frac{1}{2} \dot{\varphi}_3 + \dot{\theta}_p + \dot{\varphi}_{12} \right) \dot{\varphi}_3 + m_3 L_1 L_3 \sin \varphi_{23} (\dot{\varphi}_1 + \dot{\theta}_p)^2 \\
& + k_{2z} (\varphi_2 - \varphi_{2,0}) + b_{2z} \dot{\varphi}_2
\end{aligned} \tag{3-13}$$

$$\begin{aligned}
T_{z3} = & \frac{1}{2} m_3 g L_{c3} + \frac{1}{2} m_3 (L_{c3} \dot{J}_{1x} + L_{s3} \dot{J}_{1y}) \dot{\theta}_p + m_3 L_2 L_3 \sin \varphi_3 \left[ -\frac{1}{2} \dot{\varphi}_{12}^2 - \dot{\theta}_p \left( \frac{1}{2} \dot{\theta}_p + \dot{\varphi}_{12} \right) \right] \\
& - \frac{1}{2} m_3 L_{13} \sin \varphi_{23} (\dot{\varphi}_1 + \dot{\theta}_p)^2 + k_{3z} (\varphi_3 - \varphi_{3,0}) + b_{3z} \dot{\varphi}_3
\end{aligned} \tag{3-14}$$

$$T_{z4} = k_{4z} (\varphi_4 - \varphi_{4,0}) + b_{4z} \dot{\varphi}_4 \tag{3-15}$$

For F-2a, non-constrained forces on bird joint angles are given from Equation (3-16) to (3-17):

$$T_{y1} = -\frac{1}{2} \sum_{i=1}^3 m_i L_{ci} \dot{J}_{1x} \dot{\theta}_y - \frac{1}{2} \sum_{i=1}^3 m_i L_{si} \dot{J}_{1z} \dot{\theta}_y + k_{1y} (\beta_1 - \beta_{1,0}) + b_{1y} \dot{\beta}_1 \tag{3-16}$$

$$T_{y4} = k_{4y} (\beta_4 - \beta_{4,0}) + b_{4y} \dot{\beta}_4 \tag{3-17}$$

### Constrained forces

From the solutions to the constrained Lagrange equation of motion, the resulting constrained forces/torques  $\mathbf{F}_c = [a(\mathbf{q})]^T \boldsymbol{\lambda}$  (in X and Y global coordinates) can be derived, which have been summarized in Table 3-4. With the automated live-bird transfer application in mind, the following information is of particular interest:

- In addition to the joint torque  $\tau_l$ , the constrained force  $\mathbf{F}_{c1}$  imposed at the toe between Joint J<sub>1</sub> and the shackle resolved into two components; parallel with and perpendicular to the shackle plane. This constrained force provides a basis to design the foot-grippers on the shackling mechanism to prevent damaging the bird legs during the handling processes.

- The constrained force  $\mathbf{F}_{c5}$  and moment  $M_c$  imposed at the center (or Joint  $J_5$ ) by the (external) generalized force/moment. This constrained force and moment provide intuitive insights to the effects of the operating finger speed (and thus the exit momentum) on the center and orientation of the bird body.
- The constrained moment  $\tau_i$  at the hock, knee and hip joints ( $J_2$ ,  $J_3$  and  $J_3$ ), which are the torques manipulating the bird legs.

Table 3-4 Constrained forces

	<b>F-1 and F-2b (XY-plane)</b>	<b>F-2a (XZ-plane)</b>
$\mathbf{F}_{JIC},$	$\mathbf{F}_{c1} = \begin{bmatrix} 2J_{1x}\lambda_1 - \frac{J_{1y}}{ \mathbf{J}_1 ^2}\lambda_2 + \lambda_3 \\ 2J_{1y}\lambda_1 + \frac{J_{1x}}{ \mathbf{J}_1 ^2}\lambda_2 + \lambda_4 \end{bmatrix}$ $\tau_{z1} = \lambda_3 \sum_{i=1}^3 (-1)^i L_{si} + \lambda_4 \sum_{i=1}^3 (-1)^{i-1} L_{ci} + \lambda_5$	$\mathbf{F}_{c1} = \begin{bmatrix} 2J_{1x}\lambda_1 - \frac{J_{1z}}{ \mathbf{J}_1 ^2}\lambda_2 + \lambda_3 \\ 2J_{1z}\lambda_1 + \frac{J_{1x}}{ \mathbf{J}_1 ^2}\lambda_2 + \lambda_4 \end{bmatrix}$ $\tau_{y1} = \lambda_3 \sum_{i=1}^3 L_{si} - \lambda_4 \sum_{i=1}^3 L_{ci} - \lambda_5$
$\mathbf{F}_{J5C}, M_{5C}$	$\mathbf{F}_{c5} = \begin{bmatrix} -\lambda_3 \\ -\lambda_4 \end{bmatrix}$ $M_{c5} = L_{s4}\lambda_3 - L_{c4}\lambda_4 - \lambda_5$	$\mathbf{F}_{c5} = \begin{bmatrix} -\lambda_3 \\ -\lambda_4 \end{bmatrix}$ $M_{c5} = L_{s4}\lambda_3 - L_{c4}\lambda_4 + \lambda_5$
$\tau_i$ where $i=2, 3, 4$	$\tau_{z2} = \lambda_3 \sum_{i=2}^3 (-1)^{i-1} L_{si} + \lambda_4 \sum_{i=2}^3 (-1)^i L_{ci} - \lambda_5$ $\tau_{z3} = -L_{s3}\lambda_3 + L_{c3}\lambda_4 + \lambda_5$ $\tau_{z4} = -\lambda_5$	$\tau_{y2} = 0$ $\tau_{y3} = 0$ $\tau_{y4} = -\lambda_5$

### Force prediction at contact

For F-1 and SF-2b, the bird experiences impulsive force acting on its body when it rotates onto the shackle surface as seen from Figure 3-1, which is resolved into two components ( $F_T$  and  $F_N$ ) in the directions parallel and perpendicular to the shackle surface respectively. In Figure 3-1,  $\mathbf{P}_c$  is the contact point; and  $F_N$  and  $F_T$  denote for the normal

force and tangential force required overcoming the friction. From the Newton's second law, we have

$$\mathbf{F}\Delta t \approx m\mathbf{v}_2 - m\mathbf{v}_1 \quad (3-18a)$$

where  $\mathbf{v}_1$  and  $\mathbf{v}_2$  are the velocities before and after the contact respectively. The direction and magnitude of the initial velocity  $\mathbf{v}_1$  can be determined from the Lagrange equation of motion before contact. Since after the contact, the body slides along the shackle surface but not roll, hence the net moment on the bird center is zero.

$$F_T b - F_{c1x}(J_{4y} - J_{5y}) + F_{c1y}(J_{4x} - J_{5x}) + M_c + \tau_{z1} + \tau_{z2} + \tau_{z3} + \tau_{z4} = 0 \quad (3-18b, c)$$

$$\text{where } F_T = \mu F_N$$

where  $\mu$  is the friction coefficient between the bird body and the shackle. Therefore, from (3-18b, c), unknowns  $F_T$  and  $F_N$  can be solved. Then another two unknowns ( $\Delta t$  and  $\mathbf{v}_2$ ) can be solved simultaneously from Equations (3-18a) upon getting  $F_T$  and  $F_N$ .

### 3.4 Numerical Algorithm

The equation of motion in Equation (3-7) is solved numerically using a three-module algorithm written in MATLAB:

- The *first* module defines the system parameters and initial conditions.
- The *second* module is the numerical ODE solver.
- The *third* module is post processing for the joint coordinates and constrained forces.

Figure 3-2 shows the simulation flowchart illustrating the relationships among the modules.

System parameters and initial conditions

The system parameters are the constants used in the algorithm, most of which have been introduced in Chapter 2. Then the parameter vector  $\mathbf{P}$  is defined for all functions, as shown below:

$$\mathbf{P} = \left[ \underbrace{L_p, D_p, m_5}_{shackle}; \underbrace{a, b, c, m_4, L_4, \phi_5}_{bird\ body}; \underbrace{m_1, m_2, m_3, L_1, L_2, L_3}_{bird\ leg}; \underbrace{k_i, b_i}_{joint}; t_{max}, h \right] \quad (3-19)$$

where  $t_{max}$  is the total time for each simulation; and  $h$  is the incremental time step defined for both simulations.

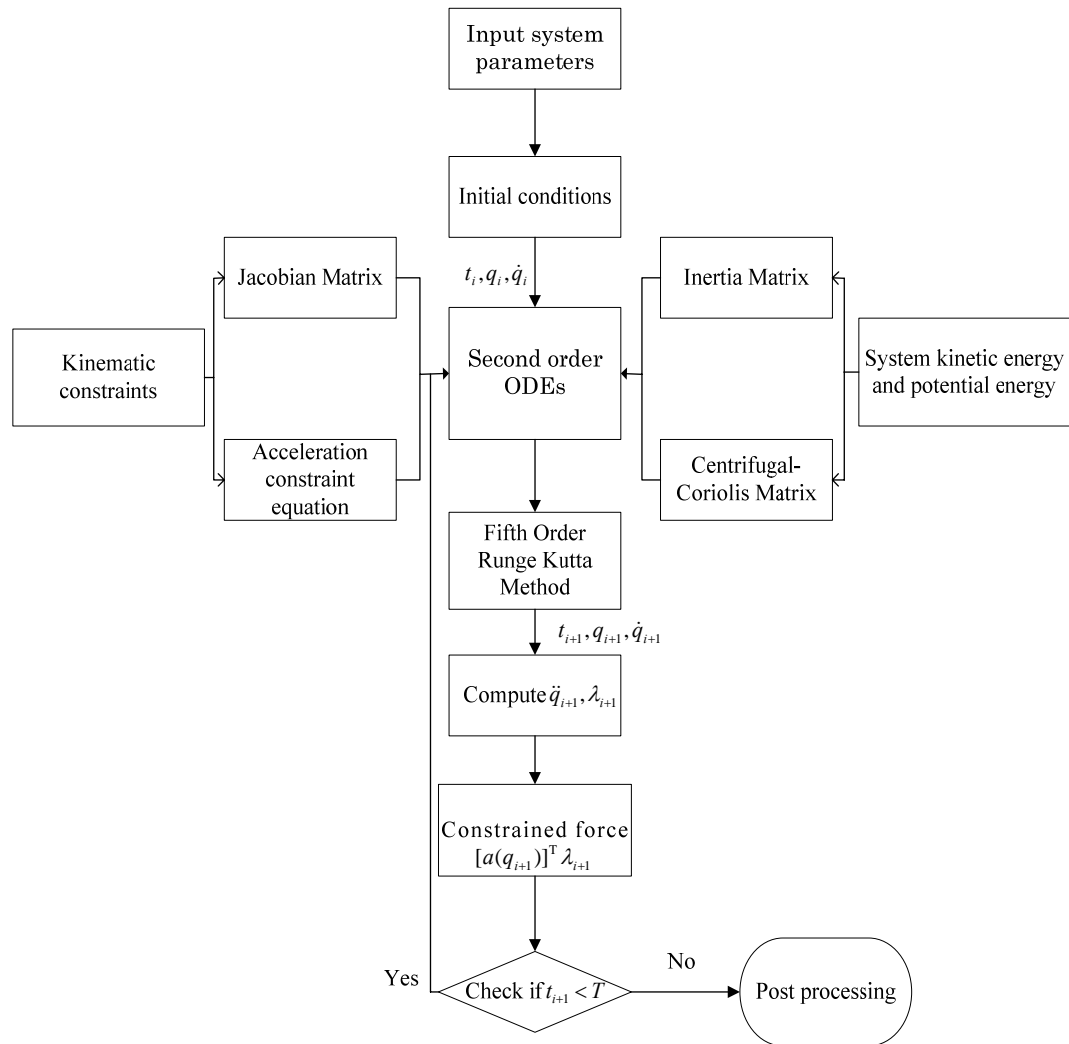


Figure 3-2 Simulation flowchart

In order to solve those ODEs, the following initial conditions at  $t=0$  are specified in terms of the system inputs and kinematics given in Chapter 2:

$$\mathbf{J}_{10} = \begin{bmatrix} D_p \cos \theta_0 \\ D_p \sin \theta_0 \end{bmatrix} = \begin{bmatrix} q_{10} \\ q_{20} \end{bmatrix} \quad (3-20a)$$

where  $\theta_0$  is the initial slope of the shackle.

$$\mathbf{J}_{50} = \mathbf{J}_{10} + \sum_{i=1}^4 (-1)^{i-1} \mathbf{L}_{i0} = \begin{bmatrix} q_{30} \\ q_{40} \end{bmatrix} \quad (3-20b)$$

where  $\mathbf{L}_{i0} = \begin{bmatrix} L_{ip} \cos \phi_{i+3,0} \\ L_{ip} \sin \phi_{i+3,0} \end{bmatrix}$ .

$$q_{i0} = \varphi_{(i-4)0} \quad \text{where } i = 5, 6, 7 \quad (3-20c, d, e)$$

$$\varphi_{e0} = \begin{cases} q_8 = \theta_{p0} + \sum_{i=1}^4 (-1)^{i-1} \varphi_{i0} - \varphi_5 & \text{F-1 and SF-2b} \\ q_6 = \theta_{y0} + \beta_{10} - \beta_{40} & \text{SF-2a} \end{cases} \quad (3-20f)$$

$$\varphi_{40} = \begin{cases} q_{90} & \text{F-1 and SF-2b} \\ q_{70} & \text{SF-2a} \end{cases} \quad (3-20g)$$

The initial values of velocities of each generalized coordinates can be acquired by taking time derivatives from Equation (3-20a) to (3-20g).

### Numerical ODE solver

The set of ODEs is solved using Butcher's fifth-order Runge-Kutta method [S. Chapra and R. Canale, 2002] as described in Equation (3-21), where  $\alpha(x, y) = dq / dt$ . At each time step,  $\alpha_j, (j = 1, 2, \dots, 6)$  is calculated from Equation (3-22) on each corresponding point.

$$q_{i+1} = q_i + \frac{1}{90} (7\alpha_1 + 32\alpha_3 + 12\alpha_4 + 32\alpha_5 + 7\alpha_6)h \quad (3-21)$$

where  $\alpha_1 = g(t_i, q_i) \quad (3-21a)$

$$\alpha_2 = g(t_i + \frac{1}{4}h, q_i + \frac{1}{4}\alpha_1h) \quad (3-21b)$$

$$\alpha_3 = g(t_i + \frac{1}{4}h, q_i + \frac{1}{8}\alpha_1h + \frac{1}{8}\alpha_2h) \quad (3-21c)$$

$$\alpha_4 = g(t_i + \frac{1}{2}h, q_i - \frac{1}{2}\alpha_2h + \alpha_3h) \quad (3-21d)$$

$$\alpha_5 = g(t_i + \frac{3}{4}h, q_i + \frac{3}{16}\alpha_1h + \frac{9}{16}\alpha_4h) \quad (3-21e)$$

$$\alpha_6 = g(t_i + h, q_i - \frac{3}{7}\alpha_1h + \frac{2}{7}\alpha_2h + \frac{12}{7}\alpha_3h - \frac{12}{7}\alpha_4h + \frac{8}{7}\alpha_5h) \quad (3-21f)$$

### Post processing

The post processing module provides the following information from the numerical solution to the ODE as a function of time for analyzing the effect of inversion and rotation processes on the bird:

- Joint kinematics
- Bird center and orientation
- Snap shot of the bird motion as it rotates
- Constrained forces and torques

The algorithm is best illustrated with simulation examples in the next section.

### 3.5 Verification of the Computational Algorithm

We compare the simulated results against FEA results (with time step of 10ms) obtained using ANSYS and LS-DYNA, a commercially available FEA package. For validating the algorithm, we simulate two examples for the same specified set of initial conditions as in [Lee and Liu, 2009], where the center and orientation trajectory are reported for SF-2a and SF-2b; and the bird is modeled as distributed masses with mechanical properties similar to rubber [Lee and Liu, 2009]. For the FEA, the geometry is initially modeled using Solidworks and ANSYS, and the data (nodes and elements)

along with the boundary conditions are then exported to LS-DYNA where the FEA modeled dynamic problem is solved.

The values of the parameters and initial conditions used in the simulation are summarized in Table 3-5. The bird model (such as its body mass, limb mass and lengths) are based on published data [Lee, 2001], while the stiffness and damping coefficients of the joints are based on experimentally data reported in [Shumway, 2002] where the stiffness for  $J_2$  and  $J_3$  are reproduced in Equation (3-22a) and (3-22b):

$$k(\varphi_2) = \begin{bmatrix} 0.74\varphi_2 - 0.09 \\ 26.5\varphi_2 + 0.17 \end{bmatrix} \text{ when } \begin{cases} \varphi_2 < \textit{Equilibrium} \\ \varphi_2 > \textit{Equilibrium} \end{cases} \quad (3-22a)$$

where  $\textit{Equilibrium} = 1.396$  radians ( $80^\circ$ )

$$k(\varphi_3) = \begin{bmatrix} 38.5\varphi_3 - 0.32 \\ -240\varphi_3^2 + 97\varphi_3 + 0.89 \end{bmatrix} \text{ when } \begin{cases} \varphi_3 < \textit{Equilibrium} \\ \varphi_3 > \textit{Equilibrium} \end{cases} \quad (3-22b)$$

where  $\textit{Equilibrium} = 2.094$  radians ( $120^\circ$ )

In [Shumway, 2002], the bird joints were experimentally modeled on the XY-plane for the hock and knee joints. Thus, for F-1 and SF-2b on the XY plane the stiffness and damping coefficients in [Shumway, 2002] are directly used. For SF-2a where the joint angle in the XZ plane, the two joints  $\beta_1$  and  $\beta_4$  modeled as similar revolute joints with similar stiffness in Equation (3-22) but the range of  $\beta_1$  and  $\beta_4$  are much smaller than the equilibrium angles.

To check the convergence of the numerical algorithm, the final state of the bird body orientation in SF-2a is computed with different time step ranging from 0.01ms to 10ms. Figure 3-3 shows the absolute value of the relative difference (with respect to the solution evaluated at the current time step) as a function of time step. The relative difference is less than the order of  $10^{-4}$  when the time step is smaller than 1ms. Therefore,

the time step of 0.4ms is chosen for the remaining computation as a compromise between computation time and accuracy.

Table 3-5 Parameters and initial conditions

Parameter	SF-2a (XZ-plane)	SF-2b (XY-plane)
<b>Shackle</b>		
Angular velocity (rad/s)	$\omega_y = 4.514$	$\omega_z = 8.727$
Gripping point m	$D\cos\theta_p = 0.281$	$D = 0.331$
Shackle slope ( $^\circ$ )	$\theta_p = 30^\circ ; 0^\circ \leq \theta_y(t) \leq 30^\circ$	$30^\circ \leq \theta_p(t) \leq 90^\circ$
Rotation radius (m)	$R = 0.152$	
<b>Bird</b>		
Body mass (kg)	$m_4 = 1.6$	
Leg mass (kg)	$m_1 = 0.03, m_2 = 0.08, m_3 = 0.1$	
Body dimension (mm)	$a = 97, b = 66$	$a = 97, c = 57$
Leg length, $i=1,2,3$ (m)	$L_i \cos\theta_p = 0.061, 0.078, 0.087$	$L_i = 0.07, 0.09, 0.1$
Hip-to-center Length (m)	$0.0215$	$0.06$
Stiffness (N-m/rad)	Equations (3-57a,b), $k_1 = 1; k_4 = 0.1$	
Damping (N-s/m)	$b_i = 0.05, b_4 = 0.005$ where $i=1,2,3$	
<b>Numerical simulation</b>	$h = 0.4\text{ms}; t_{\max} = 0.116\text{s}$	
<b>Initial Conditions of Generalized Coordinates</b>		
Toe joint (m)	$J_{1x} = -0.05, J_{1y} = -0.029$	$J_{1x} = -0.05, J_{1z} = 0$
Body center (m)	$J_{5x} = -0.1159, J_{5y} = 0.0534$	$J_{5x} = -0.1159, J_{5z} = 0$
Joint angle ( $^\circ$ ), $i=1,2,3,4$	$\beta_i = 0$	$\varphi_i = 15, 40, 68.75, 36.76$
Orientation angle ( $^\circ$ )	$\beta_e = 0$	$\varphi_e = 0$
<b>Initial Conditions of Generalized Velocities</b>		
Joint 1 (m/s)	$V_{1x} = 0, V_{1y} = 1.917$	$V_{1x} = -1.5307, V_{1z} = 2.4496$
Body center velocity (m/s)	$V_{5x} = 0.32, V_{5y} = 0.9711$	$V_{5x} = V_{5z} = 0$
Joint velocity (rad/s <sup>2</sup> )	$\dot{\varphi}_e = \dot{\varphi}_i = 0$ where $i=1, \dots, 4$	

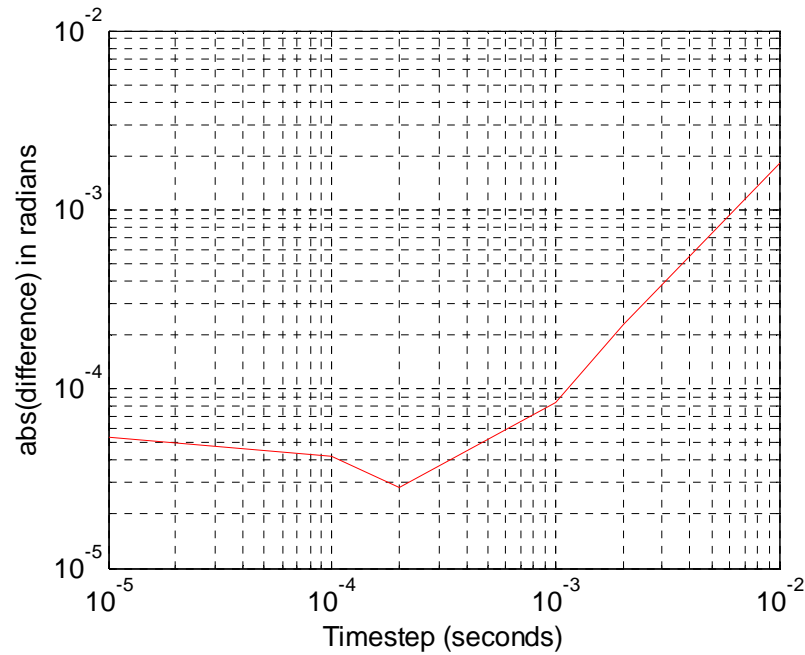


Figure 3-3 Convergence check

Results of comparison are shown from Figure 3-4 to 3-5.

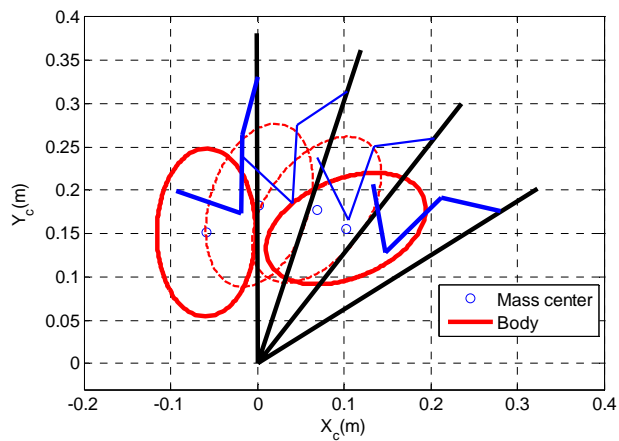
- Figure 3-4 describes the snapshot and trajectory(body center and orientation) of SF-2b from the initial position  $32^\circ$  of  $\theta_p$  to the final position of  $90^\circ$ .
- Figure 3-5 describes the snapshot and trajectory(body center and orientation) of SF-2a from the initial position  $0^\circ$  of  $\theta_y$  to the final position of  $30^\circ$ . The effect of gravity was neglected in the simulation where the bird swings on the XZ plane with the pallet.
- Figure 3-6 shows the percentage error of Y-coordinate of the body center and the orientation of SF-2b.
- Figure 3-7 shows the percentage error of Z-coordinate of the body center and the orientation of SF-2a.

The simulated SF-2b motion is similar to that predicted by FEA. The body is in contact with the shackle surface at about  $t=0.01s$ ; after that, the bird slides along the surface until the shackle rotates to its vertical position at  $t=0.116s$ . The discrepancy is in

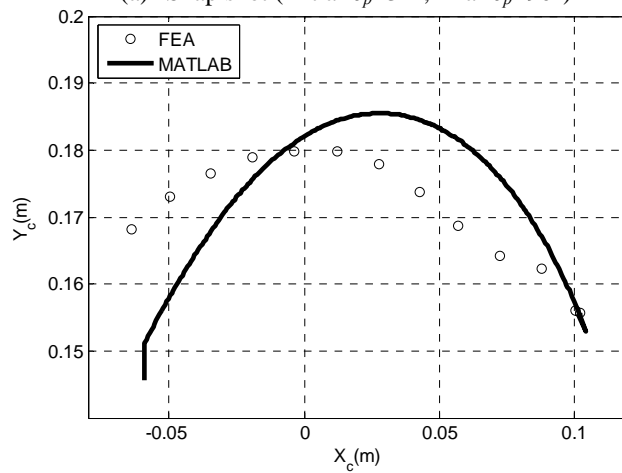
the Y trajectory where the simulated Y is faster than that by FEA. This is somewhat expected as the lumped-parameter approach results in a smaller moment of inertia than the distributed mass based in FEA. As compared to FEA, this discrepancy has three effects; it results in an earlier contact with shackle surface, a higher peak of 10cm, and a larger impulsive force during the contact with the shackle. For SF-2b, the maximum  $Y_c$  difference is 12.75% at  $X_c(t=0.12s) = -0.063m$  while the maximum difference in the body orientation occurs at  $X_c(t=0.02s) = 0.088m$  with a percentage error of 19% as shown in Figure 3-6. Similar arguments can be made when comparing the simulation against the FEA for SF-2a. As shown in Figure 3-7, the maximum difference of  $X_c$  occurs at  $Z_c(t=0.03s) = 0.004m$ , while the percentage error is 2%, and the maximum of body orientation occurs at  $Z_c(t=0.11s) = 0.063$  with a percentage error of 3.1%.

### 3.6 Summary

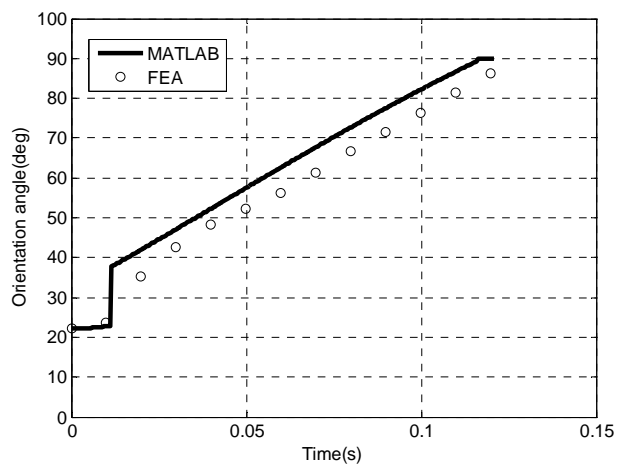
The constrained equations of motion for the generalized coordinates of the bird model have been derived, which include a detailed formulation of the inertia matrix, Jacobian matrix and system forces (consisting of non-constrained forces, constrained forces and contact forces). The numerical algorithm and its convergence were discussed. The computed results of SF-2a and SF-2b were verified by comparing against those obtained using finite element analysis. The verified model can be used for further investigations, as developed in Chapter IV.



(a) Snap shot (initial  $\theta_p=32^\circ$ , final  $\theta_p=90^\circ$ )

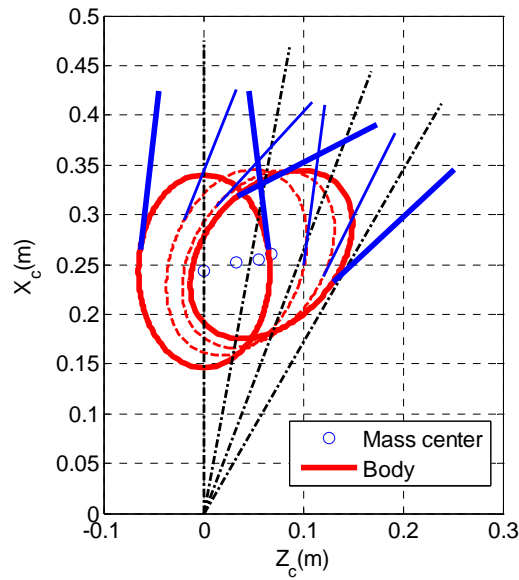


(b) Bird center

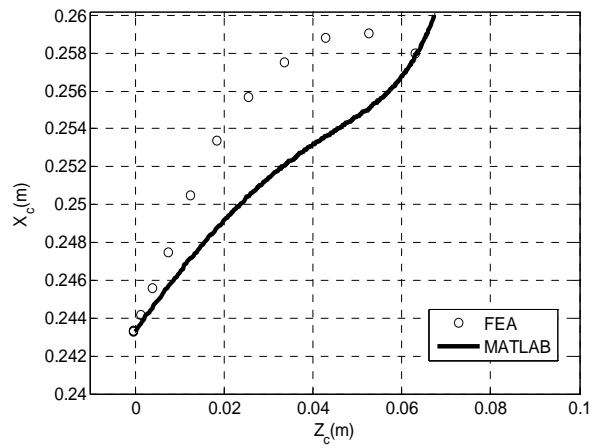


(c) Body orientation

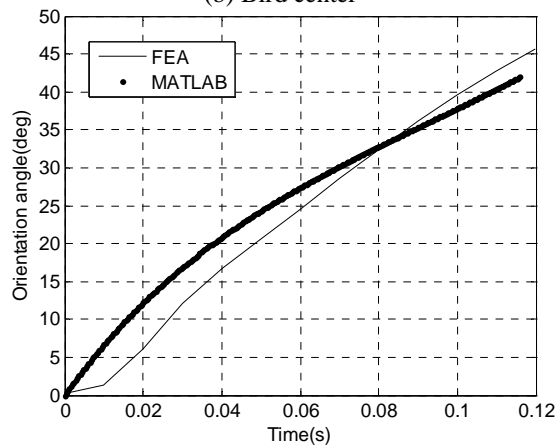
Figure 3-4 Inversion process (SF-2b on the XY plane,  $\omega_z = 8.727\text{rad/s}$ )



(a) Snap shot (initial  $\theta_y=0^\circ$ , final  $\theta_y=30^\circ$ )



(b) Bird center



(c) Body orientation

Figure 3-5 Rotation process (SF-2a on the XZ plane,  $\omega_y = 4.514\text{rad/s}$ )

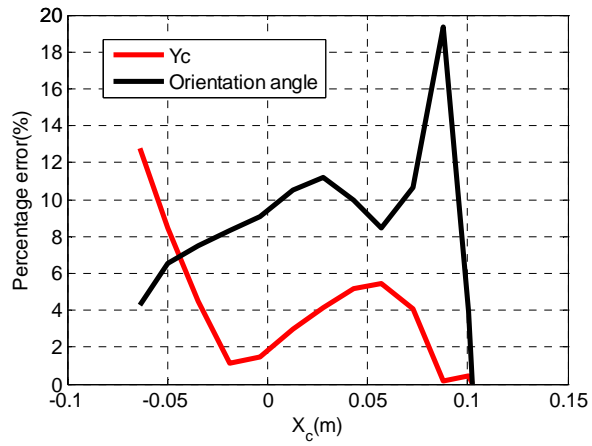


Figure 3-6 Percentage error of  $Y_c$  (SF-2b)

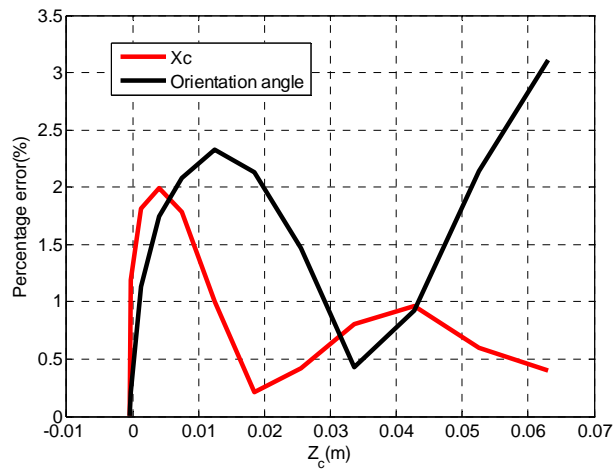


Figure 3-7 Percentage error of  $Z_c$  (SF-2a)

## CHAPTER 4

### NUMERICAL DESIGN ANALYSIS

#### 4.1 Introduction

This chapter begins with defining the parameters for executing a consecutive operation of three functions based on a medium-size bird. This is followed by investigating the effects of three bird sizes (large, medium and small) on the motion and forces. The results include comparisons of the position, velocity, and orientation as well as constrained forces imposed on the toe joint. A preliminary study on the effects of rotation on the head motion of a bird and that of the shackle sidewalls is briefly explored at the end of the chapter.

#### 4.2 Simulation Parameters

The algorithm described in Chapter 3 is applied here to simulate the three sequential functions starting with F-1, then SF-2a and finally SF-2b, and to study the effect of bird size on the motion and forces on the joints. The parametric values characterizing the bird body and legs are given in Table 4-1, where the dimension of medium size is used in Chapter 3. The time intervals ( $t_{max}$  for F-1, SF-2a and SF-2b) and the initial conditions in Table 4-2 are based on the live-bird transfer system being developed at Georgia Tech [11]; the final states of F-1 and SF-2a are the corresponding initial conditions of its subsequent function. The shackle is held stationary at a constant slope of  $30^\circ$  with respect to the horizontal axis (and hence  $\omega_z = 0$ ). With the specified initial position/orientation of the bird, F-1 is simulated for 0.22s. After that, the shackle

begins to rotate  $45^\circ$  about the Y-axis with a constant angular velocity  $\omega_y$  for 0.174s. This is immediately followed by SF-2b, where the shackle rotates from the initial slope of  $30^\circ$  to the vertical position on the XY-plane.

Table 4-1 Bird properties [16]

Property	Large	Medium	Small
<b>Body</b>			
Mass, kg	2.43	1.6	1
Size (a, b, c), mm	115.8, 64.5, 76.2	99, 57, 66	81.8, 51, 55.9
<b>Leg</b>			
Mass ( $m_1, m_2, m_3$ ), kg	0.035, 0.091, 0.116	0.03, 0.08, 0.1	0.025, 0.069, 0.841
Length ( $L_1, L_2, L_3, L_4$ ), mm	82.7, 102.7, 92.7, 72.7	70, 90, 80, 60	57.3, 77.3, 67.3, 47

Table 4-2 Parameters and initial conditions

Parameter	F-1(XY-plane)	SF-2a (XZ-plane)	SF-2b (XY-plane)
<b>Shackle</b>			
Angular velocity (rad/s)	$\omega_z=0$	$\omega_y = 4.51$	$\omega_z = 8.73$
Gripping point (m)	D=0.178	$D \cos \theta_p = 0.154$	D=0.178
Shackle slope ( $^\circ$ )	$\theta_p = 30^\circ$	$\theta_p = 30^\circ ; 0^\circ \leq \theta_y(t) \leq 45^\circ$	$30^\circ \leq \theta_p(t) \leq 90^\circ$
Rotation radius (m)		$R=0.305$	
<b>Time interval</b> , $t_{\max}$ (s)	0.22	0.174	0.116
<b>Initial Conditions of Generalized Coordinates</b>			
$(J_{1x}, J_{1y}$ or $J_{1z})$ (m)	0.154, 0.089	0.154, 0	0.154, 0.089
$(J_{5x}, J_{5y}$ or $J_{5z})$ (m)	0.127, 0.177	-0.04, 0	-0.07, 0.046
$\varphi_1, \varphi_2, \varphi_3, \varphi_4$ ( $^\circ$ )	15, 58.38, 55.27, 4.89	$\beta_1 = \beta_4 = 0$	88.8, 69.4, 116, 99
Orientation ( $^\circ$ )	$\varphi_e=0$	$\beta_e = 0$	$\varphi_e=30^\circ$
<b>Initial Conditions of Generalized Velocities</b>			
$(V_{1x}, V_{1y}$ or $V_{1z})$ (m/s)	0, 0	0, 2.07	-0.7758, 1.3437
$(V_{5x}, V_{5y}$ or $V_{5z})$ (m/s)	0, 0	0, 1	-0.3026, -0.2947

The external inputs to F-1 are the forces and moment of the fingers acting on the shackled bird:

$$\mathbf{F} = \begin{bmatrix} F_x \\ F_y \end{bmatrix} = |\mathbf{F}| \begin{bmatrix} \cos \theta_c \\ \sin \theta_c \end{bmatrix}; M = F_x \Delta Y_c - F_y \Delta X_c \quad (4-1a, b)$$

where  $|\mathbf{F}|$  is the magnitude of the contact force;  $\Delta X_c$  and  $\Delta Y_c$  are the distances of the contact point from the bird center; and  $\theta_c$  is the direction of the finger force. For the design  $\theta_c = 30^\circ$ , the initial contact point is approximated at  $\Delta X_c = 0.011\text{m}$  and  $\Delta Y_c = 0.03\text{m}$ . Based on the 2D contact force computation algorithm in Lee *et.al*, [2001], the normalized initial contact force of a rotating finger on an elliptical object as a function of time is given in Figure 4-1. More details can be found in [Lee and Yin, 2001] and [Yin and Lee, 2002].

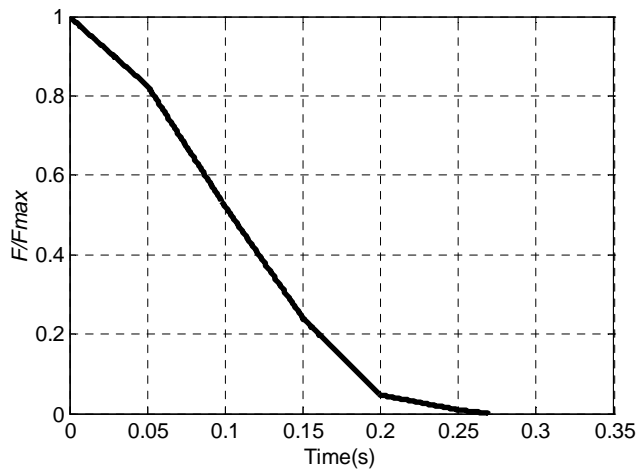


Figure 4-1 Contact force-time plot ( $F_{\max} = 25.35\text{N}$ )

### 4.3 Simulation of Three Consecutive Functions

Results are given in Figures 4-2 to 4-17, where simulations were based on the bird of the medium size.

- Figure 4-2 shows snap shots of the three consecutive functions to help visualize the motion and the corresponding 3D plots.
- Figures 4-3 to 4-7 detail the motion simulation corresponding to F-1.
  - Figure 4-3 shows the trajectory (body center location and orientation).
  - Figures 4-4(a) and (b) give the bird center position and velocity in the X and Y direction respectively.
  - Figure 4-5 shows the constrained force imposed by the shackle, which is decomposed into two components as a normal force and a tangential force.
  - Figure 4-6 gives the constrained force and moment on the bird center.
  - Figure 4-7 describes the constrained torque on the toe, hock, knee and hip joint respectively.
- Similarly, the details corresponding to SF-2a and SF-2b are given in two other sets of figures; Figures 4-8 to 4-12 for SF-2a and Figures 4-13 to 4-17 for SF-2b.
  - Unlike F-1, SF-2a is on the XZ plane. In this simulation, the effect of gravity is neglected as the bird swings with the pallet. Also, since the joint angles of hock and knee are not considered as generalized coordinates in SF-2a, only the constrained torques of the toe and hip joint are shown in Figure 4-12.
  - For SF-2b, the figure layout is the same as that in F-1.

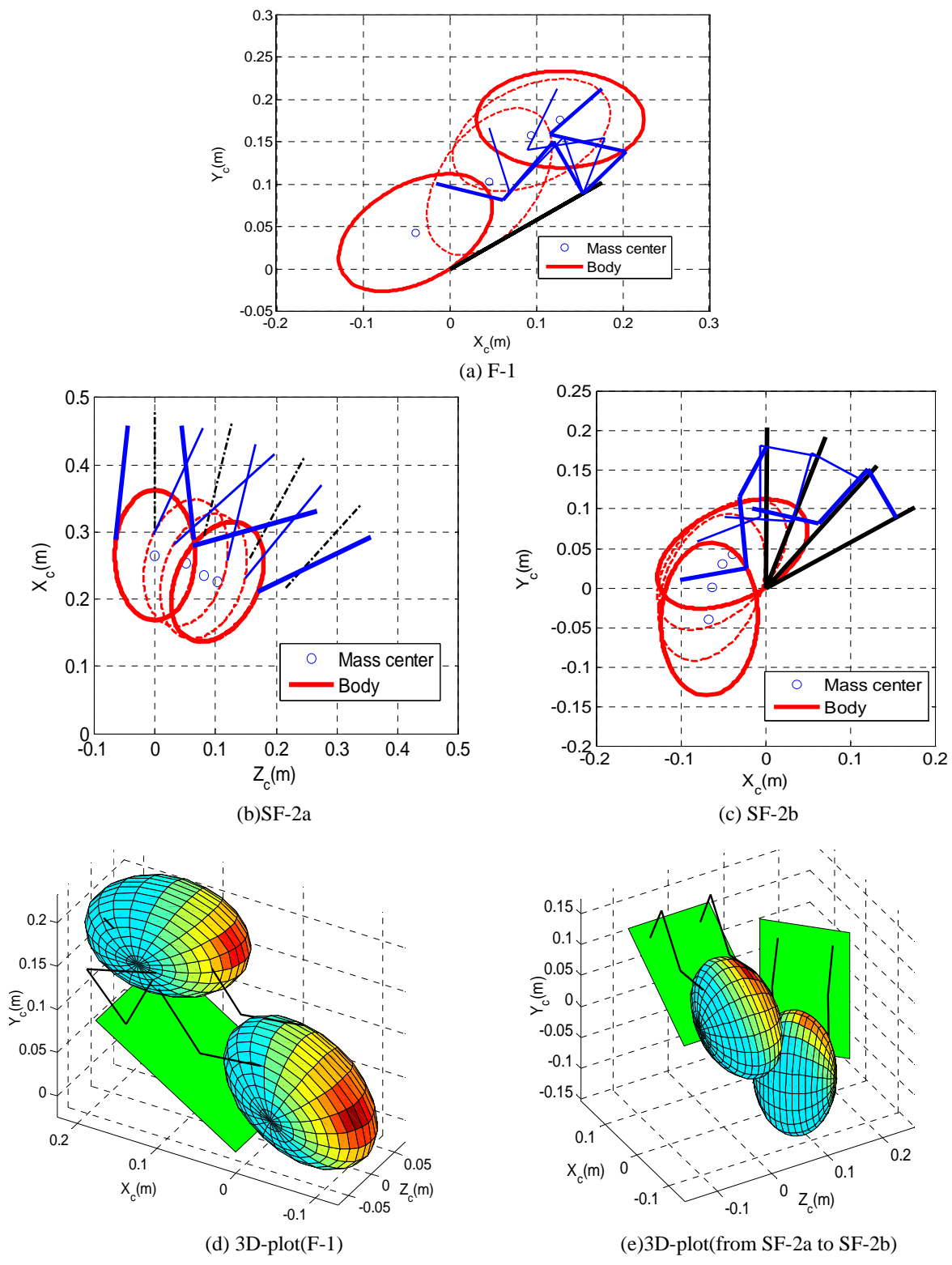


Figure 4-2 Snap shots of three consecutive functions

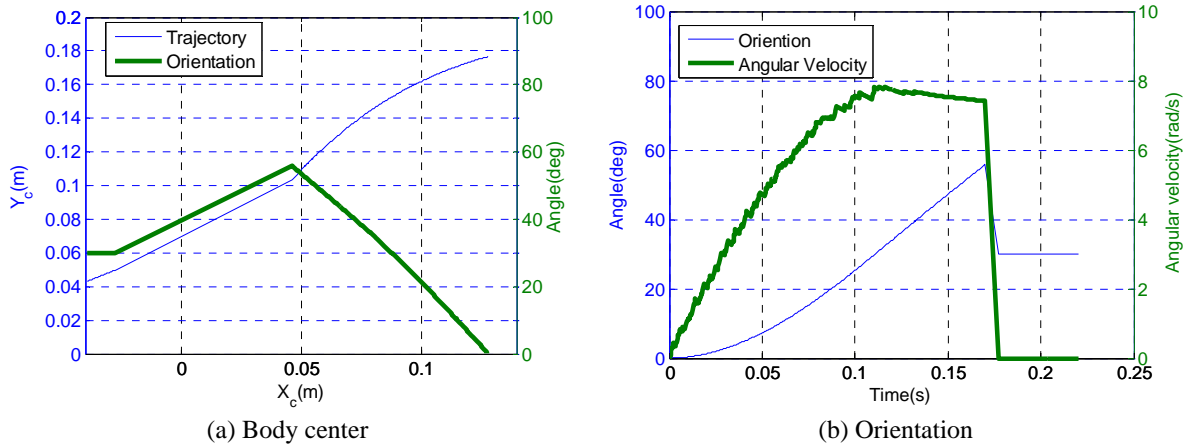


Figure 4-3 Trajectory (center and orientation in F-1)

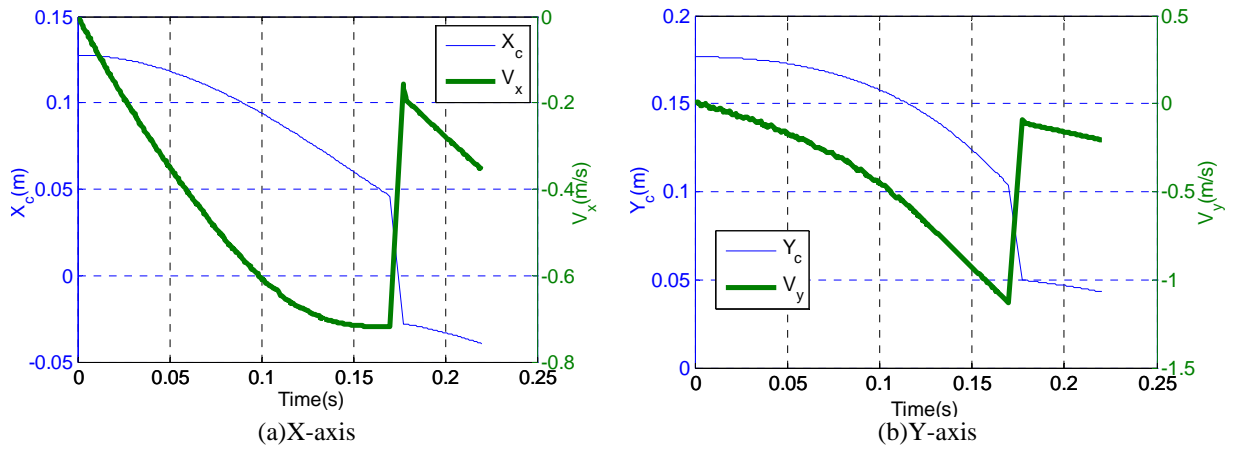
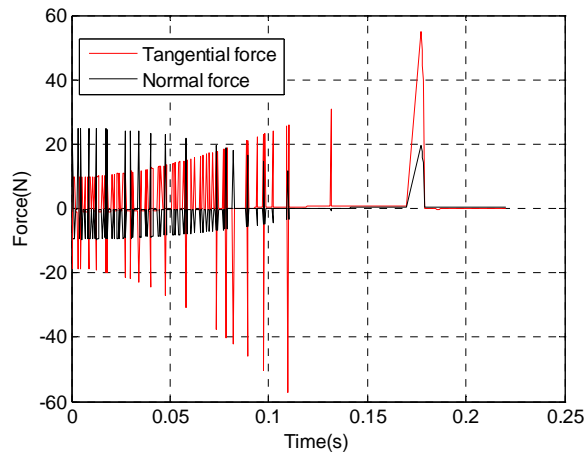
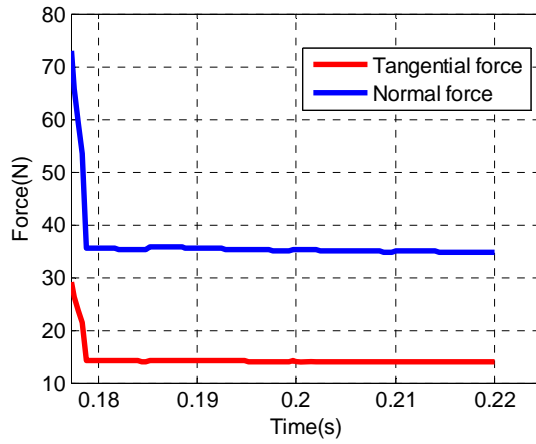


Figure 4-4 Center position and velocity (F-1)

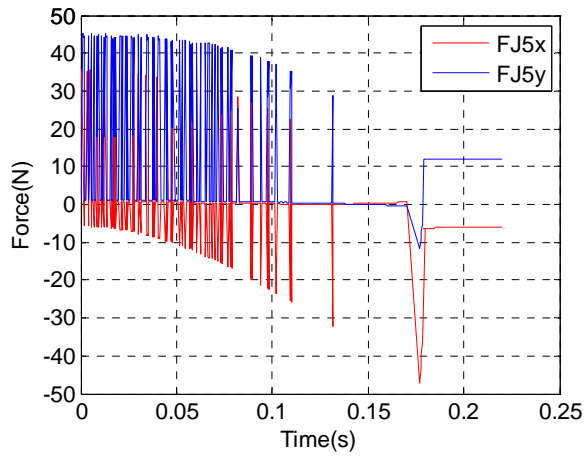


(a) Shackle force on Joint 1

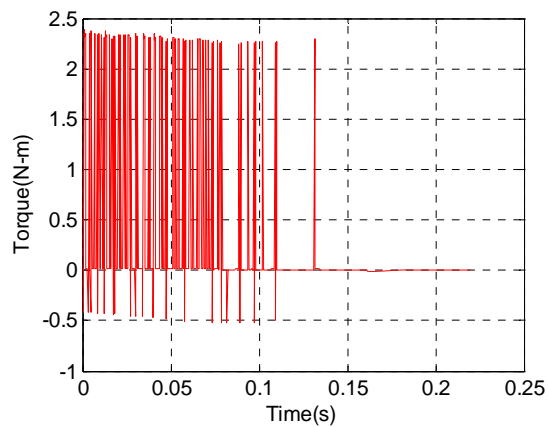


(b) Shackle force on the body after contact

Figure 4-5 Shackle force (F-1)

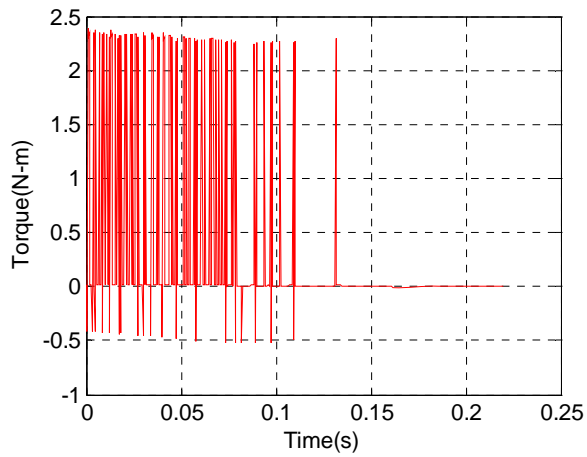


(a) Force on bird center ( $X_c$  and  $Y_c$ )

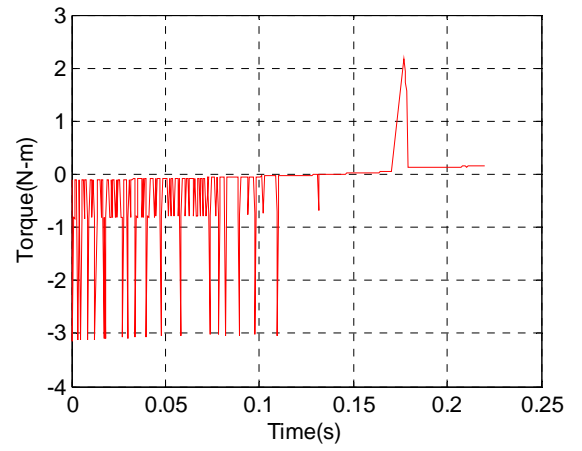


(b) Moment about bird center

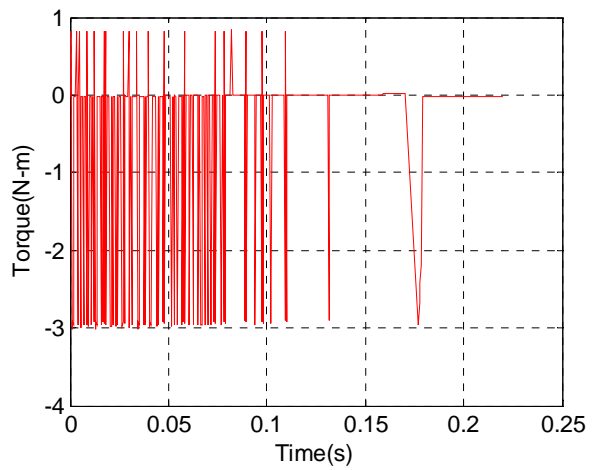
Figure 4-6 Constrained force and moment (body center in F-1)



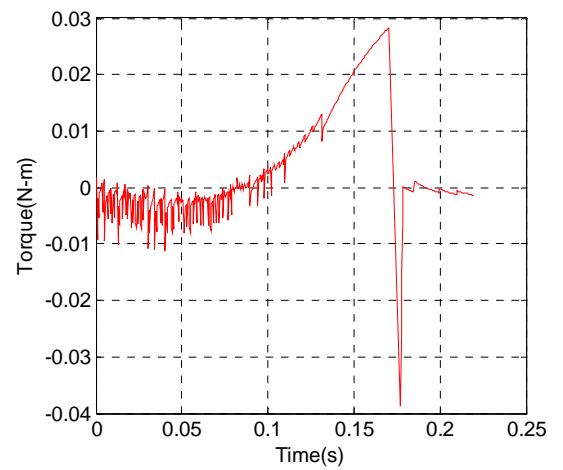
(a) Toe joint  $J_1$



(b) Hock joint  $J_2$

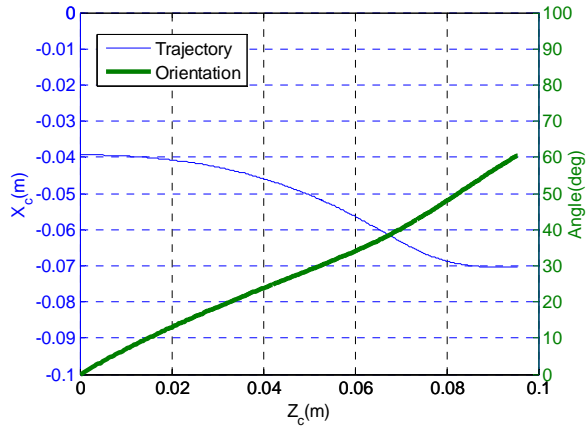


(c) Knee joint  $J_3$

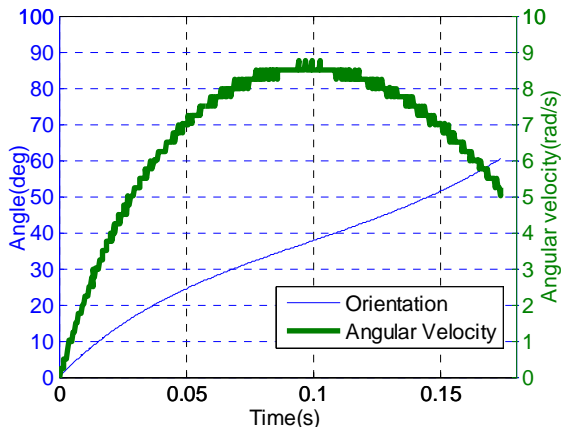


(d) Hip joint  $J_4$

Figure 4-7 Constrained torque on joints (F-1)

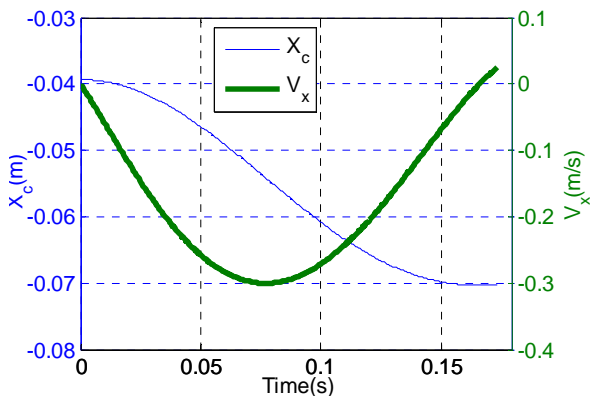


(a) Body center

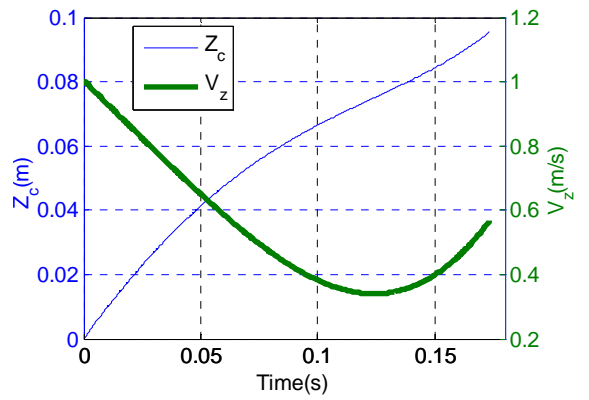


(b) Orientation

Figure 4-8 Trajectory (center and orientation in SF-2a)



(a) X-axis



(b) Z-axis

Figure 4-9 Center position and velocity (SF-2a)

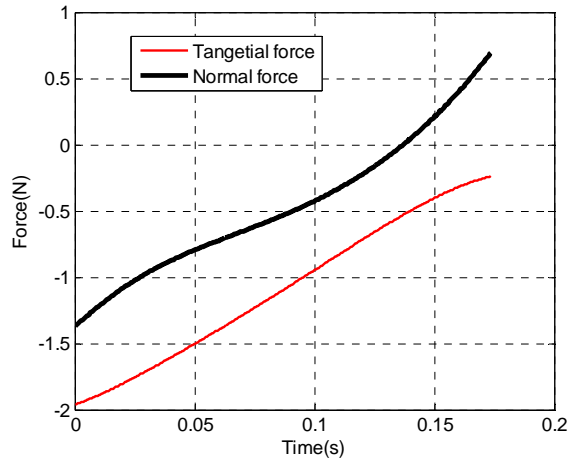
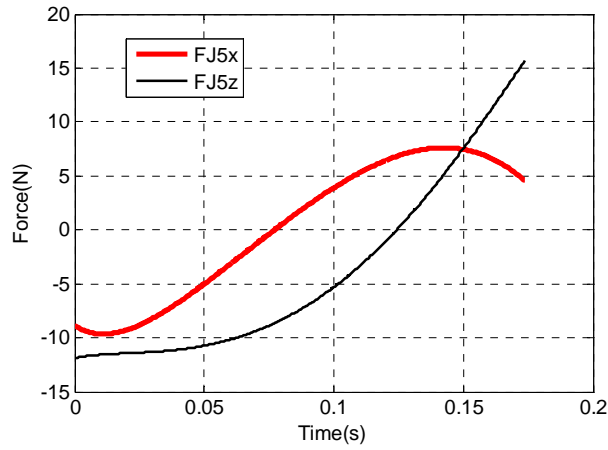
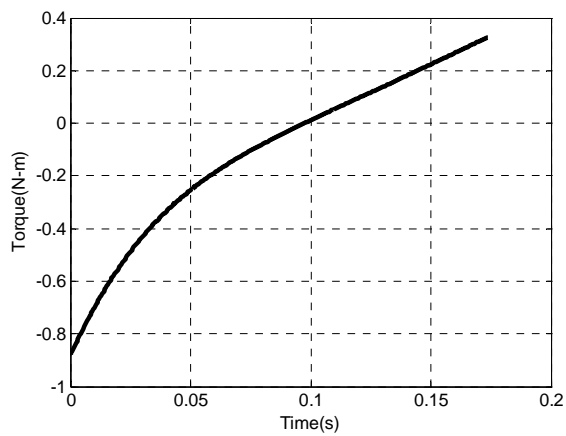


Figure 4-10 Shackle force on Joint 1 (SF-2a)

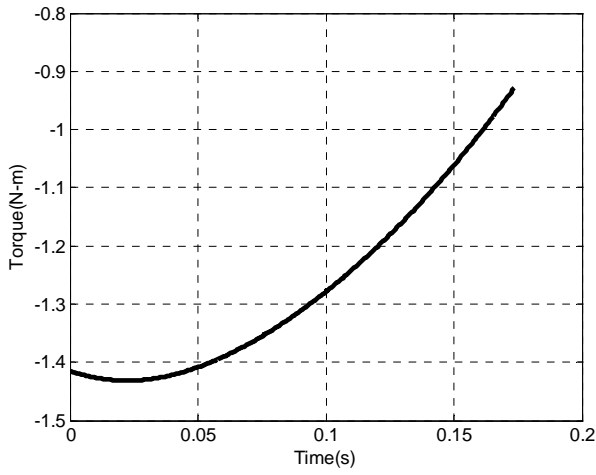


(a) Force on bird center ( $X_c$  and  $Z_c$ )

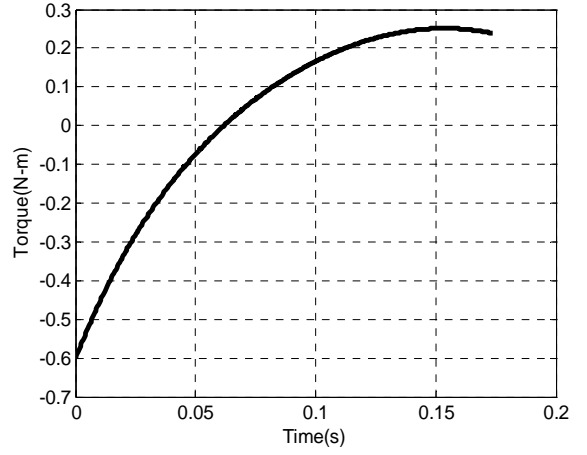


(b) Moment about bird center

Figure 4-11 Constrained force and moment (body center in SF-2a)

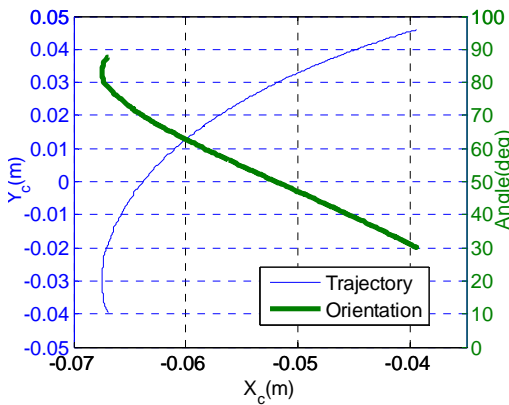


(a) Toe Joint  $J_1$

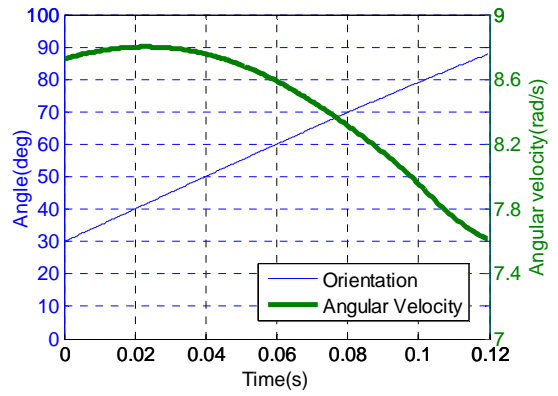


(b) Hip joint  $J_4$

Figure 4-12 Constrained torque on joints (SF-2a)

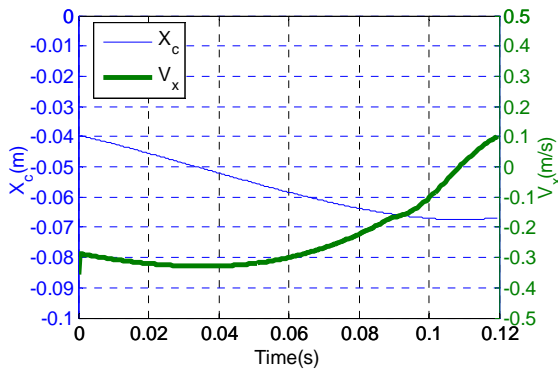


(a) Body center

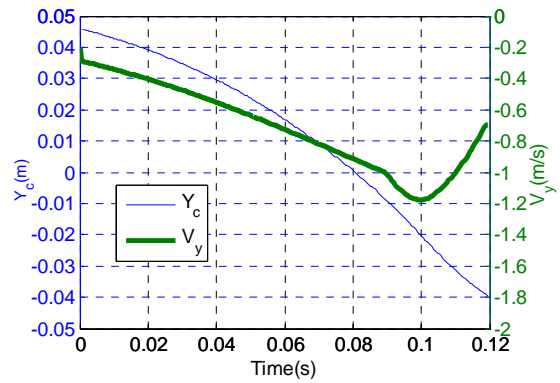


(b) Orientation

Figure 4-13 Trajectory (center and orientation in SF-2b)



(a) X-axis



(b) Y-axis

Figure 4-14 Center position and velocity (SF-2b)

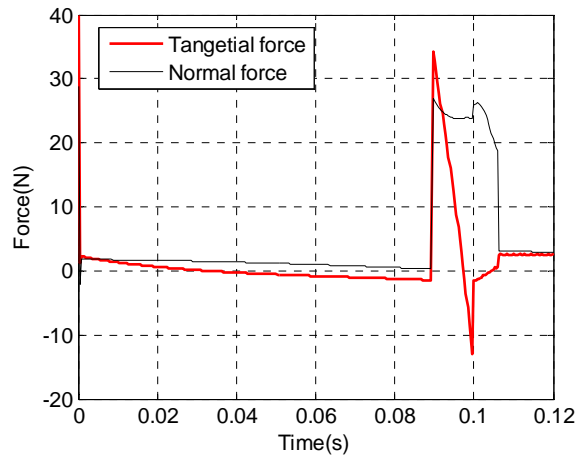
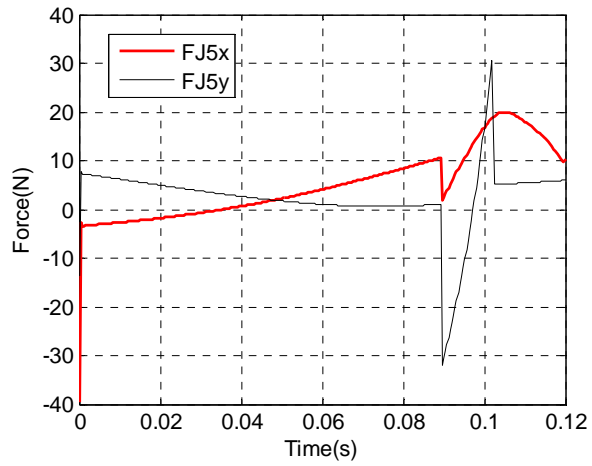
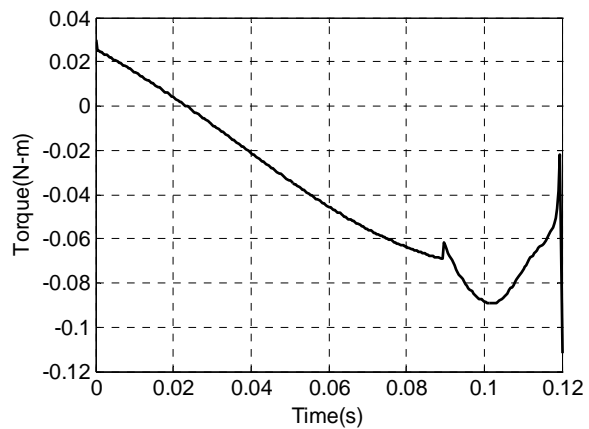


Figure 4-15 Shackle force on Joint 1 (SF-2b)



(a) Force on bird center ( $X_c$  and  $Y_c$ )



(b) Moment about bird center

Figure 4-16 Constrained force on body center and toe joint (SF-2b)

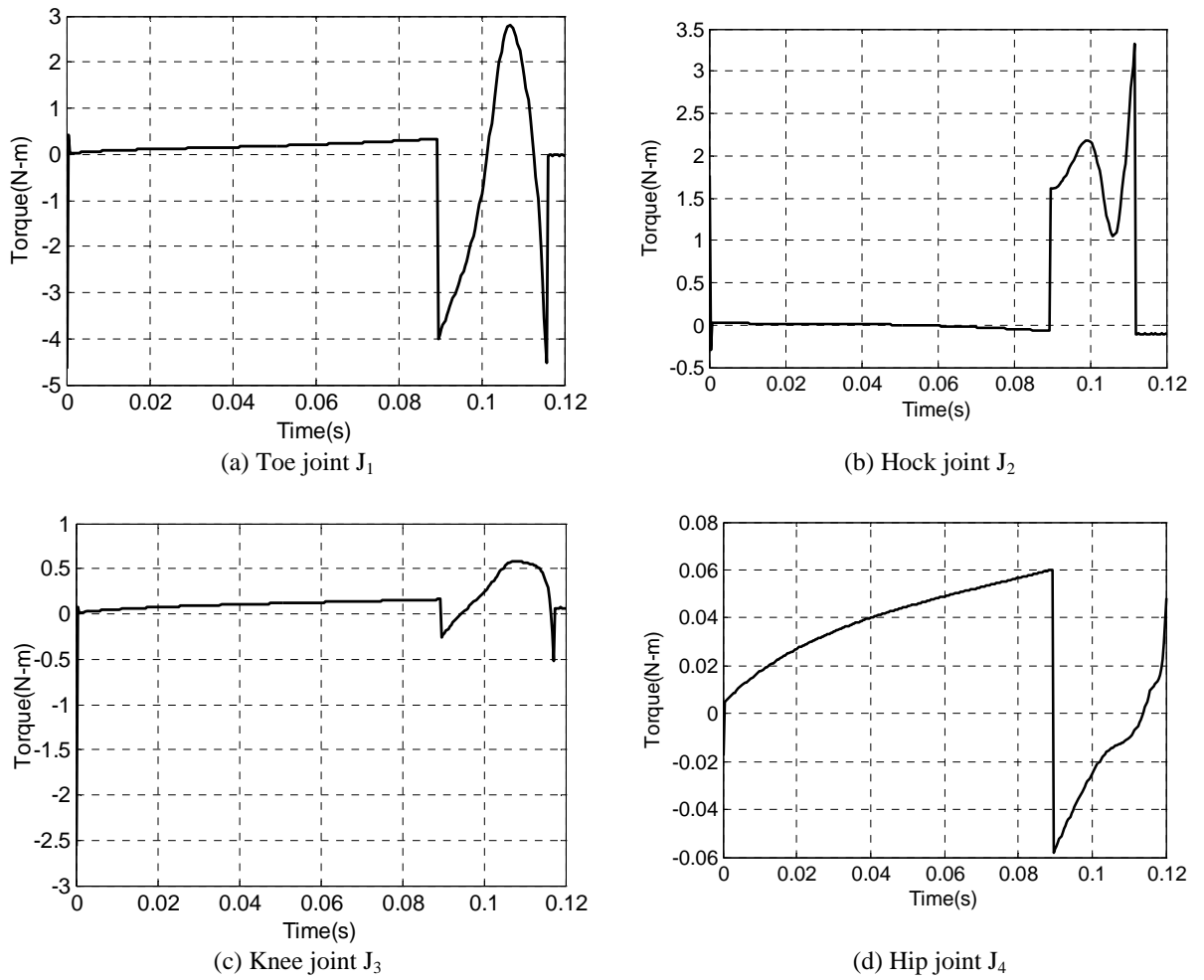


Figure 4-17 Constrained torque on the joints (SF-2b)

#### 4.4 Discussions of Integrated Three-function Simulation

Some observations made in these results are detailed below.

##### Discussion on F-1 results:

In Figure 4-2(a) that describes the snap shots in F-1, the bird (rotating under the influence of the rotating fingers and gravity) contacts with the shackle surface at  $X_c=0.0478\text{m}$ . From Equation (3-18), the impact time can be calculated to be  $\Delta t=6.8\text{ms}$ . After making contact, the bird slides along the shackle following a straight line trajectory

parallel to the shackle surface (with its orientation equal to a constant of  $30^\circ$  or zero angular velocity).

- Both  $X_c$  and  $Y_c$  move downwards after the contact point illustrating that the bird extends its legs during the contact. Due to the impulse effects, the velocity in X and Y directions reduce to  $-0.17\text{m/s}$  and  $-0.2\text{m/s}$  respectively.
- The constrained force on the toe joint imposed by the shackle can be decomposed into a normal force, perpendicular to the shackle surface, and a tangential force, parallel to the shackle surface. As seen in Figure 4-5, both component forces oscillate during the bird body rotation, and experience a sudden change when the body makes contact with the shackle, during which the tangential force reaches to its peak value of 50N. When the bird slides (with no rolling) along the shackle, both component forces reduce sharply to zero.
- Similar observations can be made for the constrained forces on the body center as well as the constrained torques on the joints. Note that the constrained torque on the body center is zero after the contact since the bird is assumed to slide along the shackle; therefore there is zero net moment about its center as shown in Figure 4-6(b).

Discussion on SF-2a results:

At  $t=0.22\text{s}$ , the bird begins to rotate on the XZ plane while keeping in contact with the shackle surface, and possesses a maximum orientation of  $60^\circ$  as well as a maximum angular velocity of  $8.7\text{rad/s}$ , as shown in Figure 4-8(a) and 4-8(b), respectively.

- Compared to the shackle forces in F-1, the normal force and tangential force in SF-2a are small, since the bird is supported on the shackle surface in SF-2a. As seen from Figure 4-11 and 4-12, the constrained force on the body center and all the joints yield

a more smooth curve than the constrained force in F-1, which indicates that the rotation on the XZ plane imposes less effects on the constrained forces.

Discussion on SF-2b results:

At  $t=0.396s$ , the bird rotates on the XY plane again driven by the rotating shackle. It will not only rotate but also slide along the shackle surface with its orientation equal to the shackle slope, as shown in Figure 4-2(c). Besides, the trajectory of the center is similar to a curvature since the bird is rotating about its center, which is also close to the pivot point of the shackle, as seen in Figure 4-2 (c) and Figure 4-13(a).

- In SF-2b, the Y-velocity reduces at  $t=0.09s$ , which is led by the leg constraint that the foot and leg move to their limits at  $t=0.1s$ , the bird may be temporarily held back at that instant.
- The above observation can be further validated by the constrained forces. Both normal force and tangential force of shackle will reach their peak value of 30N because the bird suddenly decelerates in the Y-direction. Similar trends can be found in the constrained forces/torques of the body and the joints.
- As shown in Figure 4-16(a), since the bird is rotating near the pivot point of the shackle, which is close to its natural rotation thus reducing the body force or other imposed forces, therefore the forces are smaller than that in F-1.

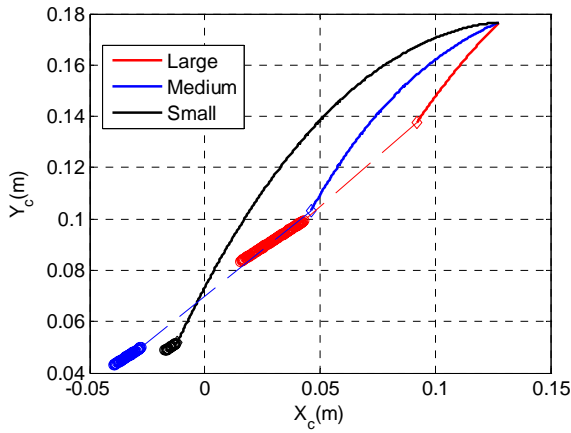
#### 4.5 Effects of Bird Sizes

This section aims to investigate the effects of different bird size when it is going through three consecutive functions. According to the experimental data in [Lee, 2001], three different bird sizes, including body and leg dimensions, are shown in Table 4-2, as being marked large, medium, small respectively.

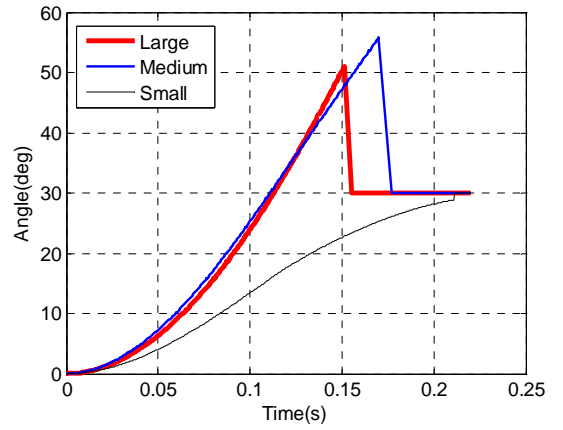
#### 4.5.1 Position, Velocity and Orientation of the Body Center

Results of position, velocity and orientation will be given from Figure 4-18 to 4-19.

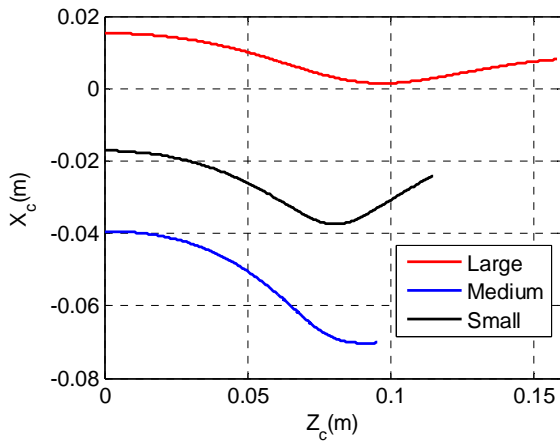
- Figure 4-18 shows the comparison of trajectory when all three birds go through three consecutive functions, where the results of F-1, SF-2a and SF-2b are shown in Figure 4-18 (a) and (b), (c) and (d), (e) and (f) respectively.
- Figure 4-19 gives the comparison of the velocity of the body center among all the birds in each function, which is decomposed into the X-axis and the Y-axis in F-1 and SF-2b, while in SF-2a, it is analyzed in the X-axis and the Z-axis.



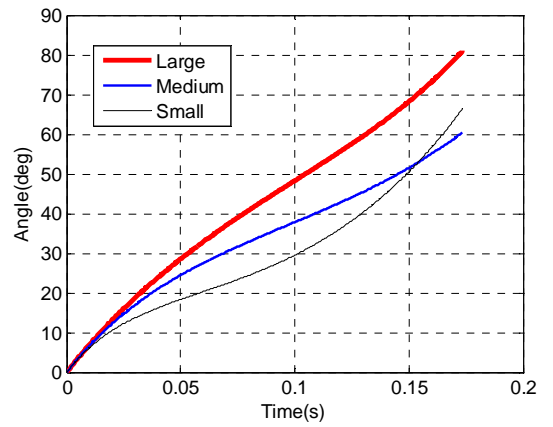
(a) Body center (F-1)



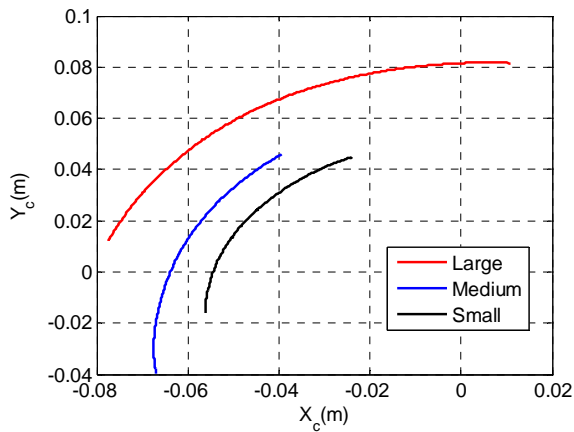
(b) Orientation (F-1)



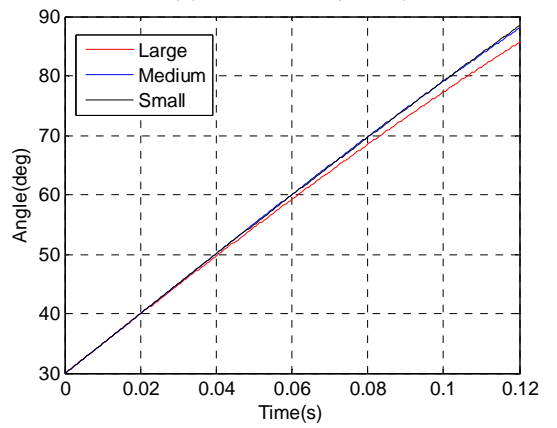
(c) Body center (SF-2a)



(d) Orientation (SF-2a)

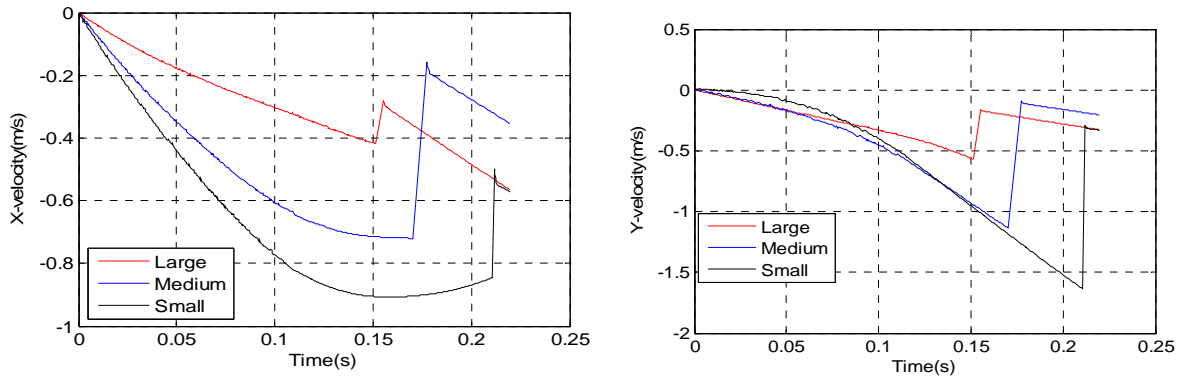


(e) Body center (SF-2b)

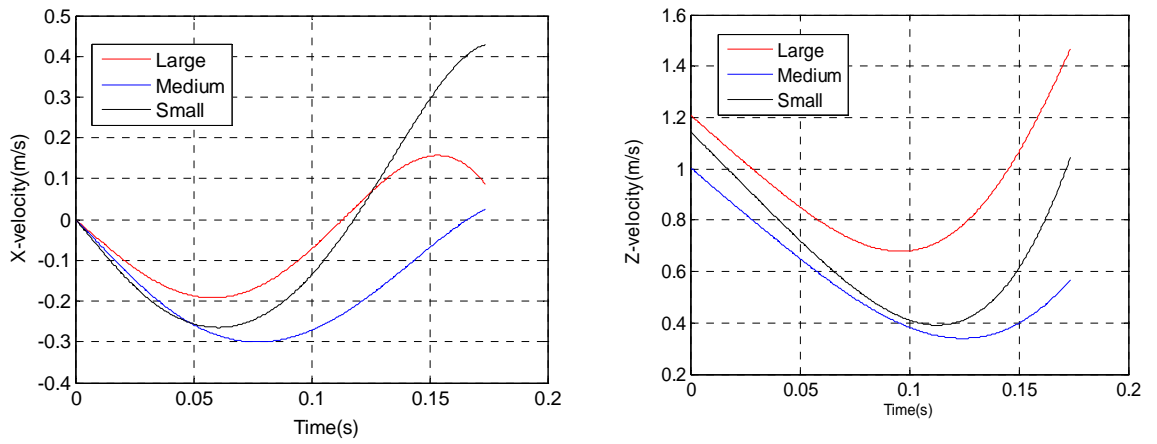


(f) Orientation (SF-2b)

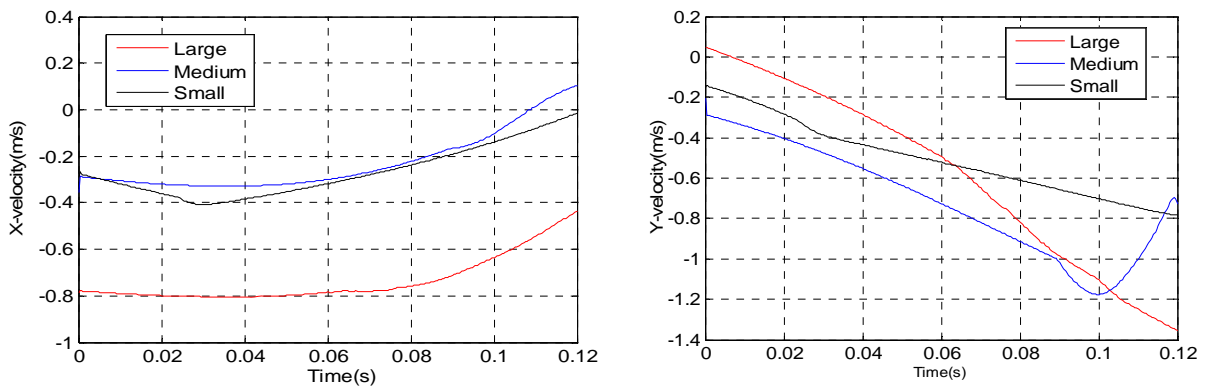
Figure 4-18 Trajectory (center and orientation)



(a) F-1



(b) SF-2a



(c) SF-2b

Figure 4-19 Center velocities

Observations on the above results are shown below:

- As can be seen from Figure 4-18(a), in F-1, the initial contact position between the bird body and the shackle surface is determined by the bird size, since for large birds, the large body makes contact occur earlier than smaller ones. The small bird will move farthest because its small dimension and the continual effects from the fingers.
- The sliding distance after the initial contact in F-1 is also determined by the bird size since a large bird has a larger gravitational force in the Y-axis, which makes it move further. However the final state of F-1 is affected more by the contact position and sliding velocities gained during the contact, which can be obtained from Equation (3-18).
- In SF-2a, as seen from Figure 4-18 (c), the range of the center trajectory will vary due to different initial conditions. The larger distance the bird has with respect to the rotation center, the further it can rotate, which means the size does not play an important role here.
- As seen from Figure 4-18 (e), in SF-2b, the size of the bird will determine the length of the rotating path. Since the final position of all the birds is near the origin, which is the rotating center of the shackle, therefore, the birds will rotate along its mass center when the shackle rotates.
- In F-1, the range of orientation is proportional to the bird mass, therefore the small bird has the minimum orientation. However, because the large bird contacts with the shackle earlier than the medium bird and then slides along the shackle, the final orientation of the large bird before the contact is smaller than that of the medium bird. After contact, all sizes of bird will have a constant orientation since they slides along

a stationary shackle. For SF-2a, the orientation angle is determined by the initial Z-velocity. For SF-2b, all the birds will slide along the surface of rotating shackle until it reaches to the vertical position, therefore all the bird orientations will go from 30° around 90° within the same time span regardless of their sizes, as seen in Figure 4-18 (f).

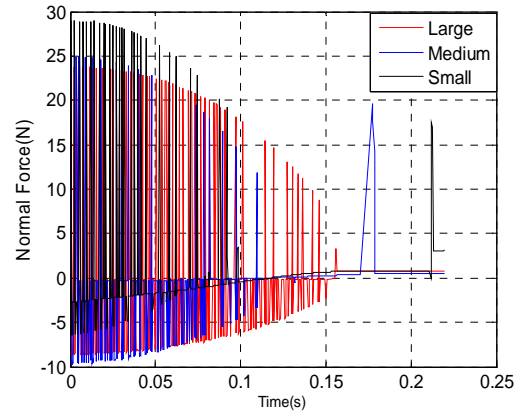
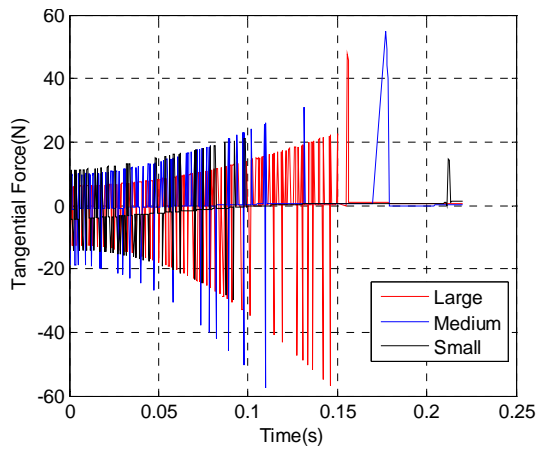
- From Figure 4-19(a), in F-1, the velocity before the contact is determined by the contact time. The longer the bird moves before the contact, the larger velocity it will gain, as determined by Equation (3-18). Figure 4-19(b) shows that the velocity of the body center oscillates in both X-direction and Z-direction, indicating a swinging motion during SF-2a. From Figure 4-19(c), since the bird body is sliding under the influence of gravitational force, the large bird will gain the largest velocity in the Y-direction.

#### 4.5.2 Bird Size Effects on the Shackle Force

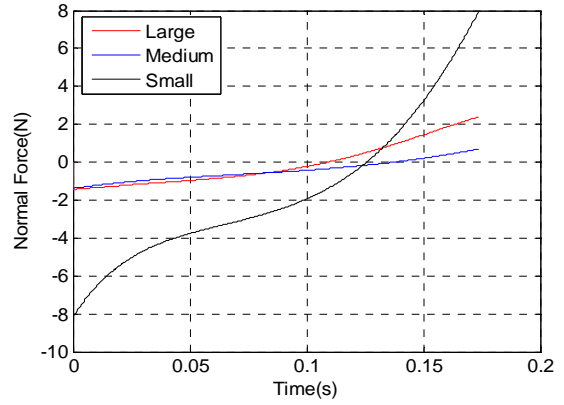
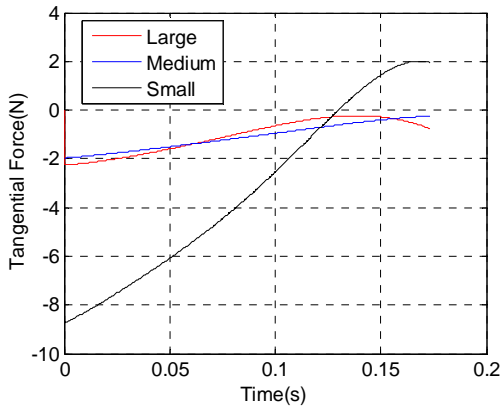
Since one of the interests in this thesis is to study the effect on the body size on the value of the imposed shackle force, this section will specifically examine the shackle force on different birds when they are going through three consecutive functions.

Results of the shackle force comparison are given in Figure 4-20

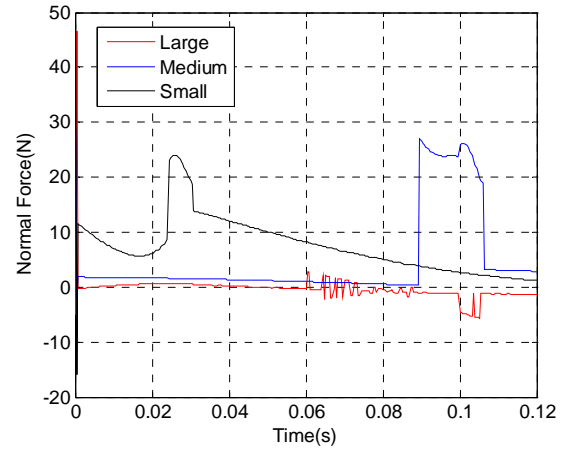
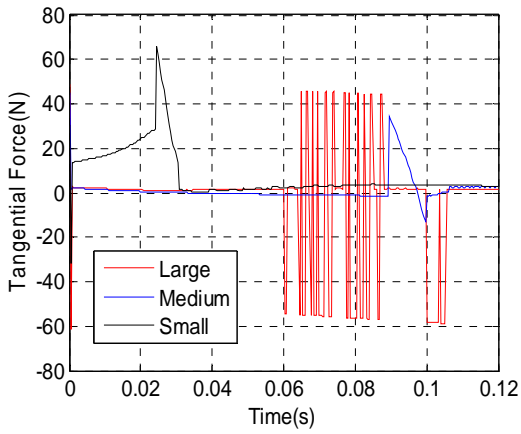
- Figure 4-20 shows the shackle forces of all three birds in each function, which is analyzed in the normal and tangential direction respectively.



(a) F-1



(b) SF-2a



(c) SF-2b

Figure 4-20 Shackle force

Observations on the results in Figure 4-20 are shown below:

- From Figure 4-20(a), the shackle forces oscillate because of the body rotation. Before the contact, the bird will experience continual effects from the shackle. The bird size affects the peak value of shackle forces, the maximum normal and tangential force from the shackle comes from the large bird, which has an absolute value around 60N and 30N respectively. Since the contact will create an impulse on the bird body, there will be a sudden change of shackle force occurring on the respective contact time. The value of this force will be related to the body mass as well as the contact time. After the contact, both tangential force and normal force will reduce to a small value since all the birds only slide along the shackle surface.
- Compared to the forces in F-1, the shackle forces in SF-2a for all the birds are smaller since no gravity is considered in the XZ plane. Most of the time, the normal force and tangential force will be negative, which indicates a pushing effect along the shackle surface while pulling the leg in the normal direction. After  $t=0.13s$ , the normal force will change its direction to support the leg when the body velocity gets larger.
- In SF-2b, compared to Figure 4-20(a), the values of both tangential and normal force from the shackle are smaller since the bird is rotating about its center of mass, which is close to the pivot point of the shackle is near the body center, thus reducing the forces from the limbs. When  $t>0.6s$ , as the bird of large size will have a longer distance with respect to the pivot point of the shackle, therefore it will gain a larger velocity, which may cause the large bird suddenly to lose the contact with the shackle hence increasing the shackle force because of the rotation. So the normal force and tangential force of the large bird will oscillate as shown in Figure 4-20 (c).

- Based on the results in Figure 4-20 (a) and (c), one advantage of this shackling system is illustrated. Compared against the shackle used in Chapter 3, the pivot point of the shackle in Chapter 4 is moving closer to the tip and hence closer to the center of the rotating bird. By doing this, the body force is minimized during rotation and thus reducing the possible injuries to the bird.

## 4.6 Preliminary Studies

This section conducts two preliminary studies on the automated transfer system. In order to provide a reference for a head handling mechanism designed in the electric stunning, head motion can be predicted by investigating effects of body rotation. Since in the actual design, there are two sidewalls on the shackle therefore their effects on the body motion need to be studied as well.

### 4.6.1 Effects of Body Rotation on Head Motion

The inverted bird must be rendered insensitive to pain before the process of neck cut, most commonly by electrical stunning. As an important welfare consideration, it is desired to accurately locate the bird head so that it can be consistently electrically stunned. Naturally, the bird head swings as its body rotates; thus we model the neck as a compliant beam and the head as a lumped mass to characterize its deflections during rotation. As an illustration, we approximate the head motion using a pseudo-rigid-body model to predict the deflection of the neck as shown in Figure 4-21.

As shown in Figure 4-21, the neck is modeled as a pin joint system (with torsion spring  $k$  and damper  $b$ ) connecting the bird body and the head, the equation of the head motion (swing angle  $\gamma$ ) is given by Equation (4-2):

$$m\ddot{\gamma} + b(\dot{\gamma} - \dot{\beta}_e) + k(\gamma - \beta_e) = 0 \quad (4-2)$$

Hence, we have the transfer function 
$$\frac{\gamma(s)}{\beta_e(s)} = \frac{bs + k}{ms^2 + bs + k} \quad (4-3)$$

To help visualize the effect of the body swing on the head motion, we approximate the neck as a 3-inch compliant beam, with properties similar to a rubber finger, which is used in an experiment introduced in the Appendix, as shown in Table A-1. Using the method proposed by [Howell, 2001], the equivalent spring constant for the pseudo-rigid-model of the rubber finger is given by Equation (4-4):

$$k = EI / \ell \quad (4-4)$$

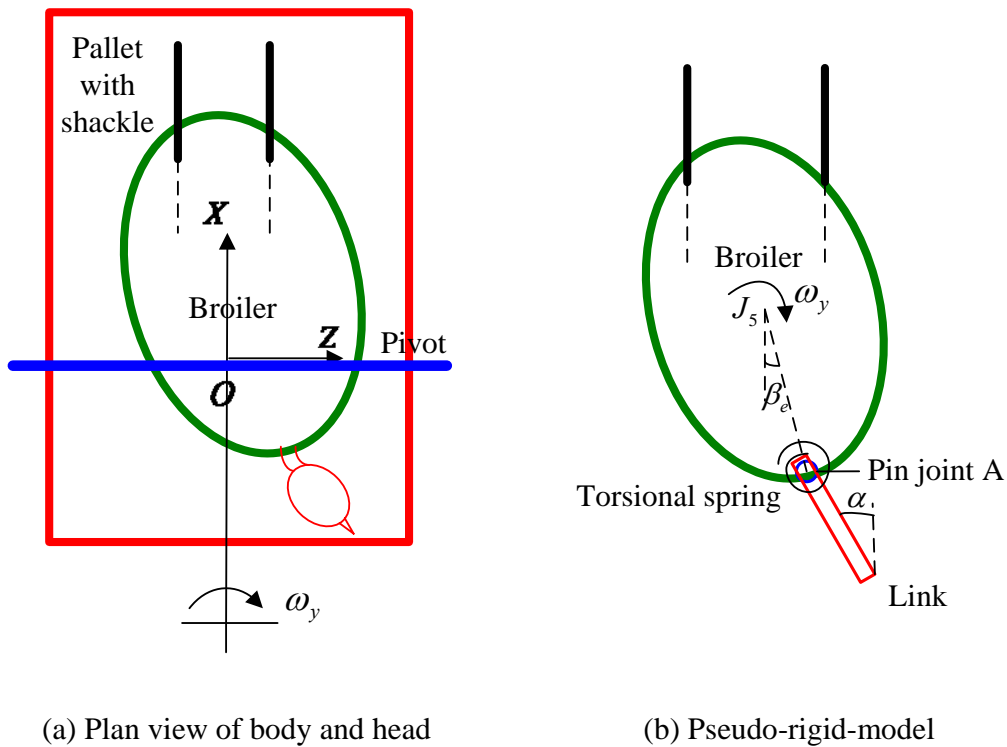


Figure 4-21 Head and its pseudo-rigid-model (plan view)

The results are given in Figures 4-22 to 4-24. Figure 4-22 shows the plot of the system input (body orientation angle) and output (head swing angle during the pallet rotation with respect to time). Figure 4-23 shows the motion of this pseudo-rigid-model

during pallet rotation. Figure 4-24 shows a plot about the link trajectory without the body. These results will help predict the head motion for designing a head grasping system that facilitates the stunning of the bird.

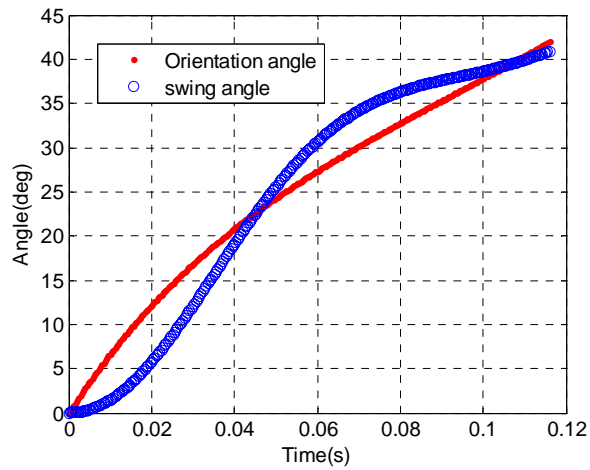


Figure 4-22 System input and output

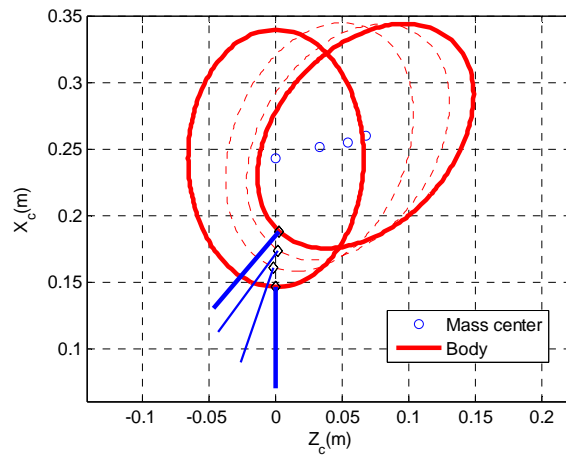


Figure 4-23 Pseudo-rigid-model motion

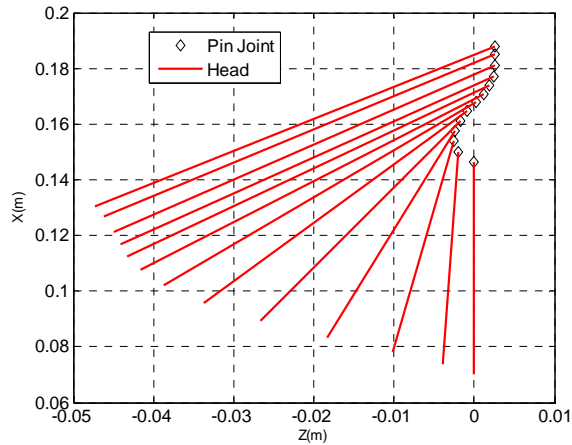


Figure 4-24 Pseudo-rigid-link trajectory

#### 4.6.2 Effects of the Shackle Sidewalls and Gravity in SF-2a

In the actual design of the system [11], there are two sidewalls on both sides of the shackle to constrain the bird motion in SF-2a. In this section, the effects of these sidewalls are investigated by using the same algorithm as in Chapter 3. Also as the bird body will contact the sidewall because of the swing motion, the contact force and the velocity after the contact are determined by the same force prediction method as mentioned in Section 3.3. In addition, the gravity is considered during the swing motion in SF-2a. The results are shown in the figures below.

- Figure 4-25 shows the snapshots of SF-2a from the initial position  $0^\circ$  of  $\theta_y$  to the final position of  $45^\circ$ .
- Figure 4-26 shows the comparison of the body center position and orientation between the simulation with the shackle and the one without the shackle.
- Figure 4-27 shows the comparison of the bird motion in 3D between the simulation with the shackle and the one without the shackle.

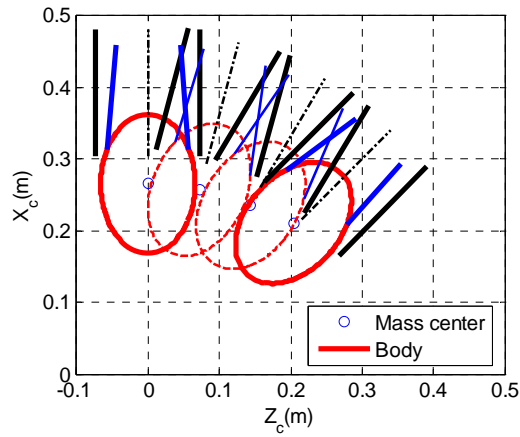


Figure 4-25 Snapshots in SF-2a (with sidewalls and gravity)

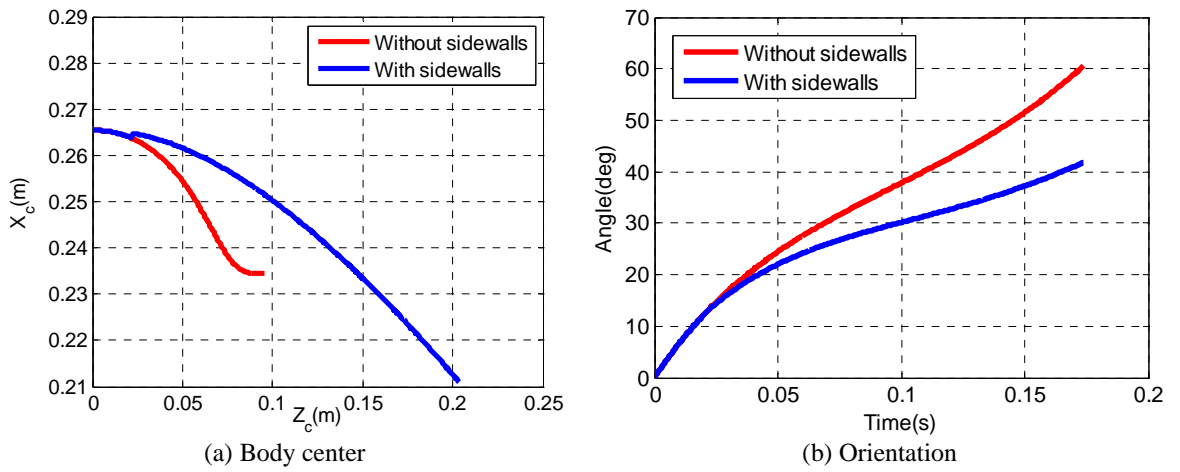


Figure 4-26 Trajectory comparison

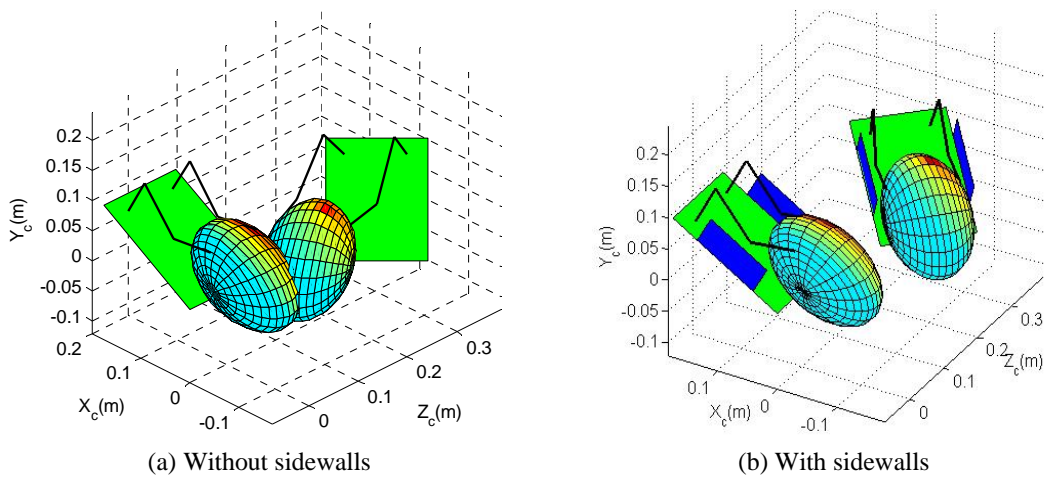


Figure 4-27 Bird motion in 3D

As shown in Figures 4-25 to 4-27, one effect of the sidewalls is to constrain the bird motion within the shackle in SF-2a on the XZ plane. In this simulation the bird has a contact with the left sidewall at  $t=0.024s$ , with a contact force of 30.1N, which can be calculated from Equation (3-18). As a result, this interaction supports the bird body to move within the region between the two sidewalls, hence the Z-displacement of the body center is larger than that without the sidewalls. Another effect of the sidewalls is to reduce the changes in the body orientation, thus reducing the possible injuries if the body swings excessively. The gravity increases the X-displacement of the body center since it pulls the body downward along the shackle.

#### 4.7 Summary

This chapter summarizes the results of the integrated three-function simulation. Taking a bird of medium size as a basis, the trajectory (center position and velocity) and constrained force/moment has been discussed to illustrate the body motion within each function. The following results were concluded:

- In F-1, the constrained forces oscillated before the contact and reduced when the bird slides on the shackle.
- In SF-2a, the rotation on the XZ plane had small effects on the constrained forces.
- In SF-2b, since the bird rotates about its center of mass, the constrained forces are smaller as compared to that in F-1 thus minimizing the potential injuries to the birds.

The effects of bird sizes have also been investigated by comparing the results among three bird sizes (large, medium and small) when going through three consecutive functions. The results show that bird sizes affect the initial positions of the subsequent function (SF-2a) after F-1, and peak values of the forces (imposed by the shackle). In SF-

2b, the shackle forces were reduced for all sizes since the birds rotate about their center of mass. However, the shackle force of the large bird could change suddenly when it temporarily loses the contact with the shackle. Swing angular motion has an effect on the head trajectory. The sidewalls of the shackle constrain the bird's motion so that it will not rotate excessively.

## **CHAPTER 5**

### **CONCLUSIONS AND FUTURE WORK**

This thesis presents an analytical model for predicting the dynamic behavior of a modeled bird under going through three consecutive functions. Numerical simulations provide an intuitive insight to optimize the design of live bird transfer system. Specifically, the bird is modeled as an ellipsoid with its legs as a pair of serial manipulators. Unlike previous studies where only a 2D side view was considered, the kinematic relationship between the joints and body center are derived in multiple 2D views providing a supplemental set of equations to solve for the bird's motion.

The equation of motion has been derived using the Lagrange method with a Jacobian matrix derived from the kinematic constraints. To solve a set of differential algebraic equations (formed by the Lagrange equations of motion and the constraints with Lagrange multipliers), acceleration constraint equations are introduced into the system. Through computer simulations programmed in MATLAB, the trajectory (position, velocity and orientation) of the bird body along with the constrained forces and torques are numerically predicted.

The dynamic model has been validated by comparing against finite element analysis. To offer a better understanding on the effects of constrained forces on the bird, the validated model is applied to analyze the design of an existing live transfer system and to investigate the effects of the bird sizes and hence.

This model can also provide a reference on system optimizations from a design perspective. As an example, we show how the motion prediction can be used to locate the bird head for subsequent process where the bird is rendered insensitive to pain before neck cut. As an illustration, we approximate the bird neck as a compliant beam and model it as a pseudo-rigid beam with a torsion spring and a damper attached on the bird body. The head swinging motion can be predicted based on the trajectory of the bird body. By predicting head motion, an appropriate head handling mechanism could be designed to grasp the head effectively.

The following are the recommendations for future works that could build upon this thesis. The first is to improve the accuracy of this dynamic model by further refining the kinematic constraint equations to better describe the imposed constraints. The second is to evaluate more parameters to investigate the possible effects on bird dynamics such as shackle length and rotating path.

## APPENDIX A

### DAMPING COEFFICIENTS OF THE RUBBER FINGER

An experiment was designed to determine the damping coefficient for the rubber finger when using free vibration. A 6-inch finger (manufactured by the Waukesha Rubber Company) was chosen in the application, the finger was flexible on the XY plane but relatively rigid in the Z-direction. A clamp was used to hold the finger, when the finger was bent over, it had some displacement with respect to its original position; when it was released, the oscillation of its end can be observed. In this experiment, a cylindrical permanent magnet is attached to the end of the finger, so that the change in the ambient magnetic field due to the finger deflection can be measured as shown in Figure A-1.

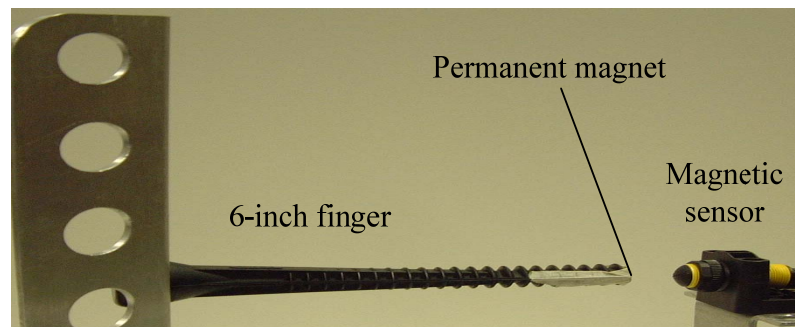


Figure A-1. Experiment setup (6-inch finger) [18]

In this experiment, the Banner S18MB magnetoresistive sensor measures the change in the earth natural magnetic field (the ambient magnetic field) caused by the introduction of a ferromagnetic object attached at the end of the finger. The sensor utilizes three mutually perpendicular magneto-resistive transducers, where the background condition and sensitivity level of the sensor can be pre-programmed by a

programmable box. The sensitivity level and the sampling time of the S18MB magnetoresistive sensor were set to 5 and 20ms (minimum) respectively.

The properties of all the equipments involved in this experiment are listed in Table A-1. The response of 6-inch finger is shown in Figure A-2.

Table A-1 Equipment properties

Sensor[1]		Permanent magnet	
Supporting voltage	10 to 30V DC	Radius(inch)	0.156
Output type	Bipolar NPN/PNP	Height(inch)	0.063
Sensing range	3 inches		
Finger properties [13][30]			
Major semi-axis	12mm		
Minor semi-axis	8.45mm		
Young's modulus	6.1 MPa		
Density	1000kg/m <sup>3</sup>		
Length	76.2mm		
Mass	0.0243kg		
Inertia	1.046kg-mm <sup>2</sup>		

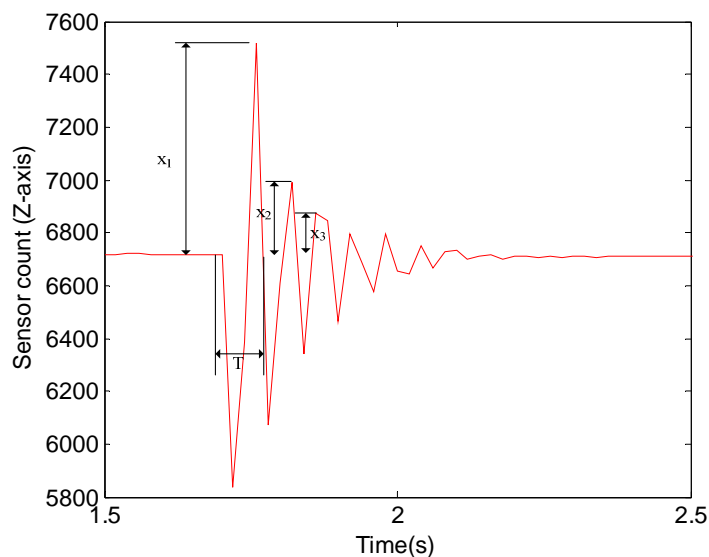
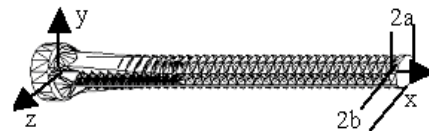


Figure A-2. Response of the 6-inch finger [18]

From Figure A-2, the damping ratio of the 6-inch finger can be calculated by from the logarithmic decrement [Ogata, 2004]:

$$\zeta = \frac{\delta}{\sqrt{4\pi^2 + \delta^2}} = 0.17 \quad \text{where } \delta = \left[ \frac{1}{n-1} \left( \ln \frac{x_1}{x_3} \right) \right] = 0.82 \quad (\text{A-1})$$

where  $x_1=800$ ,  $x_3=154$ ,  $n=3$ . The period of this finger response is  $T=0.06\text{s}$ .

## REFERENCES

- [1] Banner, INC (2006), "Manual for S18 Magneto Resistive sensor"
- [2] Boyle, C. (2001), "Dynamic modeling of compliant constant-force compression mechanisms," *Mechanism and Machine Theory*, pp. 1469-1487.
- [3] Chapra, C. and Canale, R. (2002), "Numerical Methods for Engineers," *Fifth Edition*.
- [4] Heemskerk, W.J.C., "Method for Causing Sitting Poultry to Stand Up and Apparatus for Carrying out this Method," US Patent 5.088.959, February 18, 1992.
- [5] Howell, L. (2001), "Compliant Mechanisms," *First Edition*.
- [6] Kang, B. and Mills, J.K. (2002), "Dynamic modeling of structurally-flexible planar parallel manipulator," *Robotica*, pp. 329-339.
- [7] Kövecses, J., Piedboeuf, J.-C. and Lange, C. (2003), "Dynamics Modeling and Simulation of Constrained Robotic Systems," *IEEE/ASME Transactions on Mechatronics*, pp.165-177.
- [8] Lee, K.-M. (2001), "Design Criteria for Developing an Automated Live-Bird Transfer System," *IEEE Transactions on Robotics and Automation*, August, vol. 17, Issue 4, pp. 483-490.
- [9] Lee, K.-M. (1999), "On the Development of a Compliant Grasping Mechanism for On-Line Handling of Live Objects, Part I: Analytical Model," *Proceedings of IEEE/ASME International Conference on Advanced Intelligent Mechatronics*, Atlanta, Georgia.
- [10] Lee, K.-M., "Intelligent Automated Transfer Of Live Birds To Shackle Line," Georgia ATRP 2000-2001 Final Report (August 1, 2001). Also in the 3<sup>rd</sup> Progress Report on USPE Project #557, (April 15, 2002).
- [11] Lee, K.-M., Foong, S., Liu, C., Pointextor, B. and Webster, B. (2009), "Methods of Loading Live Birds from Conveyors to Kill Line Shackles," GTRC ID 4731, Provisional application (61/147,219, January 26).
- [12] Lee, K.-M., Carey, R., Webster, B., and Lacy, M. (1997), "Intelligent Automated Transfer of Live Birds to Shackle Line," Proposal to Georgia ATRP and the US Poultry and Egg Association.

- [13] Lee, K.-M., Joni, J. and Yin, X. (2001), "Compliant Grasping Force Modeling for Handling of Live Objects," *Proceedings of the 2001 IEEE ICRA*, May 21-26, Seoul, Korea, pp. 1059-1064.
- [14] Lee, K.-M. and Shumway, C. (2003), "Dynamic Modeling of the Body Inversion for Automated Transfer of Live Birds," *Proceedings of the 2003 IEEE ICRA*, September 13-19, Taipei, Taiwan, China.
- [15] Lee, K.-M., Webster, A.B., Joni, J.H., Yin, X., Carey, R., Lacy, M.P. and Gogate, R. (1999), "On the Development of a Compliant Grasping Mechanism for On-Line Handling of Live Objects, Part II: Design and Experimental Investigation," *Proceedings of IEEE/ASME International Conference on Advanced Intelligent Mechatronics*, Atlanta, Georgia, pp.354-359.
- [16] Lee, K.-M. and Yin, X. (2001), "Design Algorithm for Automated Dynamic Grasping of Live Birds," *Proceedings of the IEEE/ASME AIM'01*, July 8-11, Como, Italy, pp. 207-212.
- [17] Liu, C.H. and Lee, K.-M. (2009), "Dynamic Analysis and Topology Optimization for Design and Modeling Automated Poultry Shackling Process".
- [18] Liu, C.H. and Wang, D. (2008), "Grasping Dynamic Analysis for Live Bird Automated Transfer System with Compliant Fingers," *Final project of ME 6124: Finite Element Method*.
- [19] Michitsuji, Y., Sato, H. and Yamakita, M. (2001), "Giant Swing via Forward Upward Circling of the Acrobat-robot," *Proceedings of the American Control Conference*, Arlington, VA, pp. 3262-3267.
- [20] Nakawaki, D., Joo, S. and Miyazaki, F. (1998), "Dynamic Modeling Approach to Gymnastic Coaching," *Proceedings of the 1998 IEEE International Conference on Robotics & Automation*, Leuven, Belgium, pp. 1069-1076.
- [21] Ogata, K. (2004), "System Dynamics," *Fourth Edition*.
- [22] Parker, A. E. Jr., "Shackling Apparatus for Live Poultry," US Patent 4,272,863, June 16, 1981.
- [23] Pop, C., Khajepour, A., Huisson, J.P. and Patla, A.E. (1999), "Application of Bond graphs to Human Locomotion Modeling," *Proceeding of the HKK Conference and Symposium*, University of Waterloo, Canada, pp. 85-90.
- [24] Summer, M.D. (2002), "Design Algorithm of a Novel Computer-Controlled Gripper for a Live Bird Transfer System," M.S.Thesis, the George W. Woodruff School of Mechanical Engineering, Georgia Institute of Technology.

- [25] Shumway, C.M. (2002), "Dynamic Modeling and Analysis of the Body Inversion," M.S.Thesis, The George W. Woodruff School of Mechanical Engineering, Georgia Institute of Technology.
- [26] Takubo, T., Inoue, K. and Arai, T. (2005), "Pushing an Object Considering the Hand by Humanoid Robot in Dynamic," *Proceedings of the 2005 IEEE International Conference on Robotics and Automation*, Barcelona, Spain, pp. 1706-1711.
- [27] Webster, A. B. and Lee, K.-M. (2002), "Toward Automation of the Transfer of Broilers to the Processing Line," *WATT PoultryUSA*, September, pp. 28-42.
- [28] Webster, A. B. and Lee, K.-M. (2003), "Automated shackling: how close is it?" *Poultry International*, Vol. 42, Number 4, April, pp.28-36.
- [29] Wojcik, L.A. (2000), "Musculoskeletal Modeling Using a Bond Graph Approach," *Proceedings of the ASME Dynamic Systems and Control Division*, pp. 35-42.
- [30] Yin, X. and Lee, K.-M. (2002), "Modeling and Analysis of Grasping Dynamics for High Speed Transfer of Live Birds," *Proceedings of the 2<sup>nd</sup> IFAC Conference on Mechatronic Systems*, Berkeley, California, December 9-11, pp. 719-724.